

Universiteit
Leiden
The Netherlands

Assembling anisotropic colloidal building blocks

Meester, V.

Citation
Meester, V. (2018, June 7). *Assembling anisotropic colloidal building blocks*. *Casimir PhD Series*. Retrieved from https://hdl.handle.net/1887/62808

Version:	Not Applicable (or Unknown)
License:	Licence agreement concerning inclusion of doctoral thesis in the Institutional Repository of the University of Leiden
Downloaded from:	https://hdl.handle.net/1887/62808

Note: To cite this publication please use the final published version (if applicable).

Cover Page



Universiteit Leiden



The handle http://hdl.handle.net/1887/62808 holds various files of this Leiden University dissertation.

Author: Meester, V.
Title: Assembling anisotropic colloidal building blocks
Issue Date: 2018-06-07

Assembling Anisotropic Colloidal Building Blocks

Proefschrift

ter verkrijging van
de graad van Doctor aan de Universiteit Leiden,
op gezag van Rector Magnificus Prof. mr. C.J.J.M. Stolker,
volgens besluit van het College voor Promoties
te verdedigen op donderdag 7 juni 2018
klokke 13:45 uur

door

Vera Meester
geboren te Amersfoort
in 1988

Promotor:	Prof. dr. M.L. van Hecke
Co-promotor:	Dr. D.J. Kraft
Promotiecommissie:	Prof. dr. W.K. Kegel (*Universiteit Utrecht*)
	Dr. T.E. Kodger (*Universiteit Wageningen*)
	Prof. dr. E.R. Eliel
	Dr. M.I. Huber
	Prof. dr. T. Schmidt

Casimir PhD Series, Delft-Leiden, 2018-11
ISBN 978-90-8593-343-4

The work described in this thesis was supported by the Netherlands Organisation for Scientific Research(NWO) through a VENI grant, 680-47-431.

The cover shows in the background a confocal microscopy image of a crystal of highly repulsive colloidal spheres adsorbed at a water-oil interface, with defects induced by dumbbell particles. The grey particles in front are scanning electron microscopy images of micron-sized patchy and anisotropic particles.

"All that I saw and learned that was new delighted me. It was like a new world opened to me, the world of science, which I was at last permitted to know in all liberty."

Maria Salomea (Marie) Sklodowska-Curie

For Science

Contents

1 Introduction **1**
- 1.1 Colloids . . . 1
- 1.2 Synthesis and fabrication . . . 2
- 1.3 Particle interactions . . . 4
- 1.4 Colloidal self-assembly . . . 7
- 1.5 This thesis . . . 9

2 Spherical, Dimpled and Crumpled Colloids with Tunable Surface Morphology **11**
- 2.1 Introduction . . . 12
- 2.2 Experimental Methods . . . 13
- 2.3 Results and Discussion . . . 15
  - 2.3.1 Synthetic approach . . . 15
  - 2.3.2 Spherical colloids with tunable surface roughness . . . 17
  - 2.3.3 Buckling mechanism for colloids swollen with mainly TPM 21
  - 2.3.4 Crumpled colloids of various shapes . . . 23
  - 2.3.5 Silica coated colloids with rough, smooth, dimpled and crumpled surface morphology . . . 25
  - 2.3.6 Hollow silica shells . . . 27
- 2.4 Conclusions . . . 28

3 Colloidal Recycling: Reconfiguration of Random Aggregates into Patchy Particles **31**
- 3.1 Introduction . . . 32
- 3.2 Experimental Methods . . . 33
- 3.3 Results and Discussion . . . 35
  - 3.3.1 Assembly strategy . . . 35
  - 3.3.2 Tunable size distribution . . . 39
  - 3.3.3 Reconfiguration parameters . . . 39
  - 3.3.4 Patchy particle configurations . . . 41
- 3.4 Conclusions . . . 45
- 3.5 Appendices . . . 47

4 Complex Patchy Colloids shaped from Deformable Seed Particles through Capillary Interactions **53**
4.1 Introduction . . . 54
4.2 Experimental Methods . . . 55
4.3 Results and Discussion . . . 57
4.3.1 The colloidal recycling method . . . 57
4.3.2 Spherical, anisotropic and patchy particles of deformable spheres . . . 60
4.3.3 Shape deformation analysis of dumbbells . . . 63
4.3.4 Patch arrangements for particles of N>5 . . . 66
4.3.5 Reconfiguration pathway . . . 69
4.4 Conclusions . . . 71

5 Patchy Particles of Various Shapes with Distinct Patches **73**
5.1 Introduction . . . 74
5.2 Experimental Methods . . . 75
5.3 Results and Discussion . . . 77
5.3.1 Patchy particles of soft and rigid spheres, size ratio 1.5 . . . 77
5.3.2 Patchy particles with chemical and physical patchiness, size ratio 4.6 . . . 80
5.4 Conclusions . . . 83

6 Anisotropic Distortions in Hexagonal Crystals at Fluid Interfaces **85**
6.1 Introduction . . . 86
6.2 Experimental Methods . . . 87
6.3 Results and Discussion . . . 90
6.3.1 Ordering of repulsive spheres at a flat fluid interface . . . 90
6.3.2 Impurities at a flat fluid interface . . . 92
6.3.3 Interfacially bound dumbbells . . . 94
6.3.4 Dumbbell orientation and crystal distortion . . . 98
6.4 Further Discussion . . . 115
6.5 Conclusions . . . 116

Summary **119**

Samenvatting **123**

Publication List **127**

Curriculum Vitae **129**

Acknowledgements **131**

Bibliography **133**

CHAPTER 1

INTRODUCTION

1.1 Colloids

Particles with at least one of their dimensions being on the order of a few nm to a few μm are referred to as colloids. Colloids can be different in phase, size, shape and material and are abundantly present in our daily life in soft material products such as drinks, foods, paint, medicine and cosmetics.[1] The particles can be a main ingredient of a product such as fat droplets in milk, but they can also be used to stabilize or encapsulate other components in, for example, shampoo or medicine. Additionally, these particles are frequently used to adapt the visco-elasticity and texture of the product.
When dispersed in a liquid, colloids are influenced by thermal fluctuations of the molecules in the liquid. These fluctuations ensure continuous movement of the particles called Brownian motion. In contrast to atoms and molecules, which are 100 to 100.000 times smaller in size, colloidal particles can be imaged with optical microscopy. This is a powerful tool, since the dynamics and interaction between the particles can be studied in real-time. Colloids are often referred to as big atoms and molecules, since their motion and phase behavior is similar.
Colloidal particles can be used as building blocks for larger structures. By varying the shape, size, material and surface chemistry of the colloids different materials can be formed.[2,3] Similations, theory and models are useful tools to predict into



FIGURE 1.1: Examples of macroscopic products that contain colloidal particles including; milk, paint, ice cream and medicine.

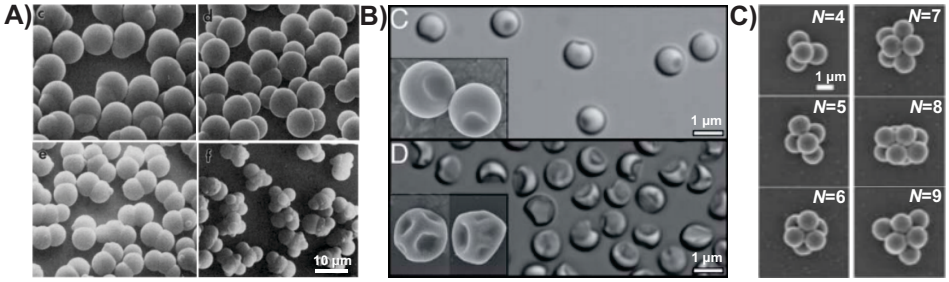


FIGURE 1.2: Polymer colloids with anisotropic shapes. A) Colloids with protrusions formed by swelling crosslinked polymer spheres with additional monomers. B) Dimpled colloids formed by buckling of an elastic shell around deformable polymer spheres. C) Colloidal clusters formed using an emulsion based evaporation method. Reprinted A) from ref. [4] and C) from ref. [5] with permission from John Wiley & Sons, copyright 1990 and 2004. B) was reprinted from ref. [6] with permission from the Royal Society of Chemistry, copyright 2011.

which structures the particles will assemble. Particles with anisotropic shapes or surface chemistry are particularly interesting, since these can assemble into novel structures which could lead to unusual material properties. Complex colloids are also promising building blocks for the assembly of 'smart' materials; materials that respond and adapt their structure to changes in their environment, such as thermo-repsonsive and light-responsive materials.

1.2 Synthesis and fabrication

Synthesis of anisotropic colloids

Colloids can be synthesized out of various materials including metals, polymers and ceramics. In this thesis polymer colloids are mainly considered. Polymer spheres of low polydispersity can be synthesized using various methods such as emulsion or dispersion polymerization.[7,8] The complexity of the particles can be increased by adapting the shape or surface properties of the polymer spheres. For example, by swelling crosslinked polymer spheres with additional monomers one or more protrusions can be formed on the seed particle, resulting in dumbbell, snowman or popcorn-like shapes (see Figure 1.2A).[9,10] The protrusions are formed due to the elastic stress exerted on the crosslinked polymer network upon swelling.[4] The shape of the final particle is determined by the crosslink density and surface properties of the seed particle, the concentration of added monomers and the dispersion medium.
Instead of protrusions, dents can also be formed on the spheres to yield

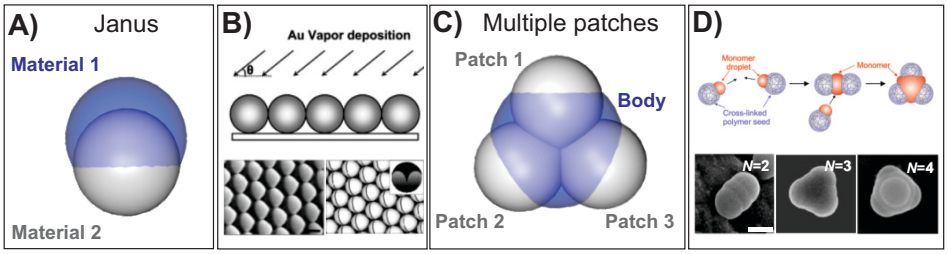


FIGURE 1.3: Patchy particles. A) Illustration of a Janus particle consisting of two different materials. B) Fabrication method for Janus particles based on the deposition of gold on one side of spheres. Scalebar is 2 μm. C) Illustration of a patchy particle with three patches and a 'body' covering the center of the cluster. D) Fabrication method for multi-patched particles based on the assembly of colloids with liquid protrusions. Scalebar is 200 nm. Reprinted B) from ref. [15] and D) from ref. [16] with permission from the American Chemical Society, copyright 2008 and 2009.

anisotropy. Dimpled and crumpled particles can be obtained by buckling an elastic shell around a spherical polymer particle (see Figure 1.2B). Buckling is induced by a pressure difference between the inside and outside of the shell due to a reduction of the volume inside the shell upon polymerization.[6,11,12]
A third example to obtain anisotropically shaped polymer particles is a cluster preparation method, where uniform spheres are assembled into colloidal clusters (see Figure 1.2C). The colloidal clusters can be formed by introducing depletion forces between the spheres[13] or by evaporation of emulsion droplets containing a number of spheres[5,14]. The geometry of the cluster depends on the formation mechanism, the number of spheres in the cluster and the wetting properties of the seed particles.

Fabrication of patchy particles

A separate class of anisotropic colloids are patchy particles. Patchy particles are defined as particles with precisely controlled patches of varying surface and interaction properties.[17–19] These particles are interesting since directional interactions could lead to, for example, reversible binding and open crystal structures.[20,21] We here distinguish between Janus particles, defined as colloid-sized particles with two regions of different surfacechemical composition[22] and particles with multiple patches, see Figure 1.3A and 1.3C, respectively.
The term Janus particles was introduced by P.G. de Gennes during his Nobel Lecture in 1992, referring to the two-faced Roman god Janus. Different methods are known to fabricate Janus particles including glancing angle deposition, where uniform particles are partly sputtercoated with a second material[15] (Figure 1.3B)

and chemical functionalization of part of the particle surface by adding reactive molecules to spheres partly immersed in emulsified molten wax[23]. Patchiness can also be achieved by swelling polymer particles with a different monomer resulting in two different 'faces' due to phase-separation.[24]
On colloids with uniform surface chemistry, patchiness can be introduced by changing the particle shape. For example, dimpled colloids can act as lock-and-key structures using the depletion interaction.[6,11] Depletion was induced by addition of a second colloidal component with the dimensions of the dimples. The overlap volume in the dimple was therefore large resulting in attraction between the dimple and the second colloidal component in the presence of depletant.
The fabrication of particles with multiple patches is often achieved by assembling smaller colloidal spheres into larger structures. For example, colloidal spheres with liquid protrusions can be assembled into patchy particles by merging of the protrusions into a larger droplet, which forms the 'body' of the patchy particle (Figure 1.3C and 1.3D).[16] The part of the spheres protruding from this droplet can act as patches. Anisotropic colloidal clusters can also be adapted to obtain patchy particles by swelling the clusters with an additional monomer, which could form the 'body' of the patchy particle.[25]

Synthesis and fabrication methods have advantages and disadvantages. Preferably, a method yields particles of uniform shape, size and surface chemistry and can be used to obtain a variety of particles with different properties. By preference, a non-toxic medium is used and the synthesis is performed in bulk to obtain a high yield.

1.3 Particle interactions

In a colloidal dispersion, both attractive and repulsive forces act on the colloids. The net interaction energy between colloids is defined as,

$$U(r)_{net} = U(r)_{att} + U(r)_{rep}, \tag{1.1}$$

where $U(r)_{att}$ is the attractive interaction energy and $U(r)_{rep}$ is the repulsive interaction energy. A stable colloidal dispersion is obtained when the net interaction energy is positive and a negative net interaction energy leads to aggregation of the particles. One source of attraction between all colloidal particles stems from the van der Waals forces. The van der Waals interaction energy between two spheres at separation distance r of equal radius R, with $R \gg r$, is defined as,

$$U(r)_{vdW} = -\frac{AR}{12r}, \tag{1.2}$$

where A is the Hamaker constant.[26] Equation 1.2 indicates that van der Waals forces are long-ranged, but typically only at short r strong enough to compete

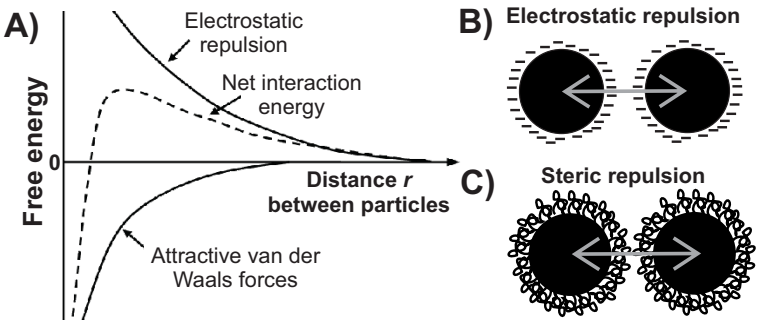


FIGURE 1.4: Colloidal stability. A) The free energy profile of two colloids at different separation distance r. At short distances particles attract due to van der Waals forces. Aggregation can be prevented by prohibiting close contact between the particles by; B) Charging the surface of the colloids resulting in electrostatic repulsion or by C) The introduction of a molecular layer of polymers at the surface of colloids.

with other forces. Aggregation can therefore be prevented by prohibiting close contact of the particles (Figure 1.4A). This can be achieved by introducing a repulsive Coulomb force by charging the colloid surface. A repulsive electric double layer will be formed around the charged particles with bound and diffusive ions from the medium accumulated at the surface. The electrostatic double layer interaction energy for two spheres with radius R at a separation distance r is defined as,

$$U(r)_{elec} = \frac{ZRe^{-\kappa r}}{2}, \tag{1.3}$$

where Z is the interaction constant, which is analogous to the Hamaker constant A, and depends only on the surface properties of the particles.[26] κ^{-1} is the Debye length which describes the characteristic length or 'thickness' of the diffuse electric double layer near the charged surfaces and is defined as,

$$\kappa^{-1} = \left(\frac{\epsilon_0 \epsilon_r k_B T}{e^2 \rho_i z_i^2} \right)^{0.5}, \tag{1.4}$$

where ϵ_0 is the vaccuum permittivity, ϵ_r the relative static permittivity, e the dielectric constant of the medium and ρ_i the ionic concentration of ions i with valency z_i in the bulk. When κ^{-1} is large enough, $U(r)_{elec} > U(r)_{vdW}$ resulting in a positive net interaction energy and thus a stable colloidal dispersion.
Colloids can also be stabilized sterically, by introducing a molecular, often polymer, layer at the surface of the colloids as illustrated in Figure 1.4C. The molecular layer prohibits close contact and thus attraction by van der Waals forces.

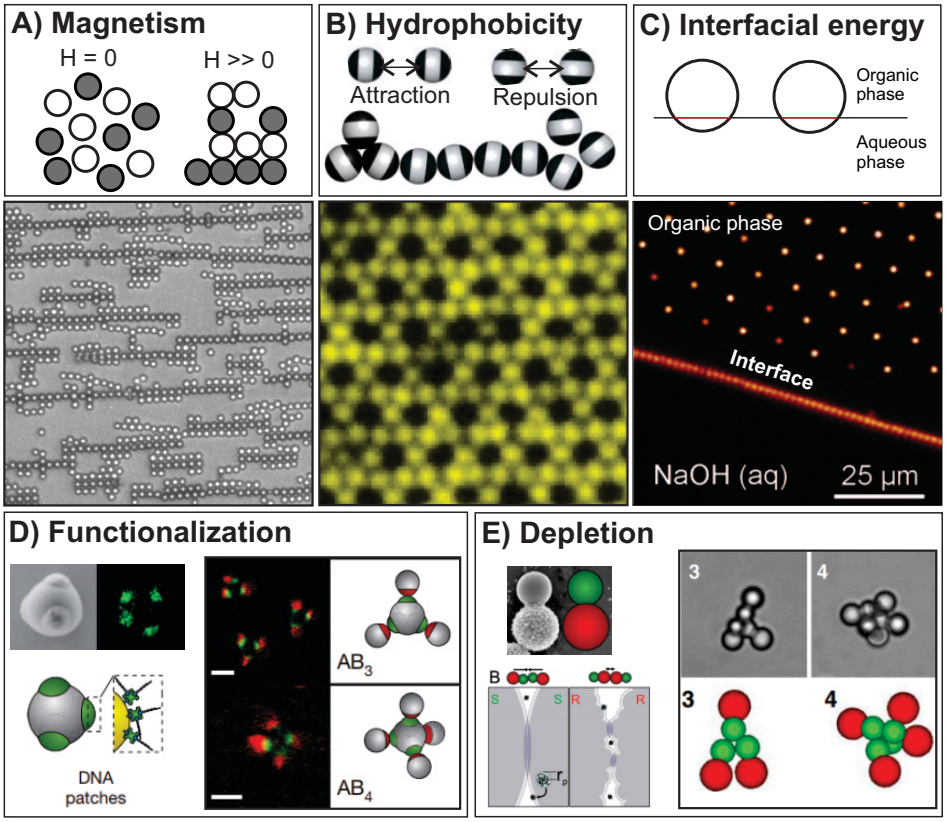


FIGURE 1.5: Microscopy images of self-assembled micron-sized polymer colloids using different assembly mechanisms. A) Dia- and superparamagnetic polymer spheres self-assembled in networks of alternating strings by aligning oppositely to an external magnetic field H. From ref. [27]. B) Triblock Janus particles arranged on a Kagome lattice due to the hydrophobic attraction between isolated patches on the spheres. C) Colloids adsorbed to a spherical organic-aqueous interface to decrease the interfacial energy. D) Particles with patches functionalized with complementary single DNA-strands assembled into colloidal molecules due to DNA binding. E) Dumbbell colloids with a rough and a smooth surface lobe, self-assembled by depletion forces. Reprinted B) from ref. [21] and D) from ref. [25] with permission from Springer Nature, copyright 2011 and 2012. C) and E) were reprinted from ref. [28] and ref. [29], respectively, with permission from the National Academy of Sciences U.S.A., copyright 2007 and 2012.

1.4 Colloidal self-assembly

Self-assembly mechanisms

Due to the Brownian motion of colloids and their tunable interaction profile colloids can self-assemble into larger structures. To obtain colloidal crystals with rich phase behavior or optical or mechanical properties anisotropic colloids or mixtures of different particles are often used. Self-assembly can be achieved via different assembly mechanisms. For example, two-dimensional networks of alternating strings of dia- and superparamagnetic polymer spheres were realized using an external magnetic field.[27]. The dia- and superparamagnetic particles aligned oppositely to the external magnetic field yielding a square packed network (see Figure 1.5A). In Figure 1.5B the hydrophobic attraction between parts of triblock Janus particles was used to form two-dimensional Kagome lattices of low packing density.[21] Colloids can also assemble at an interface between liquid and gas[30] or two immiscible liquids, as shown in Figure 1.5C for polymer spheres at an aqueous-organic interface[28]. Binding a particle to an interface decreases the interfacial area A and thus the interfacial energy, which is defined as, $E = \gamma A$, where γ is the surface tension (Figure 1.5C). Particle stabilized emulsions are referred to as Pickering emulsions, which are used in a variety of application fields including foods, cosmetics and medicine.[31]
Three-dimensional self-assembled structures were, for example, formed by particles functionalized with single DNA-strands. Mixing patchy particles with complementary DNA-strands resulted in the formation of colloidal molecules due to DNA binding (Figure 1.5D).[25] The depletion interaction was also be used to form three-dimensional structures. By introducing depletant to dumbbell shaped particles with a rough and a smooth lobe attraction between the smooth lobes was induced (see Figure 1.5E).[12,29,32] The shape of the structures depended on the number of particles in the cluster and the size ratio between the two lobes.

These examples emphasize the self-assembly possibilities of colloids. By tuning and controlling the physical properties of the colloidal building blocks and the assembly pathway, a variety of colloidal structures can be formed. This could lead to materials with advanced properties such as high material strength or 'smart' materials that change their structure under the influence of light, temperature, pH or other environmental parameters.

Colloidal crystals and defects

Colloidal crystals are ordered arrays of monodisperse colloids, where the crystal order can be described by repeating subunits.[35] Spheres often order on a hexagonal lattice where, on a planar surface, all spheres are surrounded by six neighboring spheres. Defects in hexagonal crystals appear for spheres not surrounded by

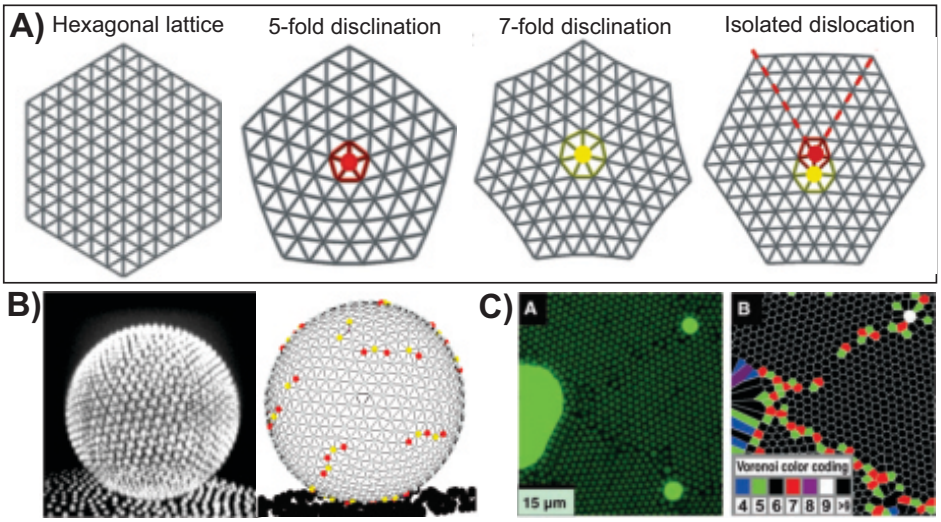


FIGURE 1.6: Colloidal crystals and crystal defects. A) Illustration of a hexagonal lattice, 5-fold and 7-fold disclinations and an isolated dislocation. B) Confocal microscopy image and Delauney triangulation of a spherical oil droplet stabilized in an aqueous phase by interfacially bound pMMA spheres. The diameter of the droplet ~ 60 μm. A) and B) were reprinted from ref. [33] with permission from Springer Nature, copyright 2012. C) Confocal microscopy image and Voronoi diagram of an planar hexagonal crystal of spheres distorted by large impurities. The impurities are connected by grain boundaries. Reprinted from ref. [34] with permission from The American Association for the Advancement of Science, copyright 2005.

six spheres, which results in disclinations and dislocations, see Figure 1.6A.[33,36] A collection of dislocations can result in the formation of a grain boundary.
In a monodisperse colloidal system crystal defects can be induced by vacancies or interstituals, substrate curvature or impurities. The number and type of defects originating from substrate curvature depends on the sign and degree of the curvature.[33,37] A confocal microscopy image of a colloidal crystal of polymer spheres adsorbed to a spherical organic-aqueous interface is shown in Figure 1.6B.[37] The fluorescent colloids arranged in a regular pattern and stabilize the organic droplet in the aqueous phase. The curvature of the interface induced the formation of topological defects; while most spheres are surrounded by six neighboring spheres, some spheres have only five or seven neighbors, resulting in disclinations, dislocations and short grain boundaries.
Large spherical impurities in a crystal of spheres induced the formation of large grain boundaries, as shown in Figure 1.6C.[34] The distortion of the hexagonal order by the impurities also frustrated the crystal growth. The presence of dumb-

bells in a hexagonal crystal of spheres also strongly affected the crystal properties. The dumbbells formed dislocation cages that restricted the dislocation motion and introduced glassy dynamics.[38,39]
The presence of defects influences the crystal properties, such as the orientation, mechanical strength and crystal melting and formation processes. By controllably introducing defects by substrate curvature or doping with impurities, the properties of crystals and thus materials can be tuned.

1.5 This thesis

In this thesis colloidal polymer spheres are used as a starting point to form anisotropic and patchy particles and to assemble and distort colloidal crystals of spheres.
In **Chapter 2** a synthetic method is presented that can be used to tune the shape and surface roughness of polystyrene particles. Linear polystyrene spheres were swollen with styrene and 3-(Trimethoxysilyl)propyl methacrylate(TPM) at different styrene:TPM ratio's. At TPM concentrations $\geq$ 50% dented colloids were formed. We hypothesize that the TPM molecules formed a shell on the surface of the particles since the silane groups in TPM prefer to be in contact with the water. At a sufficient shell thickness the TPM shell buckles when the core volume decreases, which occurs during polymerization. The surface roughness of the particles was controlled by an additional chemical component, hydroquinone, which inhibits the formation of small secundary nuclei during polymerization. Smooth surfaces were formed in the presence of hydroquinone and rough surfaces when hydroquinone was absent.
In **Chapter 3** we present a method, the "colloidal recyling" method, to reconfigure aggregates of polymer spheres into patchy particles. Colloidal aggregates were formed by the de-stabilization of charge-stabilized colloids due to the addition of salt. Reconfiguration of the aggregates was achieved by introducing organic liquid with affinity for the aggregates to the colloidal dispersion. We hypothesize that the organic liquid deposited as droplets at the contact areas between the spheres, which drastically lowers the van der Waals attraction. The spheres in the clusters could therefore rearrange their position, which lead to compact patchy shapes once the small droplets merged into one larger droplet. With this method bulk quantities of patchy particles can be assembled of various consistencies since the colloid and swelling material can be varied.
In **Chapter 4** we investigated how polystyrene spheres with different crosslink density were deformed by the capillary forces exerted by the organic droplets on the particles during reconfiguration. Clusters of seeds with low crosslink density completely merged into larger spheres, whereas the shape of the original spheres was increasingly preserved at increasing crosslink density.
In **Chapter 5** the knowledge of Chapter 3 and 4 was used to form complex par-

ticles with different patch types by combining mixtures of spheres with different sizes and crosslink density. Unique shapes were obtained by combining soft and rigid spheres and a combination of spheres with size ratio 4.6 resulted in particles with both chemical and physical patchiness.
In **Chapter 6** we assembled colloidal crystals of highly repulsive spheres at a planar water-oil interface. We introduced anisotropic impurities, dumbbells, of different lengths to the crystal and studied the dynamics and position of the dumbbell and crystal defects induced by these impurities. The crystal distortion was determined by the length of the dumbbell, where the number of neighboring spheres increased with the length of the dumbbell. We also studied the effect of the confinement of the crystal on the rotational and translational motion of the dumbbells. The motion of confined dumbbells was largely restricted and a preferred dumbbell orientation with respect to the crystal orientation was measured which was determined by the interaction energy profile between the dumbbell and the surrounding spheres.

CHAPTER 2

SPHERICAL, DIMPLED AND CRUMPLED COLLOIDS WITH TUNABLE SURFACE MORPHOLOGY

The results in this chapter have been published* and are reproduced with permission, copyright 2016 American Chemical Society.

* Vera Meester, Daniela J. Kraft,
Spherical, Dimpled and Crumpled Hybrid Colloids with Tunable Surface Morphology,
Langmuir, 2016, 32(41), 10668-10677, DOI: 10.1021/acs.langmuir.6b02952.

Abstract

Surface morphology is a tool to tune physical properties of colloidal suspensions such as the wettability, viscoelasticity and depletion attractions. Existing synthesis methods to obtain colloids with a rough surface morphology often result in colloids with non-tunable surface properties. Here, we developed a synthetic approach to obtain both spherical and shape-anisotropic hybrid colloids with tunable surface morphology. With our approach monodisperse linear polystyrene colloids, obtained in large quantities using a dispersion polymerization method, are swollen and crosslinked with styrene and 3-(Trimethoxysilyl)propyl methacrylate (TPM) in the presence of the polymerization inhibitor hydroquinone. We show that by varying only two experimental parameters, the concentration of the inhibitor and of TPM during swelling linear polystyrene colloids, three different types of particles can be synthesized. At low TPM concentration spherical colloids are obtained where the surface roughness can be tuned by varying the hydroquinone concentration. At intermediate TPM concentrations single-dimpled colloids are formed with tunable dimple size. High TPM concentrations yield crumpled colloids of various shapes. Additionally, we demonstrate that all particles can be used as templates for silica coating, resulting in electrostatically stabilized silica-coated hybrid colloids or silica shells with rough, smooth, dimpled or crumbled surface morphology.

2.1 Introduction

The surface morphology of colloidal particles plays a crucial role in many physical phenomena. For instance, theory predicts that the surface roughness of colloids is of major influence on the interactions between particles at liquid-liquid interfaces, due to nanoscopic deformations of the interface.[40–42] Recently, it has also been proposed that shear thickening behavior of colloidal suspensions is mainly governed by frictional forces.[43–45] Since frictional forces in dispersions depend on the surface morphology of the colloids, the viscoelastic properties of rough particle suspensions are expected to differ from suspensions of particles with a smooth surface.
Surface morphology can also be used as a tool to induce directional interactions between particles by tuning the strength of depletion forces through the site-specific overlap volume.[46] Using depletion interactions, rod-like, micellar or tubular structures can be assembled from anisotropic particles with smooth and a rough surface depending on whether particles with a platelet, snowman or mickey-mouse shape are employed.[29,32,46–48] Likewise, depletion forces enable the formation of lock-and-key structures from particles with an extreme degree of surface roughness, that is colloids with a dimpled surface.[11] These lock-and-key structures were assembled from dimpled particles and spheres that precisely fit the dimple and therefore are strongly attracted to it in the presence of a depletant.
Colloids with rough surfaces and dimples have been prepared by several methods. Dimpled and crumpled colloids can be obtained by inducing buckling of a rigid shell in core-shell structures, typically by dissolution or volume reduction of the core.[6,49] The rigidity and thickness of the shell and rate of deformation play a crucial role in the buckling process.[12,50–52]
Surface roughness can be achieved by depositing or growing a second type of smaller particle, for instance, inorganic nanoparticles[53], polystyrene[54] or silica spheres[55–57]. Rough polymer colloids, for example from poly(methylmethacrylate) or polystyrene, can be synthesized from linear seed particles by tuning the crosslink density, molecular weight of the polymer and type of apolar solvent during shell growth.[58–60] We recently found that hybrid colloids with a rough surface morphology can be achieved by swelling linear polystyrene colloids functionalized with poly(vinyl alcohol) (PVA) with a mixture of styrene and 3-(trimethoxysilyl)propyl methacrylate. During polymerization, secondary nucleated particles adsorbed onto the seed particles thereby yielding rough crosslinked polystyrene spheres, which we employed to create snowman particles with smooth and rough sides.[29]

In this paper, we focus on controlling the degree of surface roughness by employing the inhibitor hydroquinone (HQ) and the overall particle shape of

the polymer particles after crosslinking by systematically varying the synthesis parameters. We find that this approach not only is able to produce spherical particles with a tunable coverage with asperities, but also particles with a dimpled and crumpled morphology. Since our synthesis procedure is based on a dispersion polymerization method, we obtain monodisperse colloids in high yields. We show that by varying only two experimental parameters, that is the concentration of the polymerization inhibitor hydroquinone (HQ) in the aqueous phase and the volume ratio of styrene : 3-(trimethoxysilyl) propyl methacrylate (TPM) of the swelling solution, rough, semi-rough, smooth, dimpled and crumpled colloids with different material composition (polystyrene, polystyrene-TPM) can be obtained.
Furthermore, we demonstrate that silica coating can be achieved without loss of the particle morphology.[61–63] Silica colloids with a rough surface morphology are particularly interesting for their photoresponsive and superhydrophobic properties[53,64–67] but also as model dispersions for studying the hypothesized roughness induced shear thickening[43–45]. We provide evidence from zetapotential measurements that the silica coating changed the stabilization mechanism of the colloids from steric to electrostatic stabilization. Finally, we show that by removing the organic core hollow silica shells of different morphologies are obtained as well.

2.2 Experimental Methods

Materials

Styrene ($\geq$99%, contains 4-tert-butylcatechol as stabilizer), divinylbenzene (DVB, technical grade 55%), sodium dodecyl sulfate (SDS, $\geq$98.5%), hydroquinone (HQ, $\geq$99.5%), poly(vinyl alcohol) (PVA, Mw 72,000, 88% hydrolyzed), azobisisobutyronitril (AIBN, $\geq$98%), ammonium hydroxide(ACS reagent, 28.0–30.0% NH3 basis), Ethanol (EtOH, puriss., 96%) and 3-(Trimethoxysilyl)propyl methacrylate (TPM, 98%) were purchased from Sigma-Aldrich. Poly(vinylpyrrolidone) (PVP-40, K30, Mw 40,000) and Poly(vinylpyrrolidone) (PVP-360, K90, Mw 360,000) were purchased from Fluka, Germany. The tetraethyl orthosilicate (TEOS, 98%) was supplied by Acros Organics. All chemicals were used as received and all solutions were prepared from deionized water with 18.2MΩ·cm resistivity, using a Millipore Filtration System (Milli-Q® Gradient A10), unless stated otherwise

Methods

Linear polystryene synthesis Linear polystyrene spheres were synthesized by a dispersion polymerization method performed in ethanol.[68] Here, 20 g of PVP-40 was dissolved in 545 mL EtOH and 56 mL of water by shaking and ultrason-

ication. To the PVP-solution a swelling solution containing 554.26 mg of AIBN in 40 mL styrene was added under magnetic stirring. The reaction mixture was flushed with N_2(g) for 20 min and transferred to a preheated oil bath (75°C) where it was stirred magnetically at 320 rpm for 24h. A high yield of monodisperse linear polystyrene colloids of 910 $\pm$ 30 nm in diameter (as measured from scanning electron micrographs) was obtained.

Crosslinked polystryene synthesis Crosslinked polystyrene colloids with tunable surface morphology were obtained by swelling and crosslinking the PVP-functionalized linear polystyrene particles with a mixture of styrene and TPM including 2% wt AIBN and 1.5% v/v DVB. Before swelling, the linear seeds were washed twice with water, and subsequently they were transferred to a 1% wt PVA-solution. The final particle concentration of this dispersion was 15.1% wt. A mixture containing 4.4 mL of 1% wt PVA-solution in water, 0.88 mL of swelling solution and no, 0.0029 or 0.0185% wt HQ with respect to the total volume, was emulsified for 2 min at 8000 rpm followed by 10 s at 10,000 rpm using an IKA T18 Ultra Turrax emulsifier. Immediately after emulsification the emulsion was transferred to a 20 mL glass flask containing 1.32 g of linear polystyrene dispersion (15.1% wt). The flask was shaken gently by hand for 30-60 s, flushed with N_2(g) for 10 s, sealed with Teflon tape and placed on a tumbler covered in aluminium-foil to avoid UV-light exposure at 13 rpm. After 24h of swelling the flasks were transferred to a preheated oilbath (72°C) and rotated under a 45○ angle at 60 rpm for 24h. The following styrene:TPM v/v ratios were used: 100:0, 98:2, 94:6, 90:10, 70:30, 50:50, 30:70, 25:75, 20:80, 0:100.

Silica coating Rough and smooth colloids swollen with a styrene:TPM v/v ratio of 90:10, dimpled colloids swollen with a styrene:TPM ratio of 20:80 in the presence of 0.0183% wt HQ and crumpled colloids swollen with solely TPM were coated with silica according to a method developed by Graf et al.[61] To remove excess PVA molecules from the surface of the colloids the dispersions were washed twice with water. To coat the colloids with PVP, 1.5 mL of 10 g/L PVP-360 solution, prepared at most 2 days before use, was added to 1.5 mL of colloid dispersion (8% wt). The mixture was magnetically stirred at 250 rpm for 24h to assure adsorption of the PVP-molecules to the colloid surface. The colloids were washed once to remove excess PVP and redispersed in an ethanonl with 4.2% v/v ammonia solution by ultrasonication for 10 min. This was followed by the addition of 900 μL of TEOS in 5-10 s under vigorous magnetic stirring at 400 rpm. The reaction mixture was stirred for 18-24h and finally washed with ethanol or water to remove excess reaction components.

Silica shell formation by decompostion of organic components To obtain silica shells the silica coated colloids were heated for 5h at 450°C in a Nabertherm

B180 oven to decompose the organic polymer core.[69]

Imaging and analysis Bright field microscopy images of colloids swollen with a swelling solution containing 50:50 or 0:100 v/v styrene:TPM were acquired using a Nikon Eclipse Ti microscope with an A1R confocal scan head with a 100x oil immersion objective (NA = 1.4). The polymerized hybrid colloids were imaged using a FEI nanoSEM scanning electron microscope (SEM) at 15 kV and a JEOL JEM-1010 transmission electron microscope at 80 kV. The average diameter of the particles was determined by measuring the circumference of 50-200 particles in the SEM micrographs using ImageJ. For the diameter of the rough and semi-rough colloids the circumference of the spheres without the protruding part of the asperities was measured. The degree of roughness was determined by counting the number of small asperities positioned on the visible hemisphere of 18 representative particles per sample. Zetapotential measurements were performed using a Malvern Zetasizer Nano ZS.

2.3 Results and Discussion

2.3.1 Synthetic approach

To elucidate the formation of the surface roughness during swelling and crosslinking, we performed a systematic set of experiments where linear polystyrene colloids were swollen with several styrene:TPM v/v ratios. The linear polystyrene colloids were prepared by a dispersion polymerization yielding sterically stabilized particles 910 $\pm$ 30 nm in diameter. These colloids were swollen with a constant volume of a monomer mixture, which consisted of styrene and TPM at volume ratios ranging from 0:100 to 100:0. To the swelling solution 1.5% v/v divinylbenzene (DVB) was added as a crosslinking agent. The swelling solution was emulsified in an aqueous 1% wt poly(vinyl alcohol) (PVA) solution, before it was added to the linear seed dispersion. After swelling for 24h, we polymerized the particles by the decomposition of the radical initiator AIBN at elevated temperature and analyzed the surface morphologies of the resulting micron-sized hybrid polystyrene-TPM colloids using SEM. It was previously observed, that the surface roughness should originate from the adsorption of secondary nucleated particles during the polymerization step since the size of the asperities on the rough particles was found to be equal to the size of non-adsorbed secondary particles. Therefore, we expected that controlling the nucleation of polymers in the aqueous phase should affect the degree of surface roughness of the resulting particles. We achieved this control by the introduction of an additional component, the aromatic compound HQ, during synthesis. HQ suppresses the polymerization of monomers in the aqueous phase and thus secondary nucleation.[70]

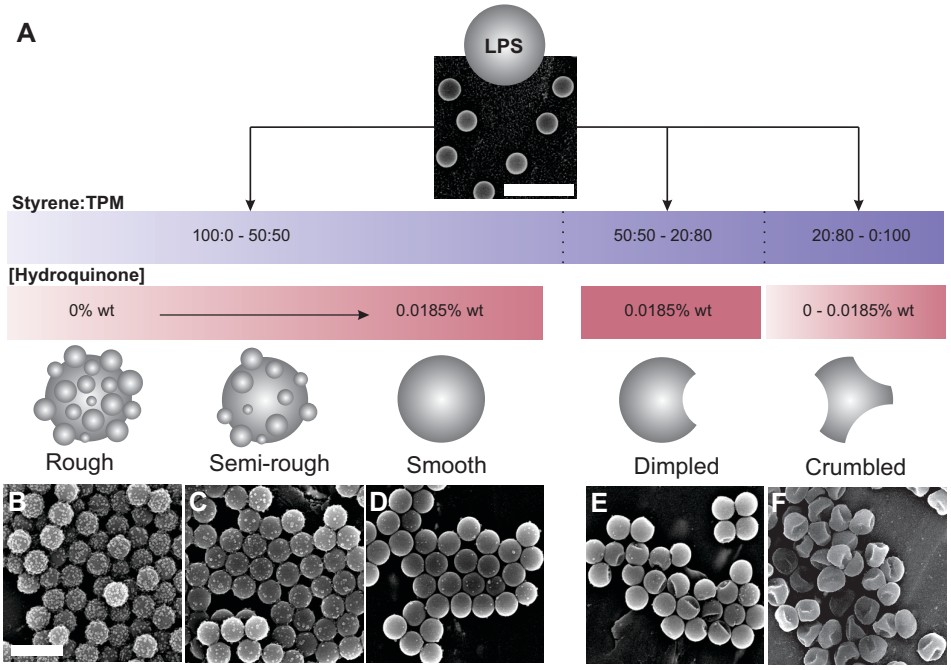


FIGURE 2.1: Synthetic approach to fabricate spherical colloids with tunable surface roughness and shape. The surface morphology is tuned by variation of the HQ concentration and styrene:TPM v/v ratio used for swelling linear polystyrene (LPS) particles. Scalebar is 3 μm. A) Spherical colloids are formed by swelling LPS particles with styrene:TPM v/v ratios between 100:0 and 50:50. By varying the HQ concentrations at these compositions, the surface morphology changes gradually from rough to smooth. Dimpled colloids are obtained after swelling with styrene:TPM v/v ratios of 50:50 to 20:80 at 0.0185% wt HQ. Crumpled colloids were observed at [TPM] $\geq$ 80% v/v. B-F) SEM micrographs of colloids with a rough (B), semi-rough (C) and smooth (D) surface morphology formed by swelling LPS particles with a 90:10 styrene:TPM v/v ratio with no, 0.0029 and 0.0185% wt HQ, respectively. Single-dimpled colloids (E) and crumpled colloids (F) were obtained by swelling with 50% v/v TPM (E, 0.0185% wt HQ) and 100% v/v TPM (F, no HQ), respectively.

Indeed, in the absence of HQ we readily obtained rough spherical colloidal particles for a wide range of styrene:TPM v/v ratios from 100:0 to 50:50, see Figure 2.1A and 2.1B. However, when we introduced increasing concentrations of HQ during swelling, the degree of surface roughness decreased, yielding a semi-rough (Figure 2.1C) and smooth (Figure 2.1D) surface morphology at 0.0029% wt and 0.0185% wt HQ, respectively. Thus, the presence of the inhibitor suppresses

the formation and adsorption of secondary particles during polymerization and thereby enables control over the surface roughness.
Surprisingly, when the TPM concentration ([TPM]) in the swelling solution was increased to $\geq$ 50% v/v, anisotropic particle shapes were formed. At intermediate styrene:TPM v/v ratios of 50:50 to 20:80 and 0.0185% wt HQ, we obtained smooth colloids with a single dimple (Figure 2.1E). At high TPM concentrations $\geq$ 80% v/v, crumpled colloids of various shapes were observed, of which one is shown in Figure 2.1F. The TPM concentration therefore influences the overall particle shape.
Thus, the swelling-based synthesis approach allows the fabrication of hybrid polystyrene-TPM colloids with tunable surface morphology by controlling the TPM and HQ concentrations. Figure 2.1 schematically summarizes the conditions that lead to the different morphologies, ranging from spheres with controllable roughness to dimpled and crumbled particles. In the following sections, we will quantify these morphologies in more detail for each of the three regimes and discuss the role of TPM and HQ.

2.3.2 Spherical colloids with tunable surface roughness

We explored the effect of the TPM concentration by systematically varying the ratio of styrene and TPM during the swelling step. For TPM concentrations below 50% v/v of the monomer mixture, we always obtained spherical colloids (Figure 2.2A). In the absence of HQ, the surface of the spherical particles is rough through the adsorption of spherical particles with a diameter of 70-180 nm. Interestingly, these asperities become gradually more submersed into the particle surface with increasing TPM concentrations, see Figure 2.2B. While at styrene:TPM ratios of 100:0 to 90:10 the asperities are only slightly embedded in the particle, the asperities are submersed roughly halfway at volume ratios of 70:30 and 50:50.
To suppress the formation of these asperities and therefore the degree of roughness, HQ was added during swelling. In the presence of 0.0029% wt HQ polymerization of the monomer in the aqueous medium is partly suppressed, resulting in semi-rough particles (Figure 2.2A, middle column). Here, the number of asperities adsorbed on the surface of the swollen seed particles is drastically reduced compared to the rough particles formed in the absence of HQ. At 0.0185% wt HQ a smooth surface morphology was obtained, indicating that secondary nucleation is completely suppressed (Figure 2.2A right column). The particles shown in Figure 2.2A are representative of the respective batch of colloids obtained under these conditions. SEM images of a larger field of view of these batches can be found in Figure 2.3.
We quantified this observation of decreasing degree of roughness with increasing HQ concentration by measuring the average number of nanoparticles per surface area of the seed particles (Figure 2.2C). An average of 31 adsorbed asperities per

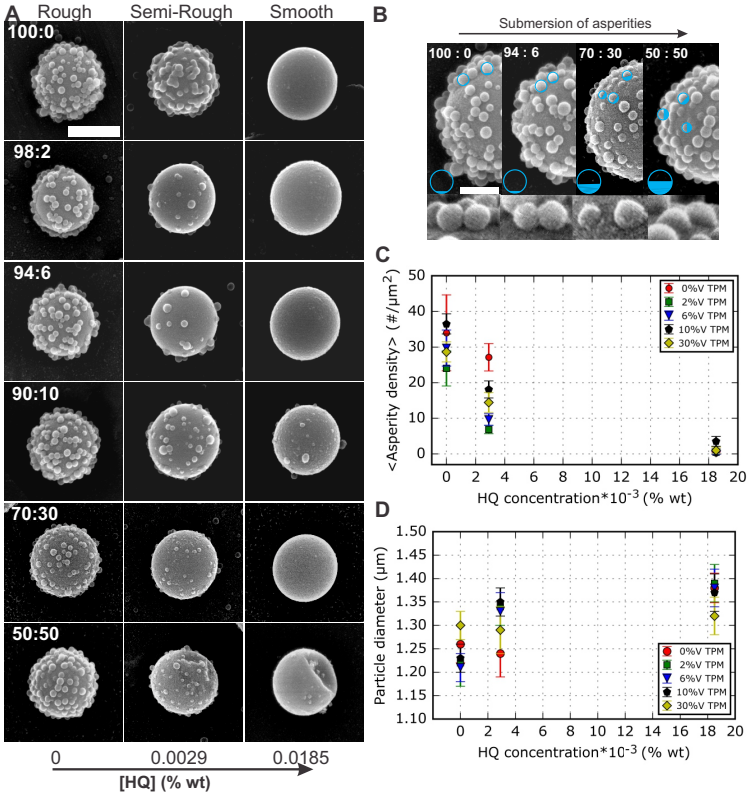


FIGURE 2.2: [HQ] and [TPM] dependent surface morphology at [TPM] $\leq$ 50% v/v. A) SEM micrographs of spheres obtained by swelling LPS colloids with styrene:TPM v/v ratios of 100:0, 98:2, 94:6, 90:10, 70:30 and 50:50. The particles were swollen in the absence of HQ (left column), in the presence of 0.0029% wt HQ (middle column) and with 0.0185% wt HQ (right column), resulting in rough, semi-rough and smooth particle surface morphologies, respectively. Scalebar is 1 μm. B) The submersion of asperities in the particle surface increases with the TPM concentration. The styrene:TPM v/v ratio is indicated on the upper left of the images. Scalebar is 500 nm. In the lower row, enlarged images of two submersed asperities of the respective samples are displayed. C) The average number of asperities per surface area decreases with the HQ concentration. D) The particle size increases slightly with the HQ concentration indicating that more monomer is absorbed by the seed particles.

μm^2 is measured for the rough particles, which decreases to 15 asperities per μm^2 for the semi-rough, and 1 for the smooth particles. The number of asperities per surface area also increases slightly with [TPM].
The part of monomer that is used for the formation of the asperities in the rough

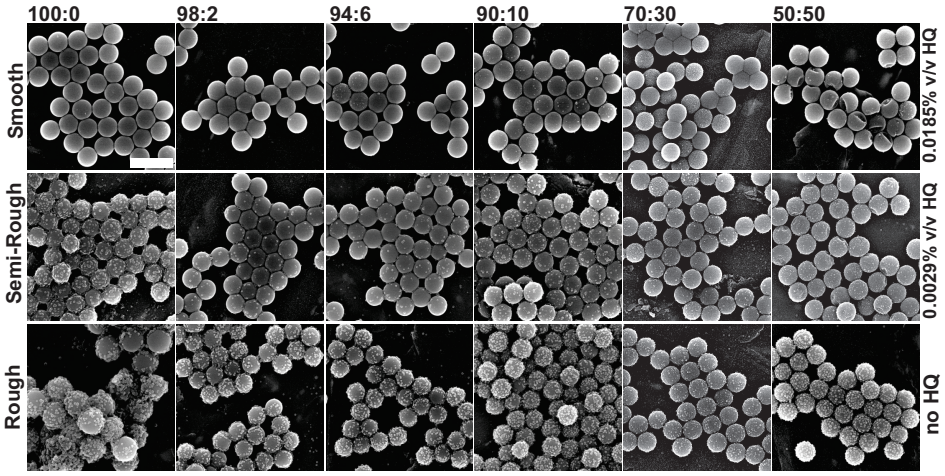


FIGURE 2.3: Spherical colloids with tunable surface roughness obtained by swelling linear polystyrene spheres with styrene:TPM ratios of 100:0 to 50:50. SEM micrographs of colloids synthesized at [TPM] $\leq$ 50% v/v corresponding to the batches of the single particles shown in Figure 2.2A. Scalebar is 3 μm.

spheres should in the presence of HQ be absorbed by the seed particles instead. As a consequence, the total absorbed monomer volume should increase, resulting in colloids of a larger size. To confirm this hypothesis, we measured the size of the rough, semi-rough and smooth particles using SEM micrographs. Here, the diameter of the colloids was measured by fitting a circle to the circumference of the colloids without taking the protruding part of the asperities into account. Figure 2.2D displays the average particle diameter as a function of the HQ concentration. On average, particles of 1.24 $\pm$ 0.04 μm in diameter are formed without HQ, which increases to 1.31 $\pm$ 0.04 μm in the presence of 0.0029% wt HQ and 1.37 $\pm$ 0.04 μm with 0.0185% wt HQ. While the particle diameter averaged over all TPM:styrene ratios clearly increases, for a given ratio this trend only becomes convincing for high HQ concentrations: all particle diameters increases significantly compared to the case when no hydroquinone was present except the sample containing 30% v/v TPM. These observations support our hypothesis that more monomer is adsorbed by the seed particles in the presence of HQ. Swelling linear polystyrene colloids with [TPM] $\leq$ 50% v/v results in particles with not only a different degree of surface roughness, but also different surface properties. Figure 2.2B already showed that submersion of the asperities increases with the TPM concentration. Besides the submersion of the asperities, we observed that the colloidal stability of these rough particles also depends on the [TPM]. When colloids were swollen solely with styrene, we frequently observed aggregates of

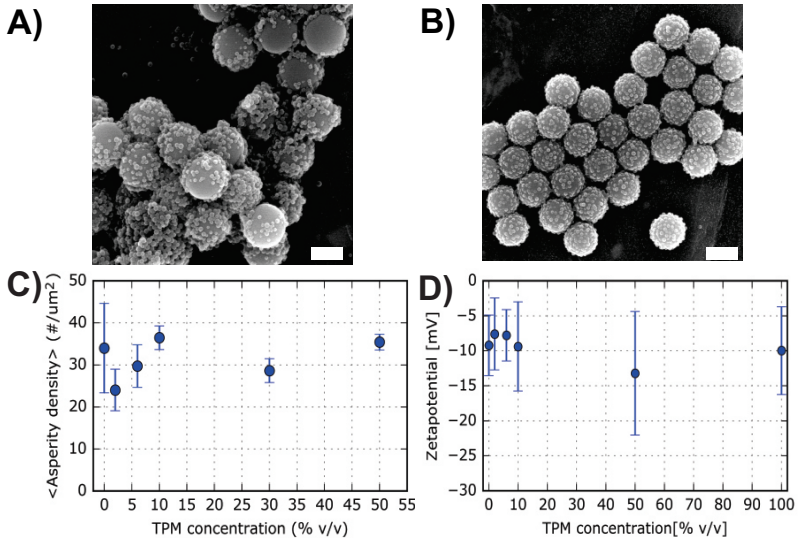


FIGURE 2.4: Surface roughness uniformity and stabilization for colloids swollen with [TPM] $\leq$ 50% v/v. Scalebar is 1 μm. A-B) SEM micrographs of LPS colloids swollen in the absence of HQ. A) Rough colloids obtained by swelling with 100% v/v styrene. The asperities on these colloids are non-uniformly distributed on the surface. (B) Rough stable colloids were formed by swelling with a styrene:TPM v/v ratio of 50:50. The particle surface is uniformly covered with asperities. C) The spread in the distribution of asperities on the surface of the particles decreases with the TPM concentration. D) Zetapotential values of polystyrene-TPM hybrid colloids, obtained by swelling with styrene:TPM ratios of 100:0 to 0:100. The zetapotential is not sufficient to contribute electrostatically to the stabilization of the colloids.

rough colloids in the SEM images, see Figure 2.4A. Furthermore, it can be seen that the asperities are non-uniformly distributed on the particle surface and that the nanoparticles seem to glue the colloids together. In contrast, when 2-50% v/v TPM was introduced in the swelling solution, stable rough particles with a uniform distribution of asperities were formed (Figure 2.4B and 2.4C).

A statistical analysis confirms that the roughness is non-uniformly distributed on the surface of colloids swollen with solely styrene: the number of asperities per surface area shows a large spread (Figure 2.4C). Already by introducing 2% v/v TPM during swelling the standard deviation of the asperity density decreases drastically, resulting in a more uniformly covered surface. The spread becomes even smaller for colloids swollen with 6-50% v/v TPM. This shows that the roughness uniformity is increased by the addition of TPM to the swelling so-

lution. Since the zetapotential of the colloids was measured to be on the order of -10 mV and independent of the [TPM], which is not sufficient to induce electrostatic stabilization, we can rule out that TPM led to an additional stabilization by charge (see Figure 2.4D). Therefore, we assume that the increased stabilization of the colloids originates mainly from the adsorbed PVA molecules on the particle surface. The adsorption of this polymer to the surface is dependent on the affinity of the PVA molecules to the particle material. Apparently, the PVA molecules have a higher affinity for TPM compared to polystyrene leading to an increase in stability in the presence of TPM. We also note that aggregation of the polystyrene colloids is not observed in the presence of HQ, pointing towards either an additional stabilization by HQ or that the secondary nucleated particles are causing this aggregation.

2.3.3 Buckling mechanism for colloids swollen with mainly TPM

Surprising results were obtained when the linear colloids were swollen with [TPM] $\geq$ 50% v/v. At these compositions, the seed particles remained spherical in shape during swelling (Figure 2.5A), but buckling occurred during polymerization leading to an anisotropy in the particle shape (Figure 2.5B). Buckling has been observed previously for hollow shell-like structures and core-shell particles.[6,50,58,71] Experiments and simulations have shown that for shell-buckling to occur the volume in the shell needs to decrease.[49,69] This can be achieved by removal of the core, or by decreasing the core volume due to changes in density or pressure. Another important parameter for shell-buckling is the ratio between the thickness of the shell h compared to the radius of the particle R.[12,72] Thinner shells from siloxanes and silica, where h/R is in the order of 0.3 and lower, are more elastic and therefore more prone to buckling due to the lack of mechanical strength.[70] For the final shape obtained after buckling the elastic properties of the shell are determinative, where elastic shells buckle into multi-dimpled colloids and less elastic shells buckle into a single dimple.[52] Besides the dimpled particles, shells can also completely collapse at high compression rates and large volume changes, resulting in crumpled particles.[51]

We believe that by swelling linear seeds with both styrene and TPM, we synthesized particles with a core-shell structure. We expect that while the styrene monomer is mostly absorbed by the linear seeds, TPM is more prone to be located at the surface of the particles since TPM is more hydrophilic compared to styrene.[73] While the styrene is a good solvent for the linear polymer in the core, TPM is known to form oligomer networks through a hydrolysis-condensation reaction, potentially creating a rigid shell at the surface, even before polymerization.[6] Upon polymerization, the volume of the swollen core will decrease with respect to the hardened shell due to the higher density of polystyrene (1.04 g/cm^3) and polymerized TPM (1.31 g/cm^3) compared to liquid styrene (0.90 g/cm^3) and

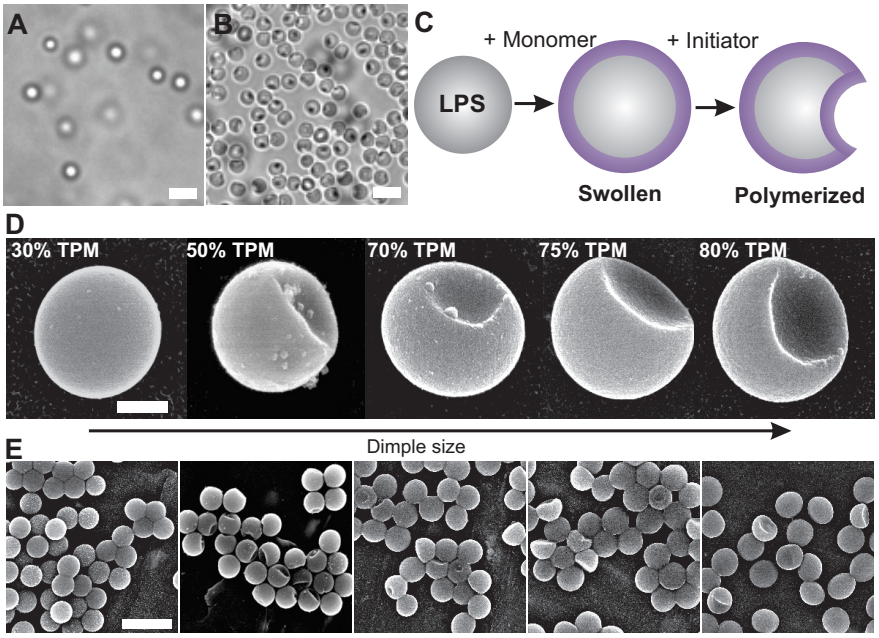


FIGURE 2.5: Dimpled colloids with tunable dimple size at [TPM] of 50-80% v/v. A) Bright field microscopy image of large spherical colloids obtained after swelling with a styrene:TPM v/v ratio of 20:80 for 23 h. B) Bright field microscopy image of dimpled colloids formed after polymerizing colloids swollen 50% v/v TPM. Scale bar in (A) and (B) is 2 μm. C) Illustration of the buckling process. First, a TPM shell is deposited on the particle during swelling. During polymerization, this shell buckles resulting in the formation of a dimple. D) Series of SEM micrographs of dimpled colloids obtained at TPM concentrations of 30-80% v/v in the presence of 0.0185% wt HQ. The dimple size increases with the TPM concentration. At [TPM] $\geq$ 75% v/v, besides dimpled, crumpled colloids were formed as well. Scale bar is 500 nm. E) SEM images of colloids in the batches corresponding to the single dimpled particles shown (D). Scalebar is 3 μm.

TPM (1.05 g/cm^3) present in the swollen state.[74,75] Since the polymerized particles were roughly 1.4 μm in diameter, which is an increase of 490 nm compared to the linear seed particles, we can estimate the decrease in volume upon polymerization to be at least 10%. This volume decrease may exert a sufficient elastic stress on the shell that can result in shell-buckling (Figure 2.5C).[12]
Indeed, for [TPM] below 50% v/v buckling was not observed (Figure 2.2A), suggesting that the [TPM] was too low to form a shell of sufficient thickness. At 50% v/v TPM, buckled colloids were only formed in the presence of HQ (Figure 2.2A). This can be understood from the observation that the monomer volume

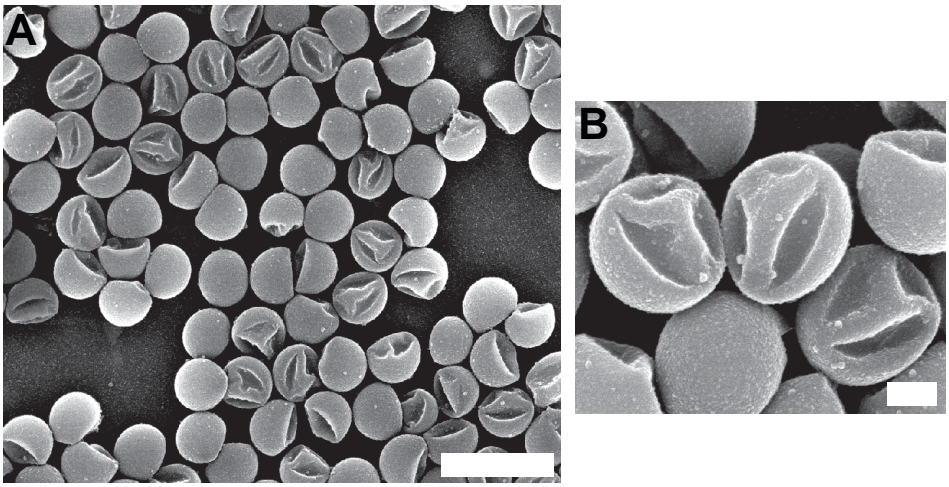


FIGURE 2.6: 'Smiley-faced' colloids. A) SEM micrograph of uniform colloids with three small dimples on one side of the sphere, obtained by swelling linear polystyrene colloids with 80% v/v TPM. Scalebar is 3 μm. B) SEM micrograph with a high magnification of three 'smiley-faced' colloids. Scalebar is 500 nm. Note: The image has won the image award of the Leiden Institute of Physics (Leiden University) in 2016.

absorbed by the seeds increases with the [HQ] (Figure 2.2D), resulting in an increase in shell thickness. At [TPM] of 50 - 80% v/v single dimpled colloids were obtained where the dimple size increased with the TPM concentration, see Figure 2.5D and 2.5E. The increase in dimple size implies a larger volume decrease upon polymerization[12,51], caused by the gradually bigger density difference between the polymerized and the swollen colloid. At [TPM] $\geq$ 75% v/v some crumpled colloids were observed as well and in a rare case, smiley-shaped colloids were obtained, where three small dimples were formed on one side of the sphere instead of one large dimple, see Figure 2.6. At even higher TPM concentrations the volume decrease during polymerization was sufficiently large to always result in the formation of crumbled colloids. These observations indicate that swelling with a mixture of styrene and TPM leads to the formation of a core-shell structure in the particles. At sufficient shell-thicknesses, the shell can buckle or crumple during polymerization if the core volume decreases strongly by the density increase.

2.3.4 Crumpled colloids of various shapes

At high TPM concentrations $\geq$ 80% v/v, we found anisotropic, crumpled shapes after polymerization. In the absence of HQ, deformed colloids with a rough surface morphology were obtained at 80% v/v TPM (Figure 2.7A). This adsorption

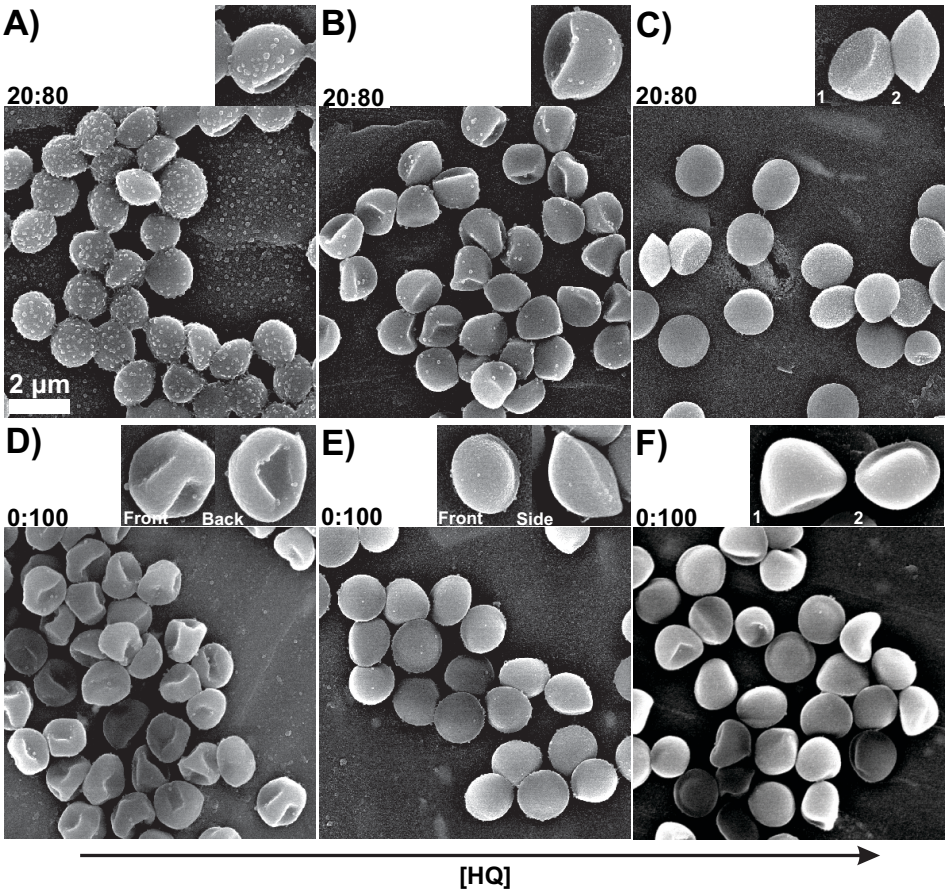


FIGURE 2.7: Crumpled colloids of various shapes at [TPM] $\geq$ 50%. SEM micrographs of crumpled colloids formed by swelling LPS colloids with a styrene:TPM v/v ratio of 20:80 or 0:100 at different HQ concentration. The enlarged images of the particle above the larger field of view is the predominant shape observed in the corresponding sample. A-C) Particles formed by swelling with 20:80 v/v styrene:TPM. A) Non-spherical deformed colloids obtained in the absence of HQ. Some asperities are adsorbed on the surface. B) Highly asymmetric shapes with several dents acquired in the presence of 0.0029% wt HQ. C) UFO-shaped and dimpled colloids are formed at 0.0185% wt HQ. D-F) Particles formed by swelling with 100% v/v TPM. D) Non-spherical colloids with three distinct dents without asperities at the surface formed in the absence of HQ. E) UFO-shaped particles with a rim in the middle, obtained at 0.0029% wt HQ. At even higher [HQ], 0.0185% wt, colloids crumpled asymmetrically (F).

of secondary particles on the surface is almost completely inhibited in the presence of HQ, resulting in particles of different shapes. An asymmetrical shape with two or more non-spherical dents was formed at 0.0029% wt HQ (Figure 2.7B) and as discussed in the previous section, dimpled and UFO-shaped colloids are found at 0.0185% wt HQ (Figure 2.7C). Dented colloids were also formed by swelling solely with TPM in the absence of HQ, see Figure 2.7D. Here, uniform shapes with two or more dents, similar to the shapes obtained at 80% v/v TPM and 0.0029% wt HQ, were observed. In the presence of HQ a rim is formed resulting in UFO-shaped colloids (Figure 2.7E and 2.7F). This rim formation was observed previously in simulations, where the UFO-shaped colloids were referred to as symmetrically crumpled particles.[12] Remarkably, when solely TPM is used for swelling, no nanoparticles adsorbed on the particle surface (Figure 2.7E-F), in line with the observation that the asperities become gradually more submersed in the particles with increasing TPM concentration (Figure 2.2B). Therefore, one would expect the same colloidal shape at all HQ concentrations. However, while in all three cases (no, 0.0029% and 0.0185% wt HQ) crumpled colloids were obtained, the crumpled shapes differ. We speculate that HQ not only suppresses the formation of secondary nuclei in solution, but also affects the formation of the TPM oligomer network and thus the elastic properties of the shell. Since shell-buckling is highly dependent on the elastic properties of the shell, different shapes were formed.[52,72] The final shape of the buckled colloids is therefore dependent on both the HQ and the TPM concentration.

2.3.5 Silica coated colloids with rough, smooth, dimpled and crumpled surface morphology

The hybrid polystyrene-TPM colloids obtained with our method are sterically stabilized by PVA. To obtain electrostatically stabilized rough, smooth and dimpled colloids we coated the particles with silica. Silica colloids are known to exhibit hard-sphere behavior which is crucial for studying for example the role of frictional forces in shear thickening suspensions.[43,45] Besides, suspensions of rough silica colloids can be used to tune wetting properties to achieve superhydrophobicity.[56,57] By coating the polystyrene-TPM hybrids with silica, colloids with the surface properties of silica are formed, but with the core properties of polystyrene-TPM. Depending on the application these coated particles can be favoured over solid silica particles because of their relatively low density and the possibility to remove the core.[69]

To improve the adhesion of silica on the colloids, we partly replaced the PVA molecules by poly(vinyl pyrrolidone) (PVP). We achieved the formation of a silica layer by the addition of tetraethyl orthosilicate (TEOS) under basic media conditions.[61] Silica colloids with a rough and smooth surface morphology were obtained using polystyrene-TPM colloids formed by swelling with a styrene:TPM

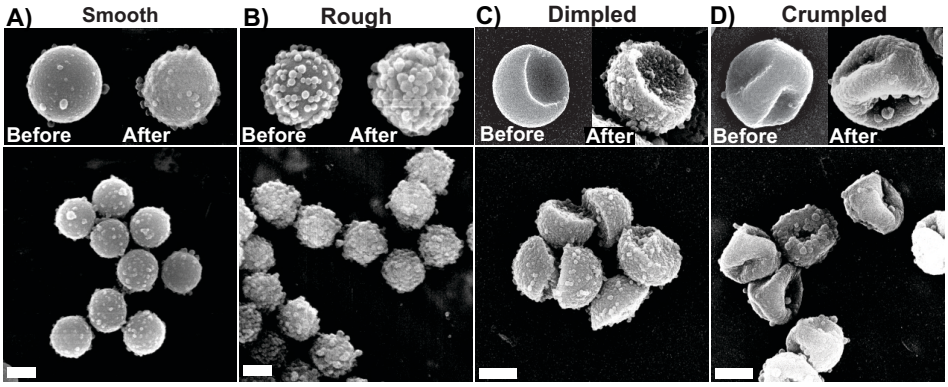
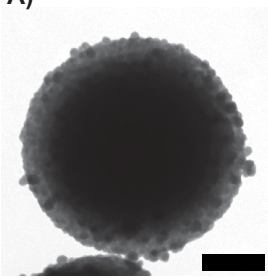


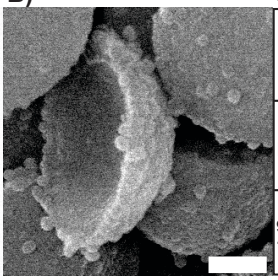
FIGURE 2.8: SEM micrographs of silica coated polystyrene-TPM hybrid colloids of various morphologies. In all cases the morphology of the colloids was preserved during silica coating. The surface roughness increased slightly. Scalebar is 1 μm. The enlarged images of the particles above the larger field of view show single particles before and after silica coating. A) Colloids with a smooth surface morphology, obtained by swelling with a 90:10 styrene:TPM v/v ratio in the presence of 0.0185% wt HQ, coated with silica. B) Colloids with a rough surface morphology formed by swelling with 90:10 v/v styrene:TPM and coated with silica. C) Single-dimpled colloids obtained by swelling with 80% v/v TPM in the presence of 0.0185% wt HQ, coated with silica. D) Crumpled colloids made by swelling solely with TPM and coated with silica.

ratio of 90:10 in the absence and presence of 0.0185% wt HQ, respectively. After coating, the initial surface morphology was mostly preserved, as can be seen in Figure 2.8A and 2.8B. From SEM images before and after coating it can be concluded that the surface of the initially smooth hybrid particles remained relatively smooth (Figure 2.8A), while for the polystyrene-TPM colloids with asperities the surface roughness increased during the silica coating. Multiple washing steps showed that the silica nanoparticles were permanently attached to the colloids.
Besides the rough and smooth particles, we also achieved a silica coating on the dimpled colloids (prepared by swelling with 80% v/v TPM in the presence of 0.0185% wt HQ) and crumpled colloids (prepared by swelling with 100% v/v TPM without HQ). Again, in both cases the shape of the coated colloids was similar to the original particles. In Figure 2.8C and 2.8D the silica coated dimpled and crumpled colloids are shown, respectively. From the analysis of TEM and SEM images we could determine the shell thickness to be on the order of 100 nm, see Figure 2.9. The shell consisted of small silica nanoparticles connected by a matrix of silica (Figure 2.9A and 2.9B). The zetapotential of the silica-coated colloids was measured to be on the order of -40 mV, whereas -10 mV was measured for the hybrid seed particles (see Figure 2.9C and 2.4D). This indicates that whereas the initial colloids were solely sterically stabilized by the PVA coating, the silica

A)



B)



C)

Zetapotential / Particle composition	Without silica [mV]	Silica coated [mV]
Polystyrene	-9.21 ± 4.32	-38.62 ± 7.61
90% Polystyrene 10% TPM	-9.38 ± 6.36	-42.54 ± 9.50

FIGURE 2.9: Properties of the silica coated colloids. A) TEM image of hybrid colloids swollen with 80% v/v TPM coated with silica. A clear distinction between the black inner organic core and the grey silica shell is observed. The shell thickness is in the order of 100 nm. B) SEM image of a broken silica shell of a 20:80 silica coated colloid. The surface morphology inside the shell is smooth indicating that the silica nanoparticles are connected by a silica matrix. C) Zetapotential measurements of polystyrene and polystyrene-TPM colloids before and after silica coating. The silica layer drastically decreases the zetapotential of the colloids providing electrostatic stabilization.

coated colloids are primarily electrostatically stabilized. These silica-coated electrostatically stabilized colloids are specifically interesting to study shear thickening behavior, superhydrophobicity and viscoelastic properties.[43,45,55,65,67]

2.3.6 Hollow silica shells

Finally, we demonstrate that hollow silica shells of various morphologies can be obtained by removal of the organic core by thermal decomposition at 450°C for 5 hours. After this treatment smooth polystyrene:TPM (90:10) spheres without silica were almost completely decomposed, see Figure 2.10A. The remnants is likely silica stemming from the TPM. For the same spheres coated with silica, hollow shells remained (Figure 2.10B). A hollow shell was obtained, indicating that the organic core was completely removed. Surprisingly, although some of the morphologies seem mechanically unstable, the majority of the shells stayed intact independent of particle shape (Figure 2.10B-E). The number of broken shells observed with electron microscopy seemed to decrease when more TPM was present during swelling. Since TPM is an alkoxysilane, we expect some of the silica after decomposition to originate from the TPM. It is thus likely, that the thickness and therefore stability of these shell-structures is enhanced by silica stemming from the TPM. Shell breakage is less frequently observed for colloids with the organic core still present. We therefore believe that this is caused by shrinking of the porous silica shell into a more dense state due to drying at high temperature or by illumination of the electron beam.[76] These effects possibly also explain

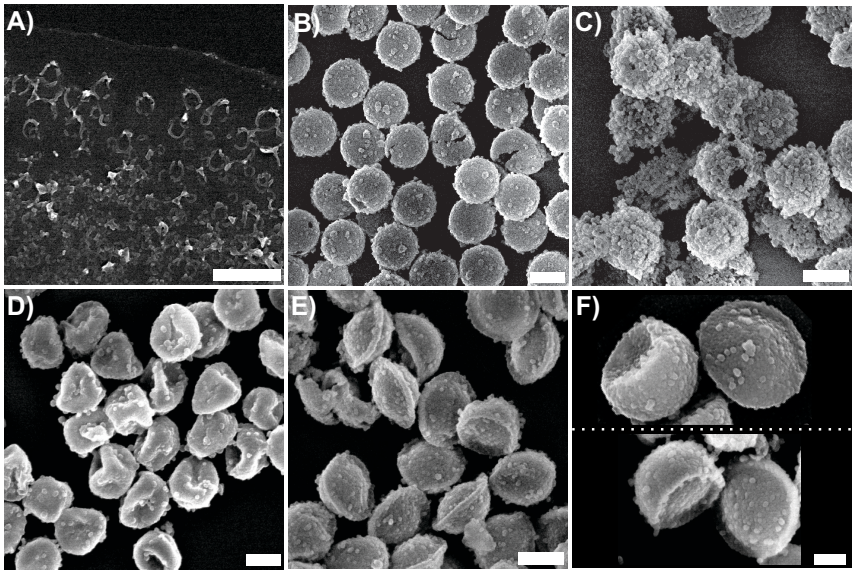


FIGURE 2.10: Silica shells after thermal decomposition of the organic compounds by heating at 450°C for 5 hours. SEM micrographs of remnants from smooth polystyrene:TPM (90:10) spheres without silica (A) and silica coated (B). Scalebar in (A) is 3 μm, in (B)-(E) 1 μm. Of silica coated rough, crumpled and dimpled particles the silica shell also remained and the shape stayed intact, see (C), (D) and (E), respectively. Although most shells stay intact some broken shells are observed as well. F) A dimpled and UFO-shaped silica colloid before (top) and after core removal (bottom). Scalebar is 500 nm.

the small differences in shape observed between the dimpled and UFO-shaped colloids (obtained by swelling with 80% v/v TPM) before and after core removal, see Figure 2.10F. Here, it can be seen that the characteristic of the shapes, such as the rim, are more pronounced after core removal. These silica shells of various morphologies can be exploited for their mechanical and cargo carrier properties.

2.4 Conclusions

We presented a robust and reliable synthesis method to obtain hybrid spherical, dimpled or crumpled colloids consisting of polystyrene, polystyrene-TPM or polystyrene-TPM-silica with tunable surface roughness. By swelling linear polystyrene colloids with a mixture of styrene and TPM not exceeding 50% v/v TPM, particles with a smooth, semi-rough and rough surface morphology could be synthesized by variation of the concentration of HQ. The asperity density on the particle surface decreases with increasing HQ concentration, since HQ in-

hibits the formation of secondary particles during polymerization. The size of the particles increases with the HQ concentration as well, indicating that a larger monomer volume was absorbed.
At TPM concentrations $\geq$ 50% v/v in the swelling solution buckling occurred upon polymerization of the swollen particles. We hypothesize that during swelling the TPM forms a shell on the surface of the swollen seed particle. Upon polymerization this shell buckles due to the high stress exerted on the shell by the volume decrease of the core, resulting in buckled colloids. At increasing TPM concentration the shell thickness increases, while the volume decreases further upon polymerization and therefore the degree of buckling increases. The final shape of the colloids depends on the thickness and elasticity of the shell and the change in volume upon polymerization.
At intermediate TPM concentrations of 50-80% v/v, single-dimpled colloids were formed with tunable dimple size. At even higher TPM concentrations, 80-100% v/v, we obtained crumpled colloids of various shapes, including three-dented and UFO-shaped colloids. We also showed that these hybrid colloids could be coated with a silica layer resulting in silica-coated polystyrene-TPM colloids with a rough, smooth, dimpled or crumpled surface morphology. By decomposition of the organic core hollow silica colloids were obtained as well. Since our approach is based on a standard dispersion polymerization method, large quantities of monodisperse colloids of various morphologies can be acquired. Our results show that by simply tuning two experimental parameters, the TPM and the HQ concentration during swelling, a wide variety of colloids with tunable surface roughness, dimple size and shape can be synthesized in a controlled fashion. These colloids are suitable for self-assembly[2,3,11] and to study the influence of surface morphology on physical properties of colloidal dispersions such as their viscoelastic behavior, wettability or stability.[43,45,55,65,67]

CHAPTER 3

COLLOIDAL RECYCLING: RECONFIGURATION OF RANDOM AGGREGATES INTO PATCHY PARTICLES

The results in this chapter have been published* and are reproduced with permission, copyright 2016 American Chemical Society.

* Vera Meester, Ruben W. Verweij, Casper van der Wel, Daniela J. Kraft,
Colloidal Recycling: Reconfiguration of Random Aggregates into Patchy Particles,
ACS Nano, 2016, 10(4), 4322-4329, DOI: 10.1021/acsnano.5b07901.

Abstract

The key ingredients to the successful bottom-up construction of complex materials are believed to be colloids with anisotropic shapes and directional, or patchy, interactions. We present an approach for creating such anisotropic patchy particles based on reconfiguring randomly shaped aggregates of colloidal spheres. While colloidal aggregates are often undesirable in colloidal dispersions due to their random shapes, we exploit them as a starting point to synthesize patchy particles. By a deliberate destabilization of the colloidal particles diffusion-limited aggregation is induced which partitions the particles into randomly shaped aggregates with controlled size distribution. We achieve a reconfiguration of the aggregates into uniform structures by swelling the polymer spheres with an apolar solvent. The swelling lowers the attractive van der Waals forces, lubricates the contact area between the spheres and drives the reorganization through minimization of the interfacial energy of the swollen polymer network. This reorganization process yields patchy particles whose patch arrangement is uniform for up to five patches. For particles with more patches, we find that the patch orientation depends on the degree of phase separation between the spheres and the monomer. This enables the synthesis of patchy particles with unprecedented patch arrangements. We demonstrate the broad applicability of this recycling strategy for making patchy particles as well as clusters of spheres by varying the swelling ratio, swelling solvent, surfactant concentration, and swelling time.

3.1 Introduction

Theoretical models and computer simulations have pointed out the tremendous potential of self-assembly for creating functional materials from the bottom up.[2,77–81] By carefully designing the building blocks' shapes, interactions, and stoichiometry, a wide range of unprecedented structures is expected to become accessible and with it, exciting new physics and concepts.[78,82,83] For example, simulations on particles with anisotropic shape showed that shape strongly affects the assembly through directional entropic forces.[84–86]Interaction directionality can also be obtained by defining specific patches of attraction or repulsion on the particle surface, which significantly alters the phase diagram and can lead to liquid states with vanishing density[87] or the coexistence of a high-density and a low-density liquid phase[88].

In experiments, a remarkable variety of novel structures has recently been observed even with low-complexity building blocks. Already particles with only one patch arrange into micellar[29,89–91] and tubular phases[47] and can form addressable and actuatable linear structures, such as ribbons and rings.[92–97] Particles with two patches on opposing ends assemble into a Kagome lattice[98], because entropy mechanically stabilizes the open lattice structure. With increasing building block complexity even richer assembly dynamics and equilibrium structures are expected. Hierarchical assembly, for instance, was demonstrated by using particles with two patches of different sizes, which assembled into networks of clusters.[99] However, there is a shortage in synthetic methods to fabricate suitable, more complex colloidal building blocks. The most important impeding factors are the limitations with respect to the particle material, the yield, and the obtainable particle complexity.[100]

Strategies based on 2D functionalization schemes such as angle-dependent vapour deposition or contact printing have an inherently low yield of patchy particles and can only be used to fabricate particles with very few patches and patch locations.[101] Bulk strategies for synthesizing anisotropic and patchy particles can achieve high yields but are limited to certain materials and particle properties.

We here present a bulk strategy for fabricating patchy particles based on the reconfiguration of randomly aggregated spheres. The reconfiguration is made possible by depositing droplets in the bond area after swelling with an apolar solvent. Surface tension and geometric constraints determine the shapes of the final patchy particles. We show that our method is able to create particles with chemical differences between the patches and the particle body. Our strategy can employ charge-stabilized polymer spheres for fabricating patchy particles with anisotropic charge distribution, which may be used in self-assembly directed by Coulomb forces or in demixing binary solvents where the wetting properties of the solvent fluctuations are determined by the charge density.[102,103] This colloidal recycling approach opens up a pathway to produce patchy particles in high yields

upon improving the control over the size distribution of the seed aggregates.

3.2 Experimental Methods

Materials

Styrene ($\geq$99%, contains 4-tert-butylcatechol as stabilizer) was obtained from Sigma Aldrich and used after passing through an inhibitor remover column (Sigma Aldrich). Divinylbenzene (DVB, technical grade 55%), sodium dodecyl sulfate (SDS, $\geq$98.5%), hydroquinone (HQ, $\geq$99.5%), poly(vinyl alcohol)(PVA, Mw 13,000–23,000, 98% hydrolysed), methylmethacrylate (MM, 99%, contains $\leq$30 ppm mono ethyl hydroquinone as inhibitor), ethylene glycol dimethacrylate(EGDM, 98%, contains 90-110 ppm mono ethyl hydroquinone as inhibitor) and azobisisobutyronitril (AIBN, $\geq$98%) were purchased from Sigma Aldrich and used as received. Potassium chloride (>99%, p.a.) and methacrylic acid(MA, 99.5%, extra pure, stabilized) were obtained from Acros Organics. The potassium peroxydisulfate ($\geq$99.0%, p.a.) and the poly(vinyl pyrrolidone) (PVP, K30, Mw 40,000) were purchased from Fluka, Germany. All solutions were prepared from deionized water with 18.2MΩ resistivity, using a Millipore Filtration System (Milli-Q® Gradient A10), unless stated otherwise. RITC-dyed polystyrene colloids crosslinked with 5% divinylbenzene and with a diameter of 1.06μm (polydispersity 5.3%) were purchased from Magsphere Inc.

Methods

Carboxylic acid functionalized particle synthesis Linear polystyrene spheres were synthesized by a single step surfactant free emulsion polymerization.[104] The obtained carboxylic acid functionalized colloids were 1.05 $\pm$ 0.02 µm in diameter (as measured from SEM micrographs) and had a zeta potential ε of -60 mV as measured by a Malvern Zetasizer Nano ZS. The colloids were filtered with glass wool and washed 3 times with Millipore filtered water at 2000g for 90 minutes. The colloids were stored in water.
To crosslink the particles, 1.7 mL swelling solution containing styrene, 2% w/w AIBN and 1.5% v/v DVB was added to 2.5 mL linear polystyrene spheres (12.4% w/w). To this mixture 10 mL SDS (0.5% w/v) and 1.0 mL HQ (0.03% w/w) dissolved in water were added. The spheres were swollen for approximately 24 hours while tumbling at 20 rpm in the dark. The swollen colloids were polymerized for 24 hours in a 70°C oil bath while rotating under an angle of 45° at 100 rpm. The colloids were washed three times and stored in water. The resulting carboxylic acid functionalized crosslinked spheres were 1.40 ± 0.06 μm in diameter (see Figure 3.1A)

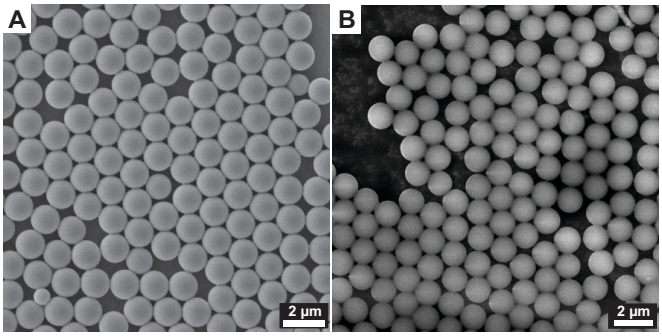


FIGURE 3.1: SEM micrographs of crosslinked polystyrene spheres synthesized by an emulsion polymerization procedure which were used as seed particles. A) Carboxylic acid functionalized spheres of 1.40 ± 0.06 μm in diameter. B) Sulfate functionalized spheres of 1.38 ± 0.03 μm in diameter.

Surfate functionalized particle synthesis Linear polystyrene spheres were synthesized by a surfactant free emulsion polymerization procedure. Here, a solution of 112.85 mg KPS in 112.5 mL water was flushed with nitrogen and heated to 70 C in an oil bath. Under magnetic stirring 22.5 mL of inhibitor-free styrene was quickly added and the reaction mixture was stirred for 24 h.
The resulting linear particles were crosslinked by adding a mixture of 2.6 mL swelling solution (styrene with 1.5% v/v DVB and 2% w/w AIBN), 2 mL of a 0.03% w/w hydroquinone solution and 23 mL of a 5% w/w PVA (Mw 13,000-23,000, 98% hydrolysed) to 5 mL of the obtained linear particle dispersion. The added mixture was emulsified at 8000 rpm for 2 min using an IKA T 18D Ultra Turrax homogenizer before it was quickly added to the linear particle dispersion. The reaction mixture was flushed with nitrogen and tumbled for 12h at 25 rpm to allow for swelling of the particles. Polymerization was performed in a 70°C oil bath for 24h while rotating at 60 rpm under an angle of 45°. The resulting sulfate functionalized crosslinked spheres were 1.38 ± 0.03 μm in diameter (see Figure 3.1B)

Formation of random aggregates Diffusion-limited aggregates of cross-linked polystyrene colloids were obtained using a salting-out quenching method.[105] Here, 200 µL of a 2 M potassium chloride solution was added to 200 µL of 2% w/w cross-linked polystyrene particles in a 40 mL graduated flask. The solution was gently swirled twice, and after an aggregation time, t_a of 1, 2, 4, or 10 min, the suspension was quenched with 30 mL water.

Formation of well-defined patchy particles To 5 mL of the random cluster dispersion various amounts (10-200 μL) of a 10% w/v SDS or PVP in water solution was added followed by a swelling solution consisting of styrene with 1% v/v DVB or 49:1 MM:MA with 1.5% v/v EGDM. We define the degree of swelling by the swelling ratio S, that is, the mass of monomer divided by the mass of the polystyrene colloids. We employed swelling ratios of 1 to 80. Immediately after the addition of the swelling solution the mixture was placed on a magnetic stirrer for 20-24 hours at 200 rpm. After swelling, the clusters were transferred to a preheated 80°C oil bath and magnetically stirred at 270 rpm. After 10–120 min a solution of 0.4 mg AIBN in 20 μL monomer was added and the particles were polymerized for 20-24 hours. The clusters were washed three times and stored in water. Additionally, carboxylic acid functionalized polystyrene seeds swollen with 49:1 MM:MA with 1.5% v/v EGDM were selectively functionalized at the polystyrene surface areas with Neutravidin according to a method described by van der Wel *et al.*[106], where the carboxylic acid groups were used as reactive sites.

Formation of colloidal clusters To 5 mL of the randomly shaped cluster dispersion, various amounts (10-200 μL) of a 10% w/v SDS in water solution were added followed by toluene of swelling ratios S=2-16. Immediately after the addition of toluene the mixture was placed on a magnetic stirrer for 20-24 hours. After swelling, the toluene was evaporated for 4-5 hours in a preheated 80°C oil bath under magnetic stirring at 270 rpm. The obtained colloidal clusters were washed three times with water.

Imaging and analysis The randomly shaped clusters formed by salting-out were imaged using a Nikon Eclipse Ti microscope with an A1R confocal scan head with a 100x oil immersion objective (NA = 1.4). The polymerized particles and clusters were imaged using a FEI nanoSEM 200 scanning electron microscope at 15 kV. The size distribution of the random aggregates and the patchy particles after polymerization was determined by statistical analysis of at least 200 clusters using the cell counter plugin in ImageJ.

3.3 Results and Discussion

3.3.1 Assembly strategy

Stability against aggregation due to van der Waals forces is arguably the most essential requirement for colloidal particles. The first step in our synthesis approach is therefore rather counterintuitive: we deliberately destabilize a colloidal dispersion. See Figure 3.2A. We reduce the colloidal stability of charge-stabilized, crosslinked polymer particles by either adding an excess amount of salt to reduce

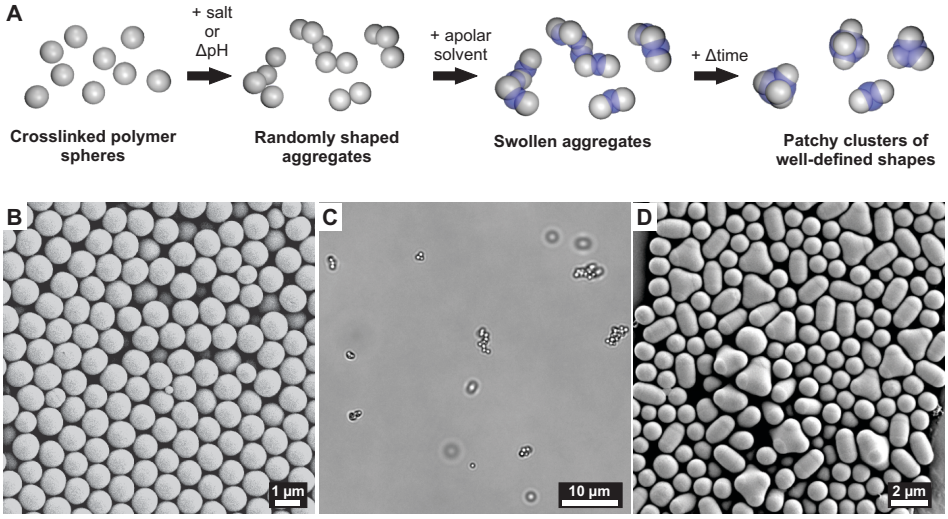


FIGURE 3.2: Colloidal recycling of random aggregates into patchy particles. (A) Schematic of the synthesis strategy. We obtain randomly shaped aggregates by destabilizing colloidal spheres, either by adding an excess amount of salt or by changing the pH to the isoelectric point. In the second step the aggregates are swollen with an apolar solvent. The apolar solvent lubricates the contact area between the spheres and reduces the attractive van der Waals forces such that the individual spheres can reconfigure into uniform patchy particles. (B) SEM micrograph of polystyrene spheres of 1.06 μm diameter with 5.3% polydispersity purchased from Magsphere Inc. (C) Bright-field microscopy image of randomly shaped aggregates obtained after increasing the salt concentration to 1.0 M potassium chloride for 2.5 min and followed by quenching with water. (D) SEM micrograph of the reconfigured and polymerized patchy particles obtained by swelling the aggregates with styrene and 1% v/v divinylbenzene at S=3.

the Debye-Hückel screening length or by adjusting the pH of the solution to the isoelectric point of the colloidal particles. The destabilization induces diffusion-limited aggregation of the colloids into small clusters[105,107], which can be brought to a halt by quenching with an excess amount of water. The resulting aggregates possess a random configuration that is not homogeneous for each cluster size as can be seen in Figure 3.2C. Here, polystyrene spheres of 1.06 μm diameter purchased from Magsphere Inc. (5% crosslink density), shown in Figure 3.2B, were aggregated by adjusting the salt concentration to 1.0M using potassium chloride. Similar random aggregates were obtained by aggregating carboxylic acid functionalized polystyrene spheres of 1.40 μm diameter (Figure 3.1A) by lowering the pH to 0 using hydrochloric acid or alternatively, increasing the salt concentration to 1.0 M (see Appendix Figure 3.8). To achieve reconfiguration, we swell the random aggregates with an apolar solvent. We define the added mass of ap-

olar solvent, $m_{solvent}$, divided by the polymer mass of the particles, $m_{polymer}$, as the swelling ratio S. The actual degree of swelling is strongly dependent on the crosslink density of the particles as well as the exact composition of particle and swelling solvent through the entropy of mixing between the polymer network and the swelling solvent.[108]

The swelling serves three purposes: firstly, it swells and softens the polymer spheres resulting in a larger contact area and partial phase separation between the apolar solvent and the polymer network.[4,7,24,109,110] This liquid-swollen polymer bridge enables particle rearrangement by lubricating the contact area between the spheres and smoothening out any surface inhomogeneity resulting from charges or roughness. The apolar liquid bridge also replaces the solvent between the polymer spheres in the area of closest contact. This change in the dielectric constant of the solvent medium affects the Hamaker constant and thus the van der Waals attraction, which binds the spheres in the randomly shaped aggregate. We can estimate the reduction of the van der Waals attraction by calculating the non-retarded Hamaker constants on the basis of Lifshitz Theory[26] for spheres fully immersed in the apolar solvent. For polystyrene spheres, the Hamaker constant reduces by a factor 600 when the aqueous medium is replaced by styrene, and by a factor 17 when replaced by toluene. The significantly lower van der Waals attraction together with the smoothing effect and the lubrication facilitates the rearrangement of the particles.

Secondly, the swelling imposes a driving mechanism to create uniform arrangements of the spheres: to minimize the interfacial energy between the apolar solvent and the water phase the spheres become close-packed. This surface tension driven rearrangement can be further enhanced by heating the dispersion to induce a larger degree of phase separation of the polymer spheres and the hydrophobic solvent, thereby creating droplets of the apolar swelling solvent at the contact points.[4,7,24,109–112] The interplay between minimization of interfacial area and the geometric constraint imposed by the spheres determines the final structures uniquely for small cluster sizes. For small clusters of N spheres we find the dimer for N=2, the triangle for N=3, the tetrahedron for N=4 and the triangular dipyramid for N=5 similar to existing droplet based cluster fabrication methods.[14,113] Finally, swelling with an apolar solvent allows for the fabrication of patchy particles when a monomer is chosen as swelling solvent. Upon heating the dispersion to 80°C, a phase separation occurs between the monomer and the polymer particles[4,16,110] creating well-defined patches that originate from the seed particles. The number of patches of a patchy particle therefore equals the number of spheres in the random cluster. The addition of a radical initiator such as azobisisobutyronitrile (AIBN) polymerizes the droplet and yields solid patchy particles. We note that the seed particles are not required to be stable in apolar solvents, and that our method for making patchy particles therefore can be applied to purely charge stabilized colloids as well.

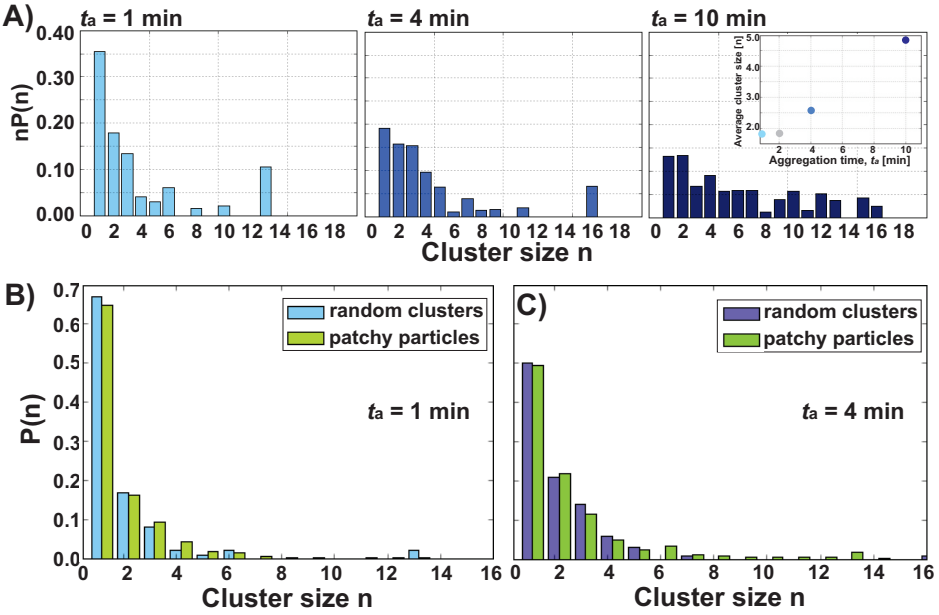


FIGURE 3.3: Tunable cluster size distribution. A) Size distribution of aggregates formed by the addition of salt to charge-stabilized colloids. The cluster size n increased with the aggregation time t_a. A linear relation between the average cluster size and the aggregation time is observed, which points to diffusion-limited aggregation. B) Probability $P(n)$ to find a cluster of n spheres for random aggregates and patchy particles made aggregating 1.06 μm polystyrene spheres for t_a = 1 min (B) and t_a = 4 min (C). The aggregates were subsequently swollen with styrene at S=7 to obtain patchy particles. The cluster size distributions of the clusters before and after swelling are in agreement.

To demonstrate the effect of swelling, we added a mixture of styrene and 1% v/v divinylbenzene (DVB) with S=3 to the salt-aggregated polystyrene spheres from Magsphere Inc. and allowed the clusters to change their configuration while stirring for a day. To prevent the particles from losing their shape during swelling, we employed crosslinked polymer spheres only. After polymerization with AIBN we imaged the obtained patchy particles using a scanning electron microscope(SEM), see Figure 3.2D. Clearly, all patchy particles of a given size share a uniform shape. For example, all random aggregates consisting of three spheres have turned into triangular clusters with three patches.

3.3.2 Tunable size distribution

By deliberately inducing colloidal aggregation, we can control the cluster size distribution of the random aggregates through an adjustment of the aggregation time, t_a. As expected for diffusion-limited aggregation, longer aggregation times linearly shift the distribution of the random clusters towards larger sizes[114], as shown in Figure 3.3A. The size distribution can furthermore be tuned by adjusting the particle volume fraction since the rate of rapid coagulation in the absence of a potential barrier is only limited by the volume fraction and particle size.[115,116] To confirm that indeed a reshaping of the random aggregates and not further aggregation is the underlying mechanism for the formation of the patchy particles, we compare the size distributions of the clusters before and after reshaping for t_a=1 and 4 minutes, see Figure 3.3B and 3.3C respectively. The size distributions of the random and patchy clusters agree very well, supporting the hypothesized reconfiguration mechanism.

3.3.3 Reconfiguration parameters

A successful reconfiguration of the spheres into patchy particles depends on the degree of swelling and the time allocated for rearrangement. In Figure 3.4A bright field images of the reconfiguration of a random aggregate of four polymer spheres of 1.06 μm diameter are displayed. The aggregate has been swollen for 20 minutes at S=7 with styrene. Once a sufficient degree of swelling is reached, the cluster changes its configuration from an open structure to a close-packed tetrahedron within several seconds. The spheres within the cluster still fluctuate around the equilibrium position in the tetrahedron structure until the swelling is completed. The polymerized patchy particles show that the final clusters have a fixed geometry.

At swelling ratios S>2, the reconfiguration of the random aggregates into uniform patchy particles of well-defined shapes occurs with high fidelity. Lower swelling ratios result in a lower lubrication of the contact area as well as a smaller driving force for rearrangement, similar to particle networks connected by a secondary fluid.[117] The reconfiguration of the insufficiently swollen spheres becomes either impossible or is significantly slowed down. For example, 1.40 μm diameter carboxylic acid functionalized polystyrene spheres made through a seeded-growth process show incomplete rearrangement for swelling ratios below S=2, as shown in Figure 3.4B, even after 24h swelling. At intermediate swelling ratios between S=2 and S=8 aggregates of the same colloidal particles reconfigure successfully into patchy particles, see Figure 3.5. A mixture of patchy particles of different sizes is obtained with well-defined structures at fixed cluster sizes (see Appendix Figure 3.9). The configuration of the resulting particles of a given cluster size is independent of the swelling ratio (see Appendix Figure 3.10 for SEM micrographs with systematic variation of S). At even higher swelling ratios, the col-

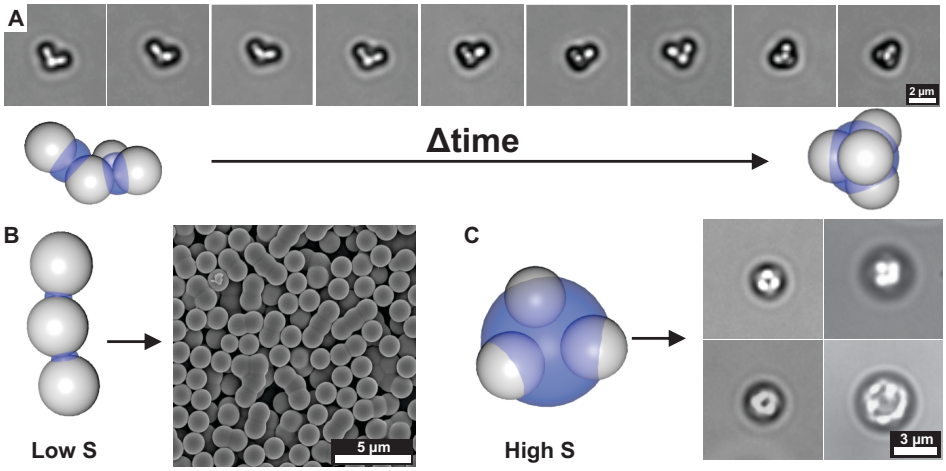


FIGURE 3.4: Reconfiguration of random aggregates into patchy particles. (A) Bright-field images of the reconfiguration process of an open random shape to a close-packed tetrahedron. The duration of the reorganization is 8 s. The aggregate consisted of four 1.06 μm in diameter polystyrene spheres and was swollen for 20 min with styrene at S=7. (B) Low swelling ratios S deposit insufficient solvent at the contact area and thus do not lead to reconfiguration. SEM micrographs of randomly shaped clusters of 1.40 μm carboxylic acid functionalized polystyrene spheres after swelling and polymerization with styrene at S=1. (C) At high swelling ratios, phase separation leads to the seed particles being adsorbed to a solvent droplet. Bright-field image of 1.06 μm cross-linked polystyrene spheres swollen with 49:1 MM:MA at S=80.

loidal particles reconfigure, but in the absence of additional stabilization by a surfactant aggregation of the clusters may occur (see Appendix Figure 3.11). The 1.06 μm polystyrene spheres (Figure 3.2B) swollen with 49:1 methylmethacrylate:methacrylic acid (MM:MA) at high swellingratios (S=80) spontaneously underwent a phase separation between the polymer particles and the apolar solvent and formed solvent droplets with the particles attached at the interface, that is, Pickering emulsions. See Figure 3.4C.

Allocating more time for rearrangement may compensate for a slow rearrangement of the spheres in the randomly shaped aggregates. For example, swelling 1.40 μm polystyrene particles at a swelling ratio S=8 for 3 hours yields non-uniform but swollen aggregates. After 23h rearrangement time, however, the spheres were able to optimize their position in the cluster and now form uniform patchy particles, see Appendix Figure 3.12.

Successful swelling relies on an efficient transport of monomer to the polymer spheres, which we enhance by adding a surfactant, 0.02–0.20% w/v SDS or polyvinylpyrrolidone (PVP), during swelling. The added surfactant also plays

a role in lowering the surface tension of the emerging droplets during phase separation and influences the wetting angle of the droplets with the polymer spheres and the water phase. Therefore, the surfactant concentration controls the patch size, as is shown in Appendix Figure 3.13. Finally, the surfactant may also adsorb onto the particle surface yielding additional stabilization of the particles by steric or ionic repulsion. This additional repulsion can lead to a re-stabilization of the individual spheres after the aggregation and thus to a disintegration of the clusters. We observed this effect for 1.38 μm sulfate functionalized polystyrene spheres in the presence of 0.4% w/v SDS, which resulted in snowman shaped particles only. See Appendix Figure 3.14.

3.3.4 Patchy particle configurations

The structures of the clusters resulting from reconfiguring the random aggregates are shown in Figure 3.5. We find that the spheres are closely packed and held together by the apolar solvent with which they were swollen. For polystyrene spheres crosslinked with 5% v/v DVB and swollen with styrene, we observe distinct patches on the particle surface that originate from the seed particles. The body of the patchy particle consists of the coalesced and polymerized styrene droplet. See Figure 3.5A for a schematic, where blue depicts the droplet body and white the spheres and Figure 3.5B for SEM micrographs. The arrangement of the spheres is determined by the constraining droplet. Therefore, the second moment of the mass distribution is minimized, resulting in arrangements in line with emulsion-based sphere packings.[14,113]
Surprisingly, when we swelled 1.40 μm carboxylic acid functionalized colloids with a lower crosslink density (1.5% v/v DVB) with styrene, MM:MA or toluene, other shapes in addition to the second moment minimizing ones are observed (see Figure 3.5D and Appendix Figure 3.8). For clusters up to N=5, again the cluster arrangements that minimize the second moment of the mass distribution are obtained, see Figure 3.5D. At N=6, however, we find that the polytetrahedron is strongly preferred over the minimal second moment arrangement found in droplet based clusters, the octahedron. For clusters consisting of N>6 spheres we found a variety of different compact configurations besides the minimal second moment arrangement (see Appendix Figure 3.15). In earlier experiments on clusters of purely attractive spheres it was found that the octahedron is favoured for long-range attractions, whereas the polytetrahedron is preferred for short-range interactions due to its larger rotational entropy.[13] Our experimental system features both short-range and long-range organizing principles: on the one hand, a significant degree of swelling and phase separation between the apolar liquid and the polymer spheres leads to droplets that coalesce and impose a cluster spanning droplet that confines and reorders the spheres, which therefore results in arrangements that minimize the second moment of the mass distribution. On the

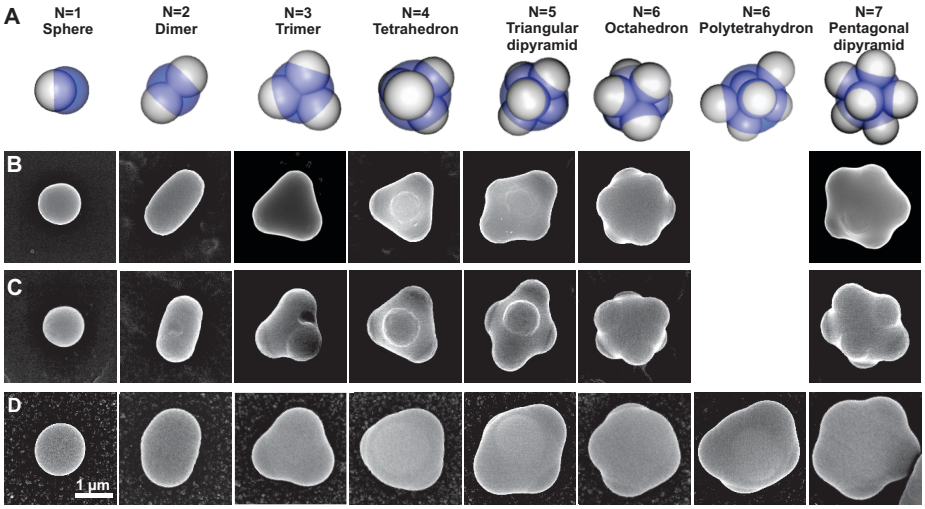


FIGURE 3.5: Reconfigured patchy particles and clusters. (A) Models of the patchy particles consisting of N=1-7 spheres. (B-D) SEM micrographs of polymerized reconfigured clusters. Patchy particles obtained from 1.06 μm polystyrene spheres (5% v/v cross-link density), purchased from Magsphere Inc. (Figure 3.2B), obtained after swelling random aggregates (B) with styrene at S=5 and (C) with 49:1 MM:MA at S=80. (D) Polymerized colloidal clusters of 1.40 μ carboxylic acid functionalized polystyrene spheres (1.5% v/v cross-link density), obtained after swelling with toluene at S=16

other hand, in the absence of a cluster-spanning droplet, the liquid bridges at the contact points only interact with their nearest neighbours. We therefore hypothesize, that the clusters of particles with a low crosslink density do not feature a cluster-spanning droplet resulting in cluster shapes preferred by entropy.[13,14] Indeed, it is known that polymer particles with a lower crosslink density also show a smaller degree of phase separation.[4] In addition, these particles are made by a seeded growth procedure where not all polymers are covalently linked to the polymer network.[4,118] Swelling the particles with a good solvent leads to migration of some polymer chains to the centre, see Figure 3.5D, possibly lowering the interfacial tension of the apolar solvent and the water phase. Excitingly, the resulting patchy particles therefore have anisotropic shapes and patch arrangements that have not been accessible by other fabrication methods until now.

The simplicity of this reconfiguration method allows it to be applied to a variety of polymer colloids and swelling solvents. The patches can be rendered functional by designing a chemical of physical difference between the polymer spheres and the swelling solvent. We demonstrate this flexibility by employing a 49:1 mixture of MM:MA as swelling monomer of the 1.06 μm diameter, 5%

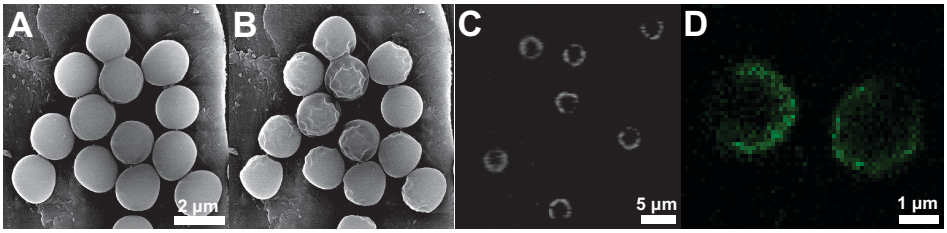


FIGURE 3.6: Functionalization of patchy particles. A-B) SEM micrographs of Janus particles with a polystyrene and a pMMA side. After severe exposure of the electron beam the pMMA crumpled (B). Confocal microscopy images of partly fluorescent particles, where the fluorescence stems from the polystyrene side of the particle originating from C) fluorescein amine and D) Neutravidin, by reaction with the carboxylic acid groups on the polystryrene surface.

crosslinked polystyrene spheres. After swelling, reconfiguration, and polymerization we obtain patchy particles possessing a pMMA body and polystyrene patches, as shown in Figure 3.5C. The resulting patchy particles have shapes that minimize the second moment of the mass distribution and show particle spanning droplets. The pMMA and polystyrene areas on the particles could be distinguished by SEM since the electron beam induced crumpling of the pMMA, see Figure 3.6A and 3.6B. Addition of fluorescein amine to the particles resulted in fluorescent polystyrene and non-fluorescent pMMA (Figure 3.6C). This indicated that the carboxilic acid groups of the polystyrene seed particles reacted with the amine groups and did not migrate on the particle surface with the pMMA during phase separation. The carboxylic acid groups could also be replaced by Neutravidin (Figure 3.6D), which can easily be used to selectively bind to biotinylated surfaces such as membranes.[106,119]
Making use of a volatile swelling solvent, toluene, we can also obtain compact clusters of spheres without patches. After heating and reconfiguration, we selectively evaporate the toluene from the swollen clusters by stirring the open sample flask in an 80°C oil bath. The resulting particles are therefore not patchy particles, but clusters of spheres, although we often find that some of the non-crosslinked polymers migrate towards the centre of the cluster.[109] When employing aggregates of the Magsphere colloids, we find clusters that minimize the second moment of the mass distribution similar to the styrene and MM:MA swollen clusters (see Appendix Figure 3.16).

In all cases, a mixture of clusters or patchy particles with well-defined geometries and low polydispersity is obtained. To quantify the uniformity of the particle arrangements, we measured the polydispersity of the distance of the seed spheres in a polymerized trimer patchy particles made from aggregates of 1.06

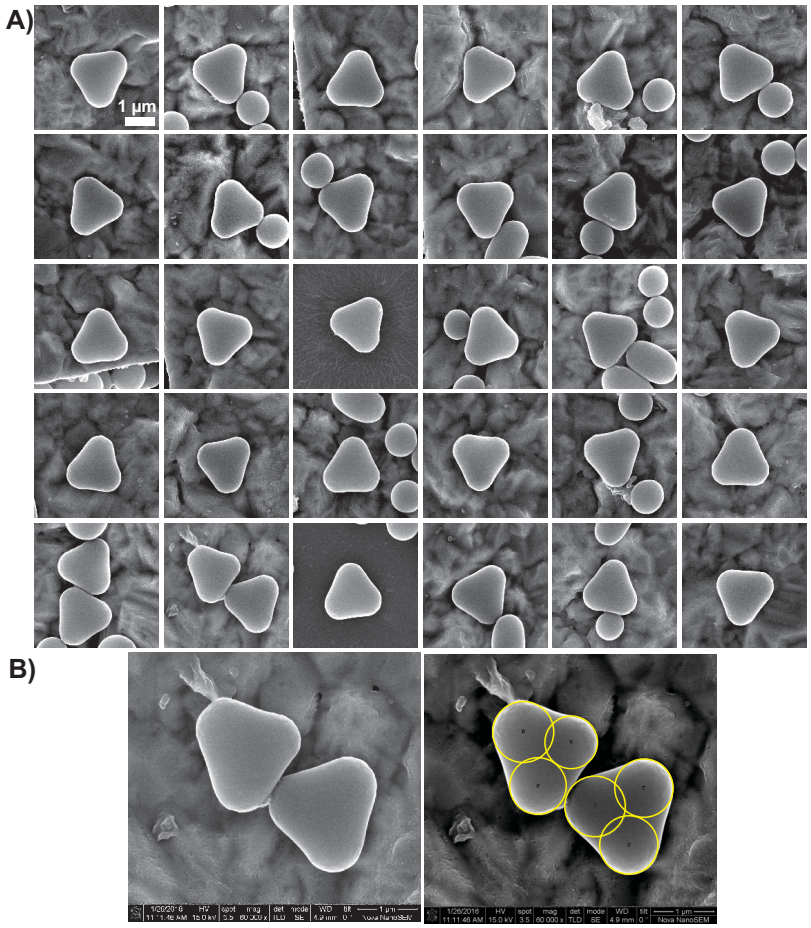


FIGURE 3.7: Patchy particle shape analysis. A) SEM micrographs of trimer patchy particles consisting of three seed particles obtained after reconfiguring aggregates of 1.06 μm polystyrene spheres(Magsphere Inc.) with styrene at S=7. B) To obtain information on the polydispersity of the clusters the center-to-center distances of the reconstructed seeds was measured using high resolution SEM micrographs of trimer particles. From the original SEM micrographs(left) the position and size of the seed particles was reconstructed by fitting a circle at the patches using ImageJ(right). The center-to-center distance in 33 trimers was measured, where an average distance of 0.95 μm was found with a polydispersity of 5.8%. This distance is slightly shorter compared to the diameter of the seed particles due to capillary forces acting on the particles during reconfiguration which can deform the polymer spheres. The polydispersity of the trimers is consistent with the 5.3% polydispersity of the seed particles.

μm polystyrene particles with styrene at swelling ratio S=7. We found the polydispersity to be 5.8%, which is comparable to the polydispersity of 5.3% for the seed particles (see Figure 3.7). The sphere arrangements are not affected by polymerization (see Appendix Figure 3.17) and the uniformity for particles with N<6 spheres indicates that these are the most stable configurations, which in principle can be stored even in the swollen state if sufficiently stabilized against further coalescence[113].

Similar to existing cluster preparation methods, a post-processing step is required to separate the different cluster sizes. Although techniques such as density gradient centrifugation are suitable for separation[14], we emphasize the need for cluster preparation methods with narrow size distributions. Our reconfiguration method provides an opportunity for achieving this, since it only requires randomly aggregates as a starting point. Therefore, any method that provides a sharply peaked size distribution of random aggregates may be used to make uniform patchy particles in high yield.

Besides the fundamentally different reconfiguration approach, our strategy distinguishes itself from existing patchy particle preparation methods by combining the arrangement of spheres into uniform structures and the formation of patchy particles into a single step. Emulsion-based strategies first require the preparation of well-defined colloidal clusters[25], before patchy particles can be formed by the addition of a swelling agent or polymerizable liquid. Because our approach combines the two steps, it does not require the seed particles to be stable in apolar solvents nor to be able to form well-defined protrusions upon swelling[16,113]. Therefore, the reconfiguration approach for making patchy particles can also be applied to purely charge stabilized colloids and colloids with a wider range of crosslink density and surface hydrophilicity. The non-toxic, aqueous environment makes our "recycling" method a user-friendly and cost-effective process that can easily be scaled up to yield large quantities of patchy particles and clusters.

Finally, we note that while we are exploiting the swelling of crosslinked polymer spheres to deposit droplets at the contact points of the spheres, the reconfiguration mechanism should be extendable to other non-polymeric colloidal systems if an alternative droplet deposition method, for example by nucleation from solution[3] or mechanical mixing[120], is employed. The generality of the principle that enables reconfiguration of particles attached by van der Waals forces by simple droplet lubrication may also offer the opportunity to create microscopic hinges that can be applied in nano-robotics, actuators, or switchable structures.

3.4 Conclusions

We presented a general method to reconfigure particle aggregates and synthesize complex patchy particles of well-defined shape. Our starting point is randomly

aggregated particles, which we obtain by deliberately destabilizing spherical colloids using an excess amount of salt or by changing the pH to the isoelectric point. The size distribution of these aggregates can be tuned by changing the aggregation time. We showed that these randomly shaped clusters can be recycled into uniform patchy particles by swelling and depositing apolar solvent at the particle contact area. These droplets significantly reduce the attractive van der Waals forces, lubricate the contact area and induce a reconfiguration of the spheres in order to minimize the interfacial energy. The resulting particles are anisotropic in size and shape, and uniform for small cluster sizes. For clusters consisting of six spheres or more, particles with a high crosslink density rearrange into structures that minimize the second moment of the mass distribution. At low crosslink density, structures with higher entropy are preferred; for example, we find that the polytetrahedron is strongly favoured over the octahedron for clusters of six spheres. We show that besides patchy particles, colloidal clusters can be formed as well using a volatile apolar solvent. Furthermore we discussed and demonstrated the broad applicability of this strategy by tuning the swelling ratio, swelling agent, surfactant concentration, and colloidal material. We believe that the principle of bond lubrication that underlies the reconfiguration is general in nature and can be transferred to other systems as well.

3.5 Appendices

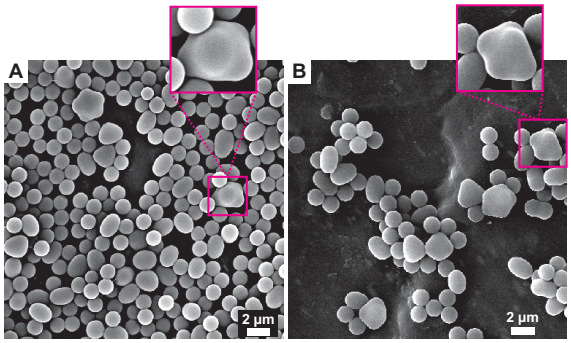


FIGURE 3.8: Different aggregation pathways give similar patchy particle shapes. SEM micrographs of polymerized patchy particles obtained by aggregating 1.40 μm carboxylic acid functionalized polystyrene spheres with 1.5% v/v crosslink density. A) in a 1M potassium chloride solution for 1.5 min B) in a 1M HCl solution for 2 min. Both samples were swollen with styrene at S=4 for 24 hours, followed by polymerization. The resulting patchy particles have similar shapes independent of the aggregation method. Furthermore, the polytetrahedral shape for clusters consisting of six spheres is observed in both samples.

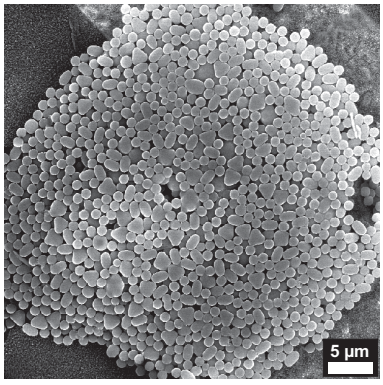


FIGURE 3.9: Large field of view by SEM of polymerized patchy particles of different sizes obtained by swelling colloidal aggregates of 1.06 μm polystyrene spheres with styrene at S=5. For each cluster size, a well-defined arrangement is obtained.

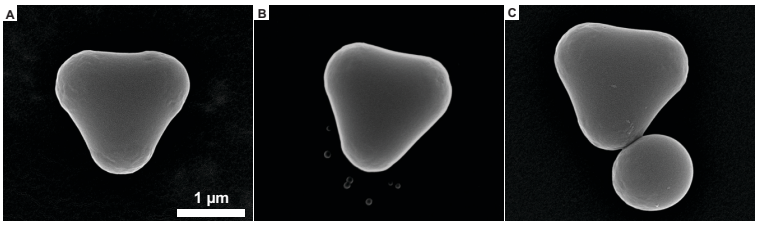


FIGURE 3.10: The shape and arrangement of the patchy particles are independent of the swelling ratio S. Colloidal aggregates of 1.06 μm polystyrene spheres were swollen with styrene at different swelling ratios. The SEM micrographs of typical trimer patchy particles obtained at A) S=2 B) S=5 C) S=8 show that at fixed sizes similar shapes and arrangements are observed, independent of the swelling ratio used.

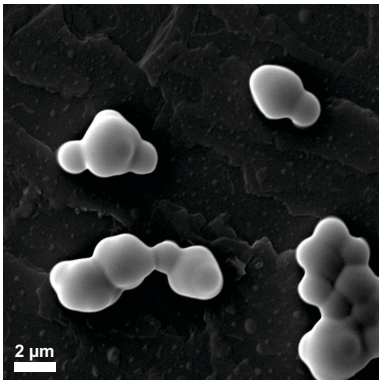


FIGURE 3.11: Patchy particles destabilize when the SDS concentration is insufficient. SEM micrograph of aggregates of patchy particles obtained by swelling aggregates of 1.40 μm polystyrene spheres with styrene at S=8. Clustering of the patchy particles was observed at this swelling ratio, since the concentration of surfactant was insufficient to stabilize the swollen patchy particles. This problem can be resolved by addition of surfactant shortly after the swelling has been initiated.

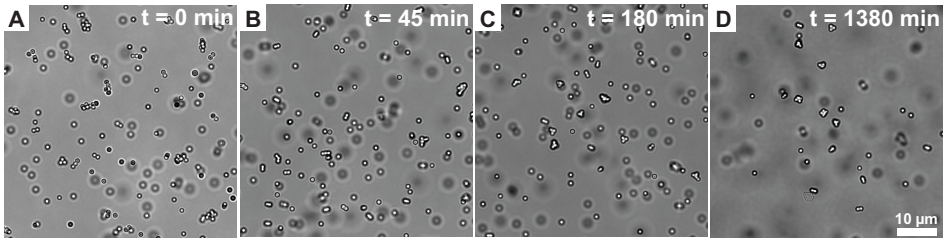


FIGURE 3.12: Swelling process of 1.40 μm carboxylic acid functionalized polystyrene aggregates with styrene at S=4 and 0.02% w/v SDS imaged with bright field microscopy over time A) After salting out for 4 min in a 1M potassium chloride solution randomly shaped aggregates were observed B) After 45 minutes of swelling the aggregates had swollen slightly, but mainly random shapes were observed C) After 3 hours of swelling part of the aggregates reconfigured into compact shapes. D) After 23 hours of swelling all swollen aggregates reconfigured into compact well-defined shapes.

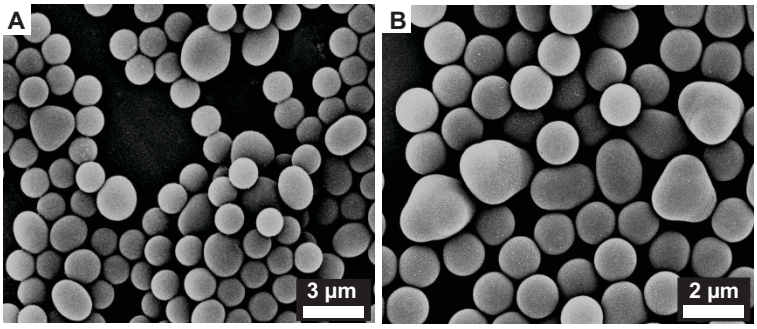


FIGURE 3.13: The concentration and timing of the addition of SDS influences the final particle shape. Colloidal aggregates of 1.40 μm polystyrene spheres were swollen with styrene at S=4 with A) 0.04% w/v SDS and B) 0.04% w/v SDS + an additional 0.04% w/v SDS added after a few hours of swelling. The additional amount of SDS leads to an increase in the transport rate of styrene to the aggregates and an increase in stability of the clusters. It also changes the surface tensions present in the system and therefore the wetting angle of the monomer with the particle. This results in patchy particles with more clearly defined patches(B).

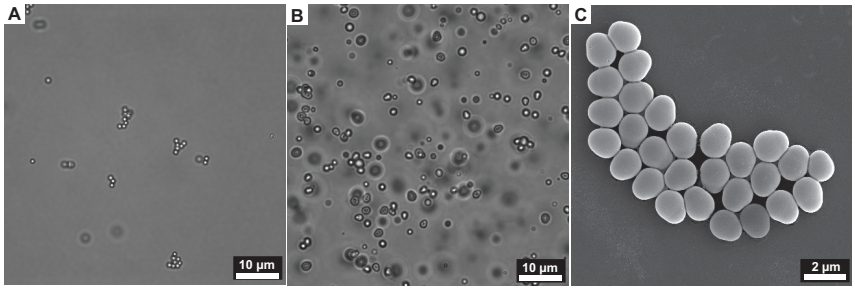


FIGURE 3.14: SDS can re-stabilize individual spheres breaking up the aggregates. Swelling of 1.38 μm sulfate functionalized polystyrene spheres A) Bright field microscopy image of aggregates formed after aggregation with salt B) Bright field microscopy image after 2 hours of swelling with styrene. The particles have non-spherical shapes and are clearly swollen C) SEM micrograph of the polymerized patchy particles. Well-defined protrusions are formed on the seed particles, displaying snowman-like shapes.

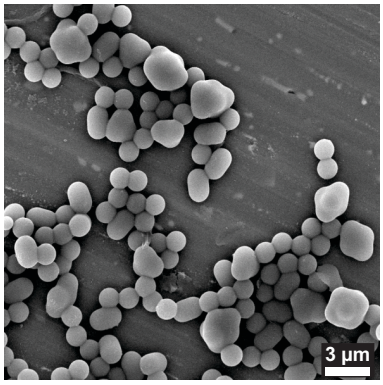


FIGURE 3.15: Large clusters shaped from low crosslink density seed particles have various shapes. SEM micrograph of patchy particles of 1.40 μm carboxylic acid functionalized polystyrene spheres with 1.5% v/v crosslink density. The patchy particles were obtained by swelling the aggregates at S=40 with MM:MA at a ratio of 49:1. Various shapes for clusters of N>5 spheres were formed.

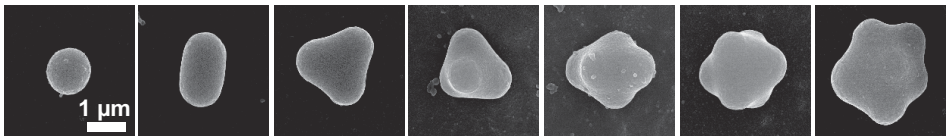


FIGURE 3.16: Colloidal clusters can be obtained by using toluene as swelling agent. SEM micrographs of colloidal clusters consisting of 1-7 spheres from left to right respectively. The colloidal clusters are obtained by swelling aggregates of 1.06 μm polystyrene spheres for 24 hours with toluene at S=8. After evaporation of the toluene well-defined colloidal clusters shapes are observed. The seed particles are slightly deformed during the process since the uptake of toluene softened the particles, leading to migration of linear polystyrene polymer out of the seed particles during the evaporation process to reduce the surface tension of the cluster.

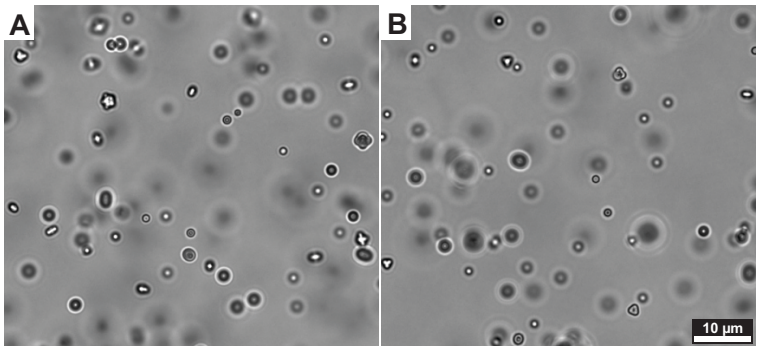


FIGURE 3.17: Comparison between swollen, unpolymerized (A) and polymerized (B) reconfigured patchy particles. A) Bright field microscopy images of patchy particles obtained from salted-out 1.40 μm polystyrene spheres (t_a=2 min, 1M potassium chloride solution) after 18 hours of swelling with styrene at S=5 B) The cluster arrangements are maintained during polymerization for 24 hours at 80°C.

CHAPTER 4

COMPLEX PATCHY COLLOIDS SHAPED FROM DEFORMABLE SEED PARTICLES THROUGH CAPILLARY INTERACTIONS

The results in this chapter have been published:

Vera Meester, Daniela J. Kraft,
Complex Patchy Colloids shaped from Deformable Seed Particles through Capillary Interactions, **Soft Matter**, 2018, 14, 1162-1170, DOI: 10.1039/C7SM02020A.

Abstract

We investigate the mechanisms underlying the reconfiguration of random aggregates of spheres through capillary interactions, the so-called "colloidal recycling" method, to fabricate a wide variety of patchy particles. We explore the influence of capillary forces on clusters of deformable seed particles by systematically varying of the crosslink density of the spherical seeds. Spheres with a poorly crosslinked polymer network strongly deform due to capillary forces and merge into large spheres. With increasing crosslink density and therefore rigidity, the shape of the spheres is increasingly preserved during reconfiguration, yielding patchy particles of well-defined shape for up to five spheres. In particular, we find that the aspect ratio between the length and width of dumbbells, L/W, increases with the crosslink density (cd) as $L/W = B - A \cdot exp(-cd/C)$. For clusters consisting of more than five spheres, the particle deformability furthermore determines the patch arrangement of the resulting particles. The reconfiguration pathway of clusters of six densely or poorly crosslinked seeds leads to octahedral and polytetrahedral shaped patchy particles, respectively. For seven particles several geometries were obtained with a preference for pentagonal dipyramids by rigid spheres, while soft spheres do rarely arrive in these structures. Even larger clusters of over 15 particles form non-uniform often aspherical shapes. We discuss that the reconfiguration pathway is largely influenced by confinement

and geometric contraints. Which key factor dominates during reconfiguration depends on the deformability of the spherical seed particles.

4.1 Introduction

Patchy colloids are excellent building blocks for self-assembly, since their anisotropy in surface chemistry allows them to form complex structures.[121–123] While spheres with isotropic interactions only crystallize in a randomly stacked hexagonal closed packed structure, particles with a single patch already assemble into micelles[29] and tubules[47,124]. Particles with multiple patches have been predicted to exhibit an even richer phase behavior[88,125], such as crystallization into dense diamond[126], body-centered-cubic and face-centered-cubic[127] lattices as well as open networks[128]. A directional interaction profile also has exciting potential for mimicking polymer chain formation[129], complex protein assemblies[130,131] and the bottom up construction of smart materials[80,132]. Patchy colloids with multiple interaction sites have been experimentally realized by, for example, partial coverage of the surface with a droplet[16,133] or a second type of colloid[134,135]. Self-assembly of such particles has been achieved by site-specific interactions based on DNA-linkers[25,136], metal coordination[20], hydrophobic interactions[98], capillary bridges[137], and depletion forces[29].

We have recently contributed to the available synthetic approaches with a strategy based on reconfiguring random aggregates of spheres into patchy particles.[138] The technique relies on the introduction of apolar droplets to the contact areas of the aggregated spheres dispersed in aqueous solution. These droplets enable rotational mobility and induce a reorganization of the spheres driven by capillary forces. By merging these capillary bridges the interfacial energy is minimized. The cluster-spanning droplet connects and partially shields the seed spheres, which creates patches. After polymerization of the droplet, this leads to patchy particles with a compact shape. Advantages of our "colloidal recycling" approach are that it can be performed in bulk in aqueous, non-toxic media and that various types of patchy particles can be obtained by variation of the initial seed particles and/or organic solvent.
In our previous study we observed that the location of the patches and the overall particle geometry is unique for each number of seed particles up to N=5 spheres. Above N=5, we found that the sphere arrangement and thus patch location depended on the type of seed particles we used. For example, we observed both a polytetrahedral and an octahedral arrangement for six spheres. In previous experiments, theoretical models and numerical calculations it was found that the preference for a certain geometry can be determined by various factors such as maximizing the number of contacts[139], the interaction profile[140,141], entropy[13], capillary forces[142], packing constraints[14], and interfacial phenomena[143].

The observation of both a polytetrahedral and octahedral arrangement in our experiments implies that the physical or chemical properties of the seed particles influence the reconfiguration process by affecting either the kinetic pathway and/or the free energy landscape of the final configuration. In our previous work we suspected that particle rigidity was the crucial difference between the seed particles, but since they had been prepared following different methods other factors could not systematically be excluded. Clearly, the key to tailor our method to create patchy particles with complex and new patch arrangements is a better understanding of the assembly pathway.

We here investigate the reconfiguration process and use this knowledge to assemble a wide variety of complex patchy particles. We analyse how spheres of different rigidity are deformed during reconfiguration and how this affects the geometry and final shape of the cluster. Quantitative results are presented of the deformation of spheres with different crosslink density. We also study the influence of the capillary forces on the reconfiguration pathway of clusters constructed from six or more spheres. The soft and rigid spheres reconfigure to different shapes, which points to different assembly pathways.

4.2 Experimental Methods

Materials

Styrene ($\geq$99%, contains 4-tert-butylcatechol as inhibitor), divinylbenzene (DVB, technical grade 55%), azobisisobutyronitril (AIBN, $\geq$98%), hydroquinone (HQ, $\geq$99.5%), sodium dodecyl sulfate (SDS, $\geq$98.5%) and perylene (sublimed grade, $\geq$99.5%) and were purchased from Sigma-Aldrich. Styrene was passed through an inhibitor remover column (Sigma-Aldrich) before use. Potassium chloride (>99% p.a.) was obtained from Fluka, Germany. The water used was deionized using a Millipore Filtration System (MilliQ Gradient A10), resulting in a resistivity of 18.2 MΩ·cm.

Methods

Seed particle synthesis Linear carboxylic acid functionalized polystyrene spheres of 1.05 ± 0.02 µm in diameter were synthesized by a surfactant free emulsion polymerization procedure[104]. The colloids were stored in water after filtration over glass wool and washing. To 13.5 mL of a 2.29% wt dispersion of these linear seeds, 0.05 g SDS, 0.034 g HQ and 1.7 mL crosslink solution was added to swell and crosslink the particles. The crosslink solution consisted of styrene with 2% wt AIBN and 0.2, 0.6, 1, 2, 3, 4, 6 or 10% v/v DVB, yielding seed particles with different crosslink density. The mixtures were rotated for 24h on a tumbler at 20

[DVB] crosslink solution % v/v	**[DVB] final seed** % v/v	**Diameter** μm
0.0	0.00	1.05 ± 0.02
0.2	0.16	1.57 ± 0.04
0.6	0.46	1.53 ± 0.06
1.0	0.68	1.42 ± 0.03
2.0	1.40	1.44 ± 0.04
3.0	2.13	1.45 ± 0.05
4.0	3.04	1.51 ± 0.02
6.0	4.31	1.46 ± 0.04
10.0	8.27	1.61 ± 0.05

TABLE 4.1: Characteristics of polystyrene seed particles synthesized including the diameter, the concentration DVB [DVB] in the crosslink solution and the [DVB] in the final seed particle.

rpm in the dark. Finally, the swollen colloids were polymerized in a 72°C preheated oil bath for 24h while rotated at 100 rpm at a 45° angle. The synthesized particles had a smooth surface morphology and a polydispersity below 4%. They were washed and stored in water. The characteristics of all synthesized particles are listed in Table 4.1 and SEM micrographs are displayed in Figure 4.1. In addition, RITC dyed polystyrene spheres of 1.06 ± 0.06 μm with a crosslink density of 10% v/v were purchased from Magsphere Inc.

Patchy particle preparation method Patchy particles were prepared using the 'colloidal-recycling' method.[138] Here, random aggregates are formed first by diffusion limited aggregation. Aggregation was induced by the addition of 100 μL of a 2M potassium chloride solution to a 100 μL electrostatically stabilized colloidal suspension (4.4% wt). After an aggregation time, t_a, of 2 min the dispersion was quenched with 15 mL water. To obtain clusters of N>15, the spheres purchased from Magsphere. Inc. were aggregated for 8 min before quenching. The random aggregates were reconfigured into compact patchy particles by the addition or organic solvent: To 5 mL of quenched dispersion containing random aggregates, 10 μL of aqueous SDS solution (10% wt) and 12.7 μL of reconfiguration solution, consisting of styrene with 1.5% v/v DVB and 2% wt AIBN, was added. The swelling ratio S, defined as the mass of the organic solvent/mass of the polymer colloids was 8 in these experiments, which is sufficient to achieve reconfiguration[138]. The dispersion was magnetically stirred for 24h to complete reconfiguration of the aggregates. The obtained patchy particles were polymerized for 24h in a preheated oil bath at 80°C. The particles were washed and stored in water.

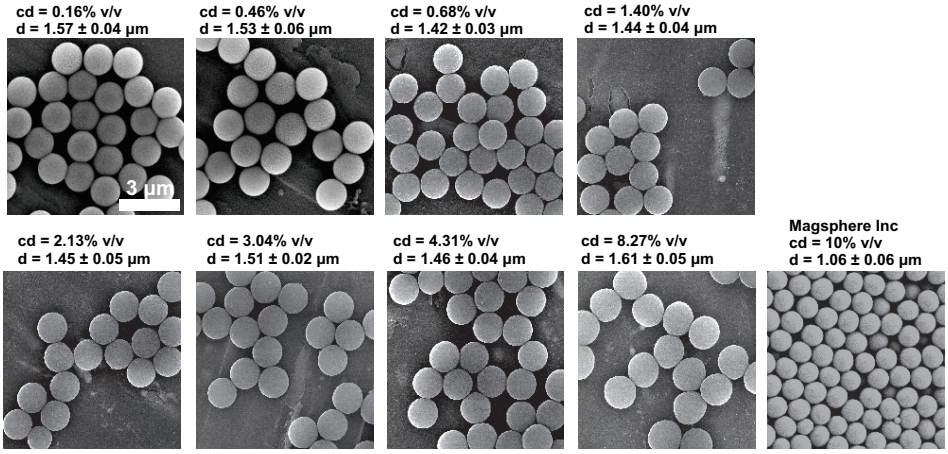


FIGURE 4.1: SEM micrographs of the seed particles used. The crosslink density (cd) and diameter (d) of the particles in the dispersion are stated above the representative images.

Imaging and analysis The synthesized polystyrene seed particles and polymerized patchy particles were imaged using a FEI nanoSEM scanning electron microscope (SEM) at 80 kV. The size of the linear and crosslinked seed particles was determined by measuring the circumference of >100 particles in SEM micrographs with ImageJ. ImageJ was also used for the analysis of patchy particles of N=2 formed by seed particles of different crosslink density. Here the long axis (L) and the short axis (W) of the dumbbell were measured of at least 30 particles per sample. For each particle the L/W ratio was determined and averaged.

4.3 Results and Discussion

4.3.1 The colloidal recycling method

We studied the shape and assembly pathway of patchy particles constructed from spheres of varying rigidity. These patchy colloids were obtained by applying the colloidal recycling method[138], illustrated in Figure 4.2A, to spheres with different crosslink density. Here, colloidal aggregates with a controlled size distribution are formed by diffusion limited aggregation induced by the addition of salt to electrostatically stabilized colloidal spheres. Reconfiguration of the randomly shaped aggregates is induced by the addition of organic solvent, which is deposited in small droplets at the contact area between the spheres. This results in the formation of capillary bridges. The droplets decrease the attractive van der Waals forces between the particles and lubricate the contact area, which en-

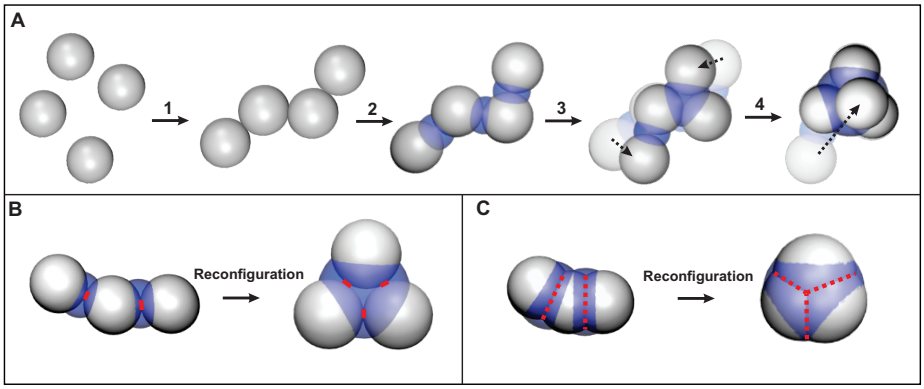


FIGURE 4.2: A) Illustration of the colloidal recycling method. 1. Destabilization of colloids resulting in the formation of aggregates. 2. By the addition of organic solvent (blue) to a random aggregate of four spheres, droplets of solvent are deposited at the contact area between the spheres. 3-4) The van der Waals attractions between the spheres are decreased, which enables rotational mobility of the aggregate leading to the coalescence of the droplets to minimize the interfacial energy of the droplet with the surrounding water. The obtained compact cluster is spanned by a single droplet creating a patchy particle. Illustrations of trimers of rigid (B) and deformable (C) spheres with the contact areas highlighted in red. The contact area between the rigid spheres is small and the shape of these spheres is largely preserved after reconfiguration. The soft spheres are largely deformed by the strong capillary forces induced by the organic droplets, which results in large contact areas and compact patchy particle shapes.

ables rotational mobility of the spheres in the aggregate. Since capillary forces dominate, the small droplets coalesce into one cluster spanning droplet to decrease the interfacial energy.[144] The aggregates therefore reconfigure into compact shapes yielding patchy particles with well-defined geometries. Since the process is purely based on reconfiguration of the initial aggregates, the size distribution of the patchy particles is equivalent to that of the aggregates and can thus be tuned by the aggregation time, t_a.[138] The size distribution can therefore be tuned by experimental parameters such as the colloid concentration, the salt concentration, the surface charge of the colloids and the aggregation time t_a. The universality of this method with respect to the particle properties of the seeds, allows us the use of various types of seed particles.

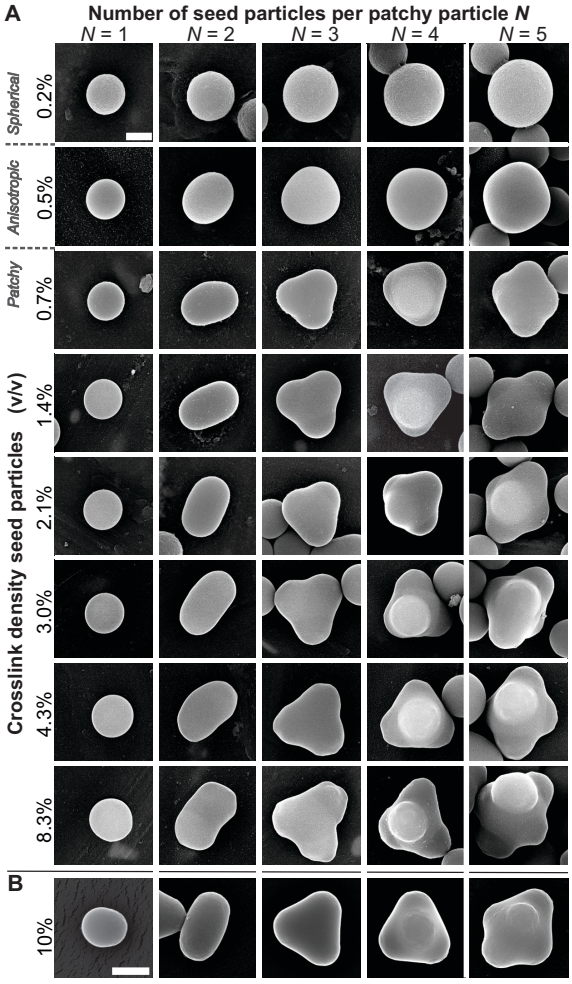


FIGURE 4.3: SEM micrographs of spherical, anisotropic and patchy particles of N=1-5 formed by polystyrene seed particles of different crosslink density (cd). Scale bar is 1 μm. A) Particles constructed by spheres of fixed crosslink density, ranging from 0.2% v/v at the top row to 8.3% v/v at the bottom row. The seeds are all synthesized following the same emulsion polymerization protocol. Per column particles consisting of a fixed number of seed particles are shown. At 0.2% v/v cd the seed particles completely merge during reconfiguration, which yields spheres with a larger diameter. Spheres with 0.5% v/v cd slightly resist deformation, resulting in anisotropic particles. At higher cd, 0.7 $\leq$ cd $\leq$ 8.3% v/v, the shape of the seeds is largely preserved and patchy particles are formed. Spheres with very densely crosslinked polymer networks, 4.3 or 8.3% v/v cd, form patchy particles with irregular features at the patches. B) Patchy particles constructed from 10% v/v crosslinked 1.06 μm seed particles purchased from Magsphere Inc. Large field of view SEM micrographs of the reconfigured particles are shown in Figure 4.5.

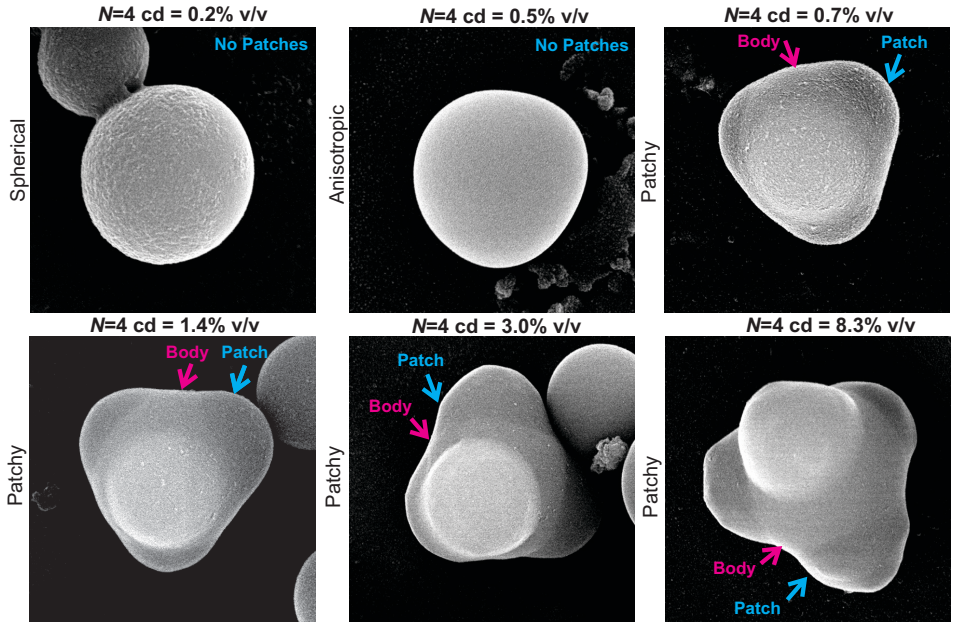


FIGURE 4.4: Spherical, anisotropic and patchy particles shaped from four seed particles. The shape of the cluster after reconfiguration was influenced by the crosslink density (cd) of the seed particles. At low crosslink density, cd=0.2% v/v the seeds merged yielding larger spheres. At cd=0.5% v/v anisotropic shapes were obtained but no patches were recognized. At cd $\geq$ 0.7% v/v patchy particles were formed where part of the original seeds can be recognized and distinguished by contrast from the polymerized droplet spanning the sphere, the body. At increasing crosslink density the contrast difference between the patches and the body became larger, making the interface between the two increasingly visible. At cd > 3.0% v/v the patches could also be distinguished from the body by a difference in the surface morphology of the patches and the body. The patches had small irregular features, which were not visible on the body of the patchy particle.

4.3.2 Spherical, anisotropic and patchy particles of deformable spheres

During the reconfiguration process strong capillary forces are acting on the spheres in the cluster. With increasing crosslink density of the polymer colloids, the rigidity of the polymer network increases and thus the ability of the particle to resist swelling and deformation induced by the capillary forces.[4,145] We therefor expect that the deformability of the seed particles influences the size of the contact area between spheres and the final shape of the reconfigured cluster (Figure 4.2B and 4.2C). To investigate how spheres of varying rigidity are influenced by capillary forces we studied particles made from spherical seed

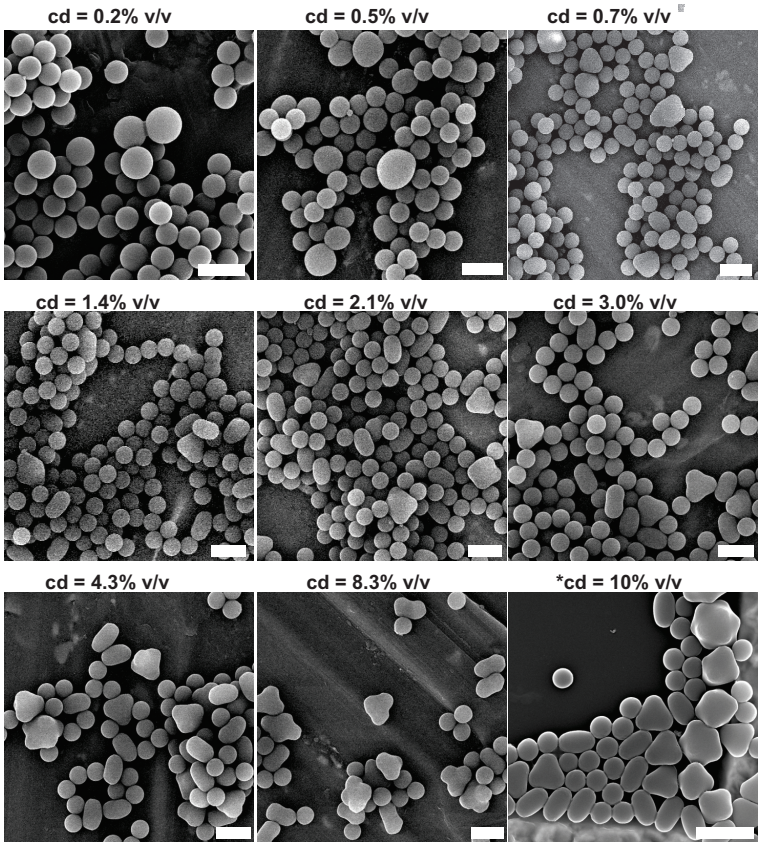


FIGURE 4.5: SEM micrographs of particles obtained by reconfiguring colloidal aggregates of seeds with different crosslink density (cd). The cd of the seeds is stated above the images and the scalebars are 3 μm. The images show typical overviews of the particles observed in the colloidal dispersions. As the crosslink density increases the shape of the original seed particles was more preserved. *The colloids with cd = 10% v/v were purchased from Magsphere Inc. and synthesized according to a different method compared to the other seed particles.

particles with a crosslink density (cd) of 0.2, 0.5, 0.7, 1.4, 2.1, 3.0, 4.3 or 8.3% v/v (volume crosslinking agent/volume styrene) and a diameter of approximately 1.5 µm, see Table 4.1 and Figure 4.1 for details and methods. The concentration of organic solvent and other experimental parameters were equal in all experiments.

After the reconfiguration process, aggregates of spheres with low crosslink density, cd = 0.2% v/v, and thus low rigidity, were deformed so strongly by

surface tension that the shape of the individual spheres could not be maintained. Instead, the seed spheres merged completely into a single, larger sphere (Figure 4.3 row 1) to minimize the interfacial energy between the organic solvent and the water phase. Spheres with 0.5% v/v crosslinking agent were sufficiently rigid to partly resist the strong capillary forces acting on the seeds, resulting in anisotropic shapes with a smooth surface (Figure 4.3 row 2).
Seeds with more densely crosslinked polymer networks, $0.7 \leq$ cd $\leq$ 8.3% v/v, deformed less during reconfiguration compared to the poorly crosslinked seeds. Here, well-defined particles were obtained where part of the original spheres can be identified as patches protruding from the central body formed by polymerization of the styrene droplet (Figure 4.3 row 3-8 and Figure 4.4). Since the seed particles and the organic droplet consist of similar material, the patches have a low wetting angle with the body. This results in a rather continuous boundary between the two phases. We identified the position of this boundary by a difference in contrast and surface morphology between the patches and the body in SEM micrographs. When no distinction could be made the particles were identified as non-patchy. For patchy particles of a given number of constituent spheres ($N \leq 5$) the same shape was obtained: the dumbbell for N=2, triangle for N=3, tetrahedron for N=4 and the triangular dipyramid for N=5. These structures have been previously observed for clusters of spheres obtained through an evaporation-driven assembly[14,143,146], long-range Lennard Jones 6-12 potentials[140], short-range interactions[13,139], capillary bridges[137,147], and hydrophobic patchy interactions[98].

Although rarely observed we note that some patchy particles have slight deviations from these geometries. Illustrative is the triangular dipyramid constructed from seeds with 3.0% v/v crosslink density (Figure 4.3 row 6). These small deviations in geometry may be attributed to the polydispersity of the seed particles in size and surface properties or inhomogeneities in the crosslinked polymer network[4,148]. The latter may also cause the formation of the irregular features arising at the patches at significant crosslink density, cd = 4.3 or 8.3% v/v (Figure 4.3 row 6-8). These irregularities are likely protrusions or local deformations of the seeds. SEM micrographs representative of the dispersions of the reconfigured particles are shown in Figure 4.5.
Further examination of patchy particles constructed from seeds with 0.7 and 8.3% v/v cd reveals that the body of the patchy particle, originating from the cluster spanning droplet, engulfs a different fraction of the original seeds, see Figure 4.4. While for the soft particles only a small part of the spheres is protruding from the body, a large part of the rigid spheres is visible. This difference is likely caused by a deformation of the spheres in the contact area and at the interfaces of droplet and solvent[149]. The degree of deformation decreases with increasing crosslink density. In addition, the crosslink density can influence the contact angle of the

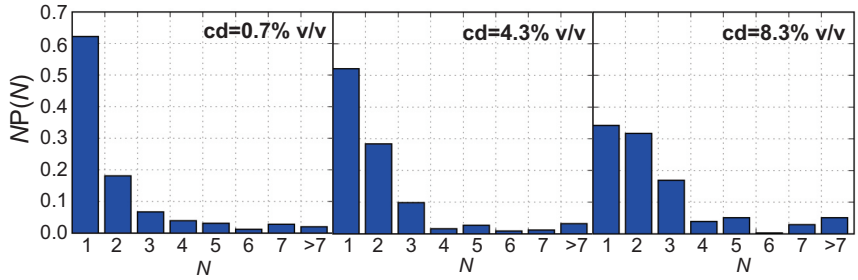


FIGURE 4.6: Size distribution of particles constructed by N after reconfiguration. These distributions are set during the aggregation step where colloids were aggregated at a colloid concentration of 2.19% wt for t_a=2 min in a 1M solution of potassium chloride. The size distribution shifts to larger cluster sizes with increasing crosslink density of the seeds.

particles with the styrene droplet as well as the degree of swelling during droplet deposition and thus the volume of the cluster-spanning droplet.[4,10] The crosslink density therefore may impact the degree of protrusion of the seed particles from the body of the patchy particles in multiple ways.
The crosslink density also affected the size distribution of the resulting particles. SEM micrographs of the dispersions of the reconfigured particles are shown in Figure 4.5. The size distributions of the particles constructed by seeds with cd = 0.7, 4.3 and 8.3% v/v are shown in Figure 4.6. These distributions are set during the aggregation step.[138] For all size distributions the probability to find a sphere in a cluster of size N decreases with increasing cluster size. The distribution also shifts to larger cluster sizes with increasing crosslink density, which indicates that the DVB concentration in the seeds changes the surface properties of the particles.

4.3.3 Shape deformation analysis of dumbbells

To study the relation between the crosslink density and the deformability of the spheres, we analysed the shape of dumbbells. SEM micrographs of multiple dumbbells formed by seeds with crosslink densities ranging from 0.2-8.3% v/v are shown in Figure 4.8. We quantified the deformation of the colloidal dumbbells by measuring the aspect ratio between the long and the short axis, the length L and width W, respectively (see Figure 4.7 inset). When two seed particles merge completely into a larger sphere, L and W are equal and therefore L/W equals 1. The higher the value of the aspect ratio the more aspherical is the dumbbell and thus less deformed are the spheres. The plot in Figure 4.7 presents the aspect ratios for dumbbells formed by seeds of crosslink densities ranging from 0.2-8.3% v/v. Slightly larger error bars are observed at 4.3% and 8.3% v/v cd due to sur-

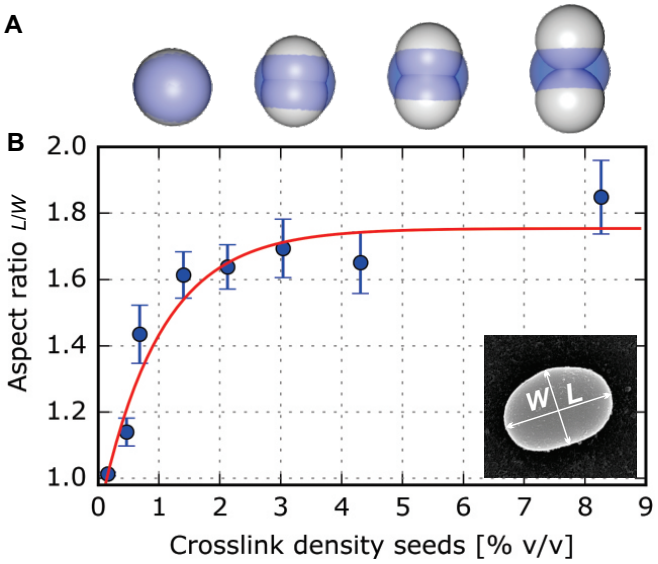


FIGURE 4.7: Deformation of dumbbells. A) Illustration of the effect of capillary forces on the shape of dumbbells constructed from deformable spheres. Sphere deformability decreases form left to right. B) The aspect ratio, L/W, of dumbbells increases with the crosslink density of the seeds. This indicates that the seed particles are less deformed upon reconfiguration at increasing rigidity. The red line is the result of a least squares fit of the data, y = 1.75 - 0.87 $\cdot$ exp(-cd/1.00).

face inhomogeneities of the patches. Yet, we found a maximum polydispersity in the L/W ratio of only 6% for any crosslink density. This shape consistency arises from the uniform properties of the seed particles such as the swelling capacity, size and wetting angle with the droplet. The low polydispersity of the dumbbells is in line with previous measurements of trimer particles, where the polydispersity in the center-to-center distance of spheres in the trimers was also only 5.8%.

The data show that L/W increases with the crosslink density, indicating that the deformation depends strongly on the density of the crosslinked polymer network[9,145]. By fitting the data with a least squares fit of the form y = B - A $\cdot$ exp(-cd/C), where cd is the crosslink density of the seeds and y the aspect ratio L/W, we find B = 1.75, A = 0.87 and C = 1.00. The saturation value at high crosslink densities, here 1.75, corresponds to a dumbbell of non-deformed spheres. Since L_{max} is equal to two times the radius of the seeds, this saturation value is determined by the thickness of the polystyrene body, which depends on the properties of the seeds such as their wetting angle with the styrene droplet as well as the

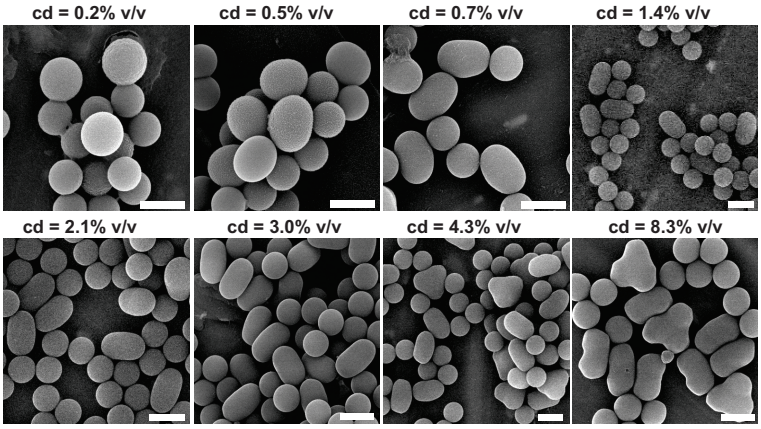


FIGURE 4.8: Typical dumbbells shaped from seed particles with different crosslink densities. The cd of the seeds is stated above the SEM micrographs and the scalebars are 2 μm. The images indicate that similar shapes were formed and as the crosslink density increases the shape of the original seed particles is more preserved, which is confirmed by a quantitave analysis.

swelling ratio.
A similar analysis was performed by Pawar *et al.* to measure the degree of merging of two 100 μm elastic oil droplets.[109] The rigidity in these droplets originated from wax crystals incorporated in the oil, where the elastic modulus increased with the wax concentration. They further calculated the strain ε, which is defined as the difference of the length of the long axis of the dumbbell before and after coalescence, ΔL, divided by the initial length L_0. We obtained qualitatively similar results to the non-Brownian elastic droplets, although a quantitative comparison is not possible since this analysis method cannot be applied to our colloidal dumbbells. The reason is that ΔL is influenced by the volume increase of the spheres during swelling with organic solvent and the degree of swelling also depends on the crosslink density of the seeds[4]. Pawar *et al.* found that the degree of deformation depended on the balance between the elasticity of the droplets and the interfacial energy, where total coalescence was observed for droplets with low elasticity, $\varepsilon = 0.37$, and total stability for elastic droplets, $\varepsilon = 0$. We observed that two colloids of low crosslink density and thus low rigidity also completely coalesced resulting in an aspect ratio L/W equal to 1. At increasing crosslink density the particles are increasingly able to resist deformation leading to higher L/W values, up to a saturation value of 1.75.

4.3.4 Patch arrangements for particles of N>5

While for particles shaped from up to five spheres a fixed geometry is observed for each cluster size, the arrangement of large clusters depends on the underlying organizing principle such as packing constraints[14], particle wettability[143], interaction potential[140,141] and entropic effects[13]. For N=6 this may lead to a polytetrahedral or octahedral structure. Surprisingly, in our initial study we have observed both the octahedral and the polytetrahedral arrangement of the patches for different batches of seed particles.[138] This points towards the fact that the physical and/or chemical properties of the seeds play an important role in determining the outcome of the reconfiguration process. Because the two batches of particles strongly differed in the particle softness, we have speculated that the rigidity may be origin of the observed difference.

To single out the effect of particle rigidity we here investigated the patch arrangements for polystyrene seeds with crosslink densities 0.7, 2.1, 4.3 and 8.3% v/v synthesized following the same protocol. The patchy particles resulting from the reconfiguration process exhibit a striking transition from the polytetrahedron at low crosslink density to the octahedron at high crosslink density (Figure 4.9A). Clusters of six seeds with low crosslink density, cd=0.7% v/v, reconfigured only into the polytetrahedron. At 2.1% v/v crosslink density the polytetrahedron was formed predominantly, while at 4.3% v/v mainly the octahedron was observed. At 8.3% v/v crosslink density we only found the octahedron. This is in line with what we had observed previously for patchy particles made from highly crosslinked (10% v/v) 1.06 μm polystyrene particles obtained from Magsphere Inc., which also only show the octahedral arrangement. Clearly, an increase in the crosslink density induces the transition from the polytetrahedral to the octahedral arrangement.

For N>6 the number of possible arrangements increases dramatically with each additional sphere. Already for patchy particles consisting of N=7 spheres, it becomes difficult to distinguish the different arrangements from 2D SEM images. In experiments and free energy calculations of clusters of seven spheres with short range attractions six geometries were observed, see Figure 4.10A for point group notations and illustrative models. Figure 4.10A also shows the sides of a polytetrahedron where the seventh sphere is positioned to form the N=7 structures. Qualitatively, we observe that the rigid spheres with cd=10% v/v arrange in all these geometries, with the pentagonal dipyramid (D_{5h}) and C_{2v} structures being dominant (Figure 4.10B). Spheres of 0.7% v/v cd do only rarely achieve the pentagonal dipyramid structures and dominantly form the C_2 and C_{3v} point group clusters (Figure 4.10C). For even larger clusters (N>15), we find that the rearranged structure take up a slightly elongated spherical shapes (see Figure 4.11) which occasionally feature protruding spheres or bulges. This suggests that the reconfiguration got arrested in a non-equilibrium state. The final shape of large clusters is therefore largely dependent on the reconfiguration pathway.

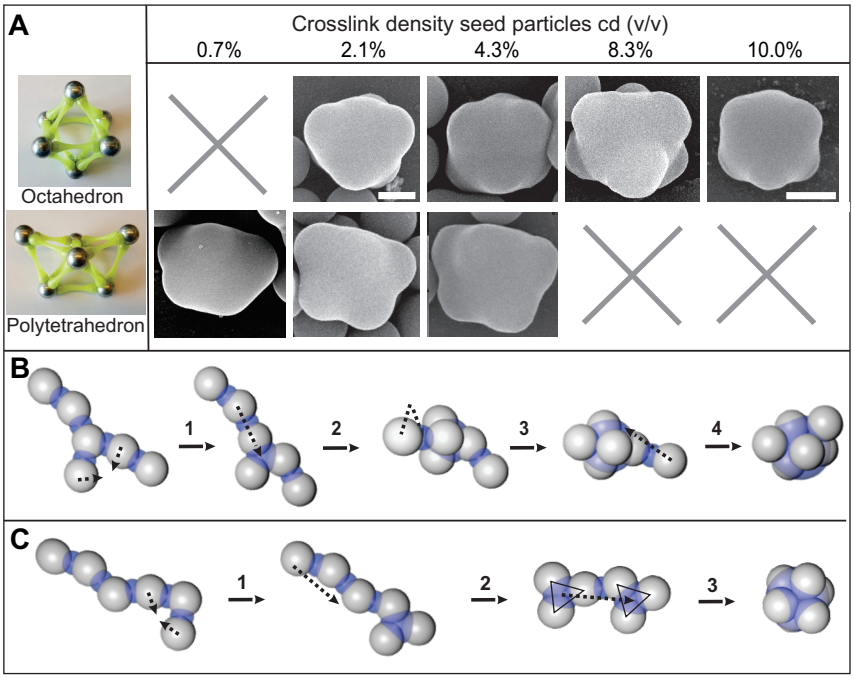


FIGURE 4.9: Patch arrangements and reconfiguration pathway of patchy particles of N=6. A) Schematic illustration and SEM micrographs of the octahedron (top row) and the polytetrahedron (bottom row) constructed from seed particles with cd = 0.7, 2.1, 4.3, 8.3 and 10% v/v cd. The seed particles with 10% v/v crosslink density are commercially purchased from Magsphere Inc. and synthesized by a different procedure. The octahedron is not formed by spheres with low crosslink density and the polytetrahedron is not observed for rigid spheres. Scalebar is 1 μm. B) Illustration of the reconfiguration pathway of a cluster of six spheres into the polytetrahedron. Upon coalescence of the small droplets into a larger droplet subsequently a triangle, step 1, and a tetramer, step 2, are formed. From the tetrahedron the reconfiguration continues leading to the triangular dipyramid, step 3, and eventually the polytetrahedron with a single droplet spanning the cluster, step 4. D) Reconfiguration pathway leading to the octahedron geometry. To form this geometry two trimers have to be formed, without the formation of a tetramer, which assemble on top of each other to yield the octahedron. The formation of the octahedron is therefore less likely to occur compared to the polytetrahedron.

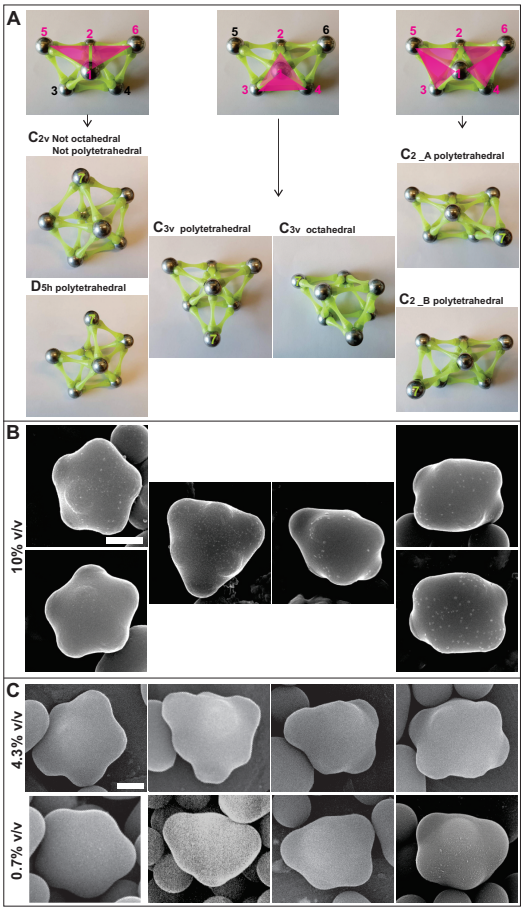


FIGURE 4.10: A) Models of typical minimal free energy geometries for clusters of N=7. The Schönflies notation is written above the image. Above the N=7 models a polytetrahedron is shown with in magenta the position where the seventh sphere can be positioned to form the N=7 structures. The pentagonal dipyramids C_{2v} and D_{5h} can be differentiated by the subtle bond distance between the two spheres on the pentagon, $1.09d$ vs $1.05d$, respectively, where d is the diameter of the sphere. C_{3v} has a polytetrahedral and an octahedral version. The polytetrahedral C_2 geometry knows two chiral enantiomers. B) and C) SEM images of patchy particles constructed from seven spheres of different crosslink density. Scalebars are 1 μm. B) For patchy particles of spheres with 10% v/v crosslink density, purchased from Magsphere Inc., all six N=7 geometries can be identified and these rigid spheres predominantly reconfigure into the pentagonal dipyramid geometries (C_{2v} and D_{5h}). C) Patchy particles with a cd of 4.3% v/v reconfigure into all geometries although we were unable to distinguish between the C_{2v} and D_{5h} geometry and only one C_2 structure is shown. At low crosslink density, 0.7% v/v, the pentagonal dipyramids C_{2v} and D_{5h} are rarely observed.

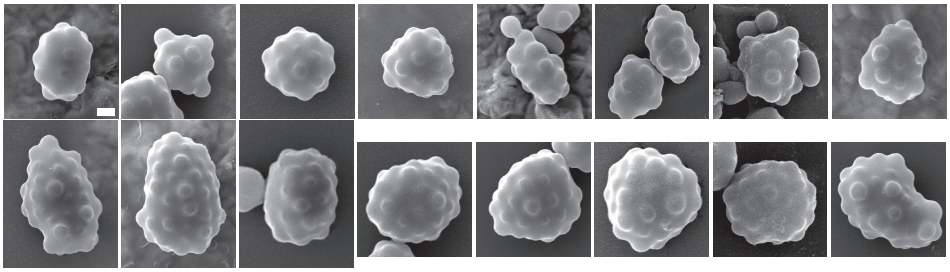


FIGURE 4.11: Patchy particles of N>15 constructed from 1.06 μm seed particles with 10% v/v crosslink density. The scalebar in the SEM micrographs is 1 μm. The patchy particles are of non-spherical, often elongated shapes. Protruding spheres and bulges are visible, suggesting that the reconfiguration got arrested in a non-equilibrium state. The final shape is therefore dependent on the reconfiguration pathway.

Previous experiments and numerical analyses on particle-covered droplets found that the preferred arrangement of the spheres depends on the particle wettability and the droplet volume.[142] Similarly, for the formation of clusters upon slow droplet evaporation it was found that the final configurations arise almost entirely from geometric constrains during the drying process and depend on particle wettability.[5,14,150] The latter process inherently leads to compact clusters, possibly with several spheres inside the cluster. Our reconfiguration approach is different from earlier work in that it is essentially a bottom-up assembly of particles connected by capillary bridges that merge into a larger droplet instead of a top down approach, which starts with the adsorption of multiple spheres on a single, large droplet. Equilibrium wetting arguments alone may not be sufficient to explain our observations since capillary interactions and kinetic effects are expected to be important as well. We therefore consider the reconfiguration process itself.

4.3.5 Reconfiguration pathway

After deposition of the droplets at the contact areas of the spheres, the consecutive merging of the droplets due to the capillary interactions determines the step-wise folding into the compact structure. Crucial for coalescence and thus reconfiguration to occur is a sufficient volume of the droplets. We have studied the effect of the amount of organic liquid previously by adding different volumes of organic liquid to the colloidal aggregates.[138] The volume was tuned by the swelling ratio S, which is defined as the mass of the organic liquid/mass of the polymer particles. At S<4, reconfiguration did often not occur likely because the droplets at the contact areas between the spheres were too small to merge into a larger droplet. At S$\geq$4 reconfiguration occured. Here, we employed S=8 to ensure a high success

rate for reconfiguration.

For simplicity, we examine the reconfiguration of a random aggregate of N=6 spheres more closely, but similar arguments should hold for aggregates containing more spheres as well. Initially, the coalescence of two droplets yields triangular arrangements. This may happen at any location in the aggregate, and we randomly chose one for illustration purposes in Figure 4.9B. The merging of the capillary bridge of a fourth and fifth sphere and subsequent minimization of the droplet interface leads to a tetrahedral and triangular dipyramid arrangement, respectively, as was seen for N=4 and N=5 clusters (Figure 4.3). The rearrangement of the final sphere results in a polytetrahedral geometry through local minimization of the interface, at least in first instance. While there exist many possible routes towards the polytetrahedron due to the different possible starting locations, the assembly of an octahedral arrangement requires either the formation of two triangles and their subsequent stacking (see Figure 4.9C), or a rearrangement of the polytetrahedral structure.
The capillary interactions that drive the reconfiguration are not only very strong but they are also long-ranged.[151,152] We are not aware of any predictions of the ground states of clusters of spheres interacting through capillary interactions, but presumably they are similar to the lowest energy state for spheres with long-ranged attractions, such as a Lennard-Jones 6-12 potential[140]. In this case, the ground states are the octahedron for N=6 and the pentagonal dipyramid (D_{5h}) for N=7. If the volume of the cluster-spanning droplet exceeds a critical value, capillary interactions can drive this rearrangement from the polytetrahedral state to the octahedron or pentagonal dipyramid.

Why do we observe the rearrangement only for rigid spheres? There are a number of possible explanations. The more crosslinked the seed particles are the better they resist deformation and disintegration by the organic liquid. They also protrude more from the droplet. This implies that they occupy less volume inside the droplet, which makes rearrangements already at a lower droplet volume possible. Furthermore, since rigid spheres likely experience less friction at their smaller contact areas than the soft spheres (Figure 4.2B and 4.2C), a rearrangement from the polytetrahedral to the octahedral state or pentagonal dipyramid should also be significantly easier with increasing crosslink density. Conversely, the strong deformation of the soft spheres in the presence of the confining droplet may impose additional geometric constraints that prevent rearrangement. Finally, the additional contribution from the elastic energy may render the polytetrahedral arrangement the state with the lowest energy for the softer spheres. Theoretical considerations or simulations may give conclusive insights.
Interestingly, we observed that particles with a higher crosslink density showed irregular features on the surface which impeded the reconfiguration process. We

found that the probability to find a not-fully reconfigured cluster increased with the crosslink density. For smooth spheres with cd=0.7% v/v this probability is only 1% and it increased to 8% and 12% for spheres with small (cd=4.3% v/v) and large (cd=8.3% v/v) surface irregularities, respectively. Still, when six rigid spheres do reconfigure, we always observed the octahedron.
That the reconfiguration pathway naturally leads to polytetrahedral arrangements can be exploited for creating particle with unusual patch arrangements. By tuning the deformability of the seed particles, we there were able to switch from patchy particles with six patches in an octahedral to a polytetrahedral arrangement.

4.4 Conclusions

A large variety of colloids can be formed by reconfiguration of random aggregates of deformable seed particles through capillary interactions. The final shape of the particles depends on the crosslink density of the seeds, since this influences the balance between interfacial energy and the shape-conserving forces due to particle rigidity. A quantitative analysis of dumbbell shape aspect ratio reveals that the deformation of the original spheres decreases with increasing crosslink density. Seed particles with a poorly crosslinked polymer network deform strongly during reconfiguration due to strong capillary forces that drive to minimize the interfacial energy between the water and the organic solvent. The resulting particles are spherical or slightly anisotropic. At higher crosslink densities well-defined patchy particles are obtained for clusters of N=1-5.
Interestingly, the deformability of the seed particles also influences the reconfiguration pathway for larger clusters, leading to distinct geometries. Clusters of six strongly deformable colloids arrange in the polytetrahedron, while rigid particles rearrange into the octahedron. For seven spheres, the rigid particles were found in pentagonal dipyramids, whereas the soft spheres only rarely achieve this structure since the number of pathways to form this geometry is lower compared to other configurations for N=7. We put forward that initial compaction leads to polytetrahedral configurations and that it can be followed by a rearrangement into the state of lowest energy driven by capillary interations. Geometric constraints, friction and the assembly path all are likely to affect the structure of the resulting patchy particles. The rigidity of the seeds is therefore a tool to guide the reconfiguration of the cluster to the desired structure.

CHAPTER 5

PATCHY PARTICLES OF VARIOUS SHAPES WITH DISTINCT PATCHES

Abstract

We fabricated complex patchy particles with distinct patches by applying the "colloidal recycling" method to binary mixtures of colloidal spheres. Aggregates constructed from the binary mixtures were reconfigured into patchy shapes by the addition of organic solvent. We combined spheres of different size and rigidity which yielded patchy particles of all permutations and therefore various shapes. The rigidity of the seeds influenced the final shape of the binary patchy particle, since soft spheres strongly deformed during reconfiguration whereas rigid spheres remained spherical. At low size ratio, 1.5, the geometry of the patchy particle was determined by the total number of spheres. At size ratio 4.6, the large spheres arranged in a compact geometry and the small particles positioned at the contact areas between these spheres. Large numbers of small spheres formed a 'jacket' around the cluster, where the patches of the small spheres introduced surface roughness at the center of the patchy particle. This yielded particles with both chemical and physical patchiness, which may be used for depletion induced self-assembly in the future.

5.1 Introduction

Functional materials can be realized by the bottom-up assembly of complex building blocks. Since patchy particles can be anisotropic in both shape and surface chemistry, these particles are in particular promising building blocks. Complex colloids with multiple patches are often formed by assembling a number of identical seed particles, such as colloidal spheres[25,153], Janus particles[137] or colloids with liquid protrusions[16], into larger structures. With our recently developed 'colloidal recycling' method we can fabricate patchy particles by recycling aggregates of uniform spheres.[138] The recycling involves the reconfiguration of aggregates induced by the addition of organic solvent. With this method a wide variety of patchy particles can be obtained by tuning experimental parameters such as colloid material, swelling agent and particle rigidity.[138,154]

By assembling non-identical seed particles into larger structures, colloids with different patch types and shapes can be realized. Although this is a promising approach to create complex particles, only a few examples are known where non-identical seeds are combined to form clusters with higher complexity. Ni *et al*. formed colloidal clusters consisting of two to four different spheres using a capillary-assisted assembly technique.[155] Using a template-based substrate the composition and the shape of these clusters could be controlled. However, since this template-based technique cannot be performed in bulk, low quantities were obtained. Cho *et al*. showed that colloidal clusters could be constructed from binary mixtures of spheres by evaporation of emulsion droplets containing a number of spheres. The spherical confinement and strong capillary forces acting on the spheres during evaporation bind the spheres into colloidal clusters of compact shapes.[134,156] Since all possible permutations could be formed, a wide variety of shapes was yielded. The geometry of these clusters was determined by the size ratio between the two seed types. At size ratio's ≥ 3, the geometry of the cluster was determined by the larger spheres whereas at size ratios ≤ 2 it was determined by both components. In all cases the geometries the same as those obtained for clusters of identical spheres. At a fixed number of spheres N, the dumbbell was formed for N=2, the triangle for N=3, the tetrahedron for N=4 and the triangular dipyramid for N=5. In particular particles with distinct and separated patches are highly promising for the bottom-up construction of materials, since the interaction between the patches can be localized and tuned by the size and location of the patches.[157]

We fabricated particles with distinct patches by employing the 'colloidal recycling' method to binary mixtures of colloidal spheres. The spheres differed in size and rigidity, which led to various shapes and patch compositions. Since soft spheres deformed during the reconfiguration process, but the rigid spheres

remained spherical, asymmetric shapes were obtained when the two were combined. We found at size ratio 1.5 that the geometry of the cluster was determined by the total number of spheres, whereas at size ratio 4.6 solely the larger spheres were involved. Interestingly, at size ratio 4.6, we formed particles that were both chemically and physically patchy.

5.2 Experimental Methods

Materials

Styrene ($\geq$99%, contains 4-tert-butylcatechol as inhibitor), divinylbenzene (DVB, technical grade 55%), azobisisobutyronitril (AIBN, $\geq$98%), hydroquinone (HQ, $\geq$99.5%), sodium dodecyl sulfate (SDS, $\geq$98.5%), vinyl acetate (contains 3-20 ppm hydroquinone as inhibitor), potassium peroxodisulfate (KPS, puriss. p.a. ACS reagent, $\geq$99.0%) and perylene (sublimed grade, $\geq$99.5%) were purchased from Sigma-Aldrich. Styrene was passed through an inhibitor remover column (Sigma-Aldrich) before use. Potassium chloride (>99% p.a.) was obtained from Fluka, Germany. The water used was deionized using a Millipore Filtration System (MilliQ Gradient A10), resulting in a resistivity of 18.2 MΩ·cm.
RITC dyed polystyrene spheres of 1.06 ± 0.06 µm with a crosslink density of 10% v/v were purchased from Magsphere Inc.

Methods

Synthesis of 1.6 μm sized polystyrene spheres Linear carboxylic acid functionalized polystyrene spheres of 1.05 ± 0.02 µm in diameter were synthesized by a surfactant free emulsion polymerization procedure[104]. The colloids were stored in water after filtration through glass wool and washing. To 13.5 mL of a 2.29% wt dispersion of these linear seeds, 0.05 g SDS, 0.034 g HQ and 1.7 mL crosslink solution was added to swell and crosslink the particles. The crosslink solution consisted of styrene with 2% wt AIBN, 2% v/v DVB and 15.78 mg perylene. Perylene was added during swelling to allow imaging by confocal microscopy. The mixtures were rotated for 24h on a tumbler at 20 rpm in the dark. Finally, the swollen colloids were polymerized in a 72°C preheated oil bath for 24h while being rotated at 100 rpm at a 45° angle. The polymerized colloids were washed and stored in water. The spheres had a smooth surface morphology and were 1.59 ± 0.07 μm in diameter with a crosslink density of 1.6% v/v (see Figure 5.1).

Synthesis of 0.2 μm sized polystyrene spheres Smaller polystyrene particles were synthesized according to an emulsion polymerization method developed by Mock *et al.*[110] Here, a solution containing 225 mL water, 0.25 g SDS and 21.15

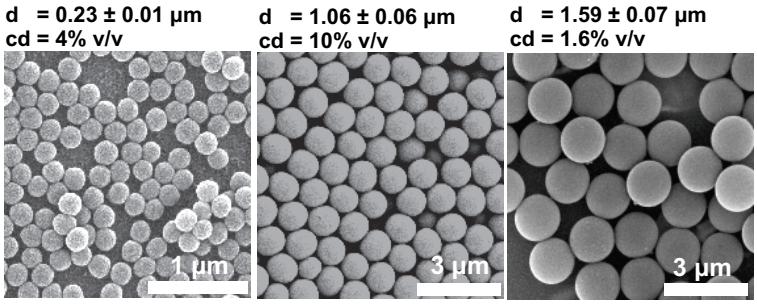


FIGURE 5.1: SEM micrographs of the polystyrene seed particles used in this study. The diameter and crosslink density are listed above the images.

g styrene with 0.97 mL DVB was heated for 1h in a 80°C oil bath under magnetic stirring, before polymerization was initiated by the addition of 0.78 g KPS in 38 mL water. The reaction was continued for 24h yielding 229 ± 8 nm particles with a crosslink density of 4% v/v. To increase the hydrophobicity of the particle surface and therefore the wetting angle of the particles with styrene, the polystyrene particles were coated with vinyl acetate. Here, 100 mL of this dispersion (7.66% wt) was heated in a 80°C oil bath under magnetic stirring for 45 min before a solution of 0.17 g KPS in 25 mL water was added. This was followed by the addition of 183 μL vinyl acetate every 15 min until a total volume of 732 μL (0.68 g) was added, leading to a surface coverage of 3.56 x 10^{-21} g/nm^2.[110] The reaction was stopped after 24h. A SEM micrograph of the colloids is shown in Figure 5.1

Formation of patchy particles Patchy particles were prepared using the 'colloidal-recycling' method.[138] We first formed random aggregates by diffusion limited aggregation of charge-stabilized colloidal spheres. Aggregates of spheres with size ratio 1.5 were formed by adding 100 μL of a 2M potassium chloride solution to a mixture of 60 μL of 1.59 μm (2.9% wt) and 40 μL 1.06 μm polystyrene particles. After an aggregation time, t_a = 6 min, the aggregates were quenched with 20 mL water. For size ratio 4.6, 60 μL of a 2M potassium chloride solution was added to 40 μL of the 1.06 μm sized colloids (1.8% wt) for t_a = 5 min followed by the addition of 40 μL of 229 nm particles (0.3% wt). The total t_a before quenching was 9 min. The aggregates were reconfigured into compact patchy particles by the addition of organic solvent: To 5 mL of the quenched dispersion, 10 μL of aqueous SDS solution (10% wt) and 10 μL of reconfiguration solution, consisting of styrene with 1.5% v/v DVB and 2% wt AIBN, was added. The dispersion was magnetically stirred for 24h to complete reconfiguration of the aggregates. The obtained patchy particles were polymerized for 24h in a preheated oil bath at 80°C. The particles were washed and stored in water.

Imaging and analysis The synthesized polystyrene seed particles and polymerized patchy particles were imaged using a FEI nanoSEM scanning electron microscope (SEM) at 80 kV. The size of the polystyrene seed particles was determined by measuring the circumference of >100 particles in SEM micrographs with ImageJ. The aggregates of the binary mixtures were studied with a Nikon Eclipse Ti microscope with an AIR confocal scan head with a 100x oil immersion objective (NA = 1.4). The 1.06 μm Magsphere particles and the 1.59 μm polystyrene spheres with a crosslink density of 1.59% v/v, were excited with a laser wavelength of 405 or 561 nm, resulting in blue and red fluorescence, respectively.

5.3 Results and Discussion

With the 'colloidal recycling' method randomly shaped aggregates of colloidal spheres are reconfigured into compact shapes by the addition of organic solvent. We have thoroughly investigated the reconfiguration mechanism and the shapes obtained after reconfiguration for aggregates of identical seed particles.[138,154] Well-defined structures were formed for a fixed number of spheres in the cluster, N, for N<6. The geometries obtained include the dumbbell for N=2, triangle for N=3, tetrahedron for N=4 and the triangular dipyramid for N=5. For aggregates of six or more identical spheres the geometry obtained after reconfiguration was determined by the deformability of the seeds.[154] While six soft spheres reconfigured to the polytetrahedron, six rigid spheres assembled into an octahedron. We found that the reconfiguration pathway was largely influenced by confinement of the cluster and geometric contraints.
Our understanding of the reconfiguration mechanism and of the shapes formed by clusters of identical colloids motivated us to explore the colloidal recycling method further using binary mixtures of seeds. The binary mixtures contained spherical colloids of different sizes and with different particle rigidity yielding patchy particles with distinct patches.

5.3.1 Patchy particles of soft and rigid spheres, size ratio 1.5

We applied the colloidal recycling method to mixtures of soft and rigid spheres to obtain particles with distinct patches and shapes. The rigidity of the seed particles was controlled by the crosslink density (cd) of the polystyrene colloids. We previously showed that the final shape of reconfigured clusters depends on the crosslink density of the seed particles.[154] Spheres with low crosslink density (cd$\leq$0.5% v/v) were strongly deformed during reconfiguration by capillary forces, resulting in complete or partial merging of the seeds in the covering droplet. More densely crosslinked seeds reconfigured into patchy particles and the deformation of the spheres decreased with increasing crosslink density.

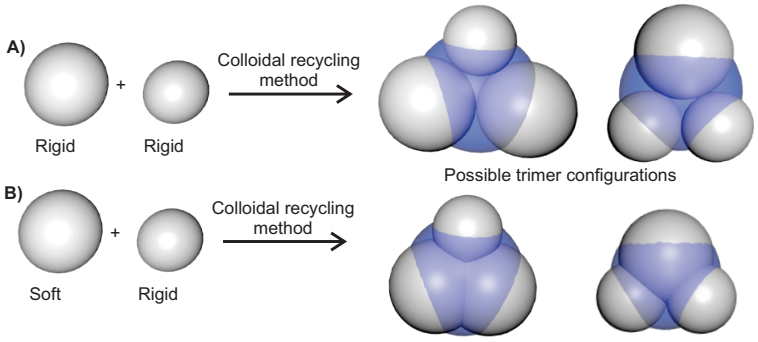


FIGURE 5.2: Illustration of patchy trimers that can be constructed from two seed types with size ratio 1.5. A) Rigid seed particles are not deformed by the capillary forces during reconfiguration, resulting in patchy particle shapes solely determined by the size ratio between the particles. B) By combining soft and rigid seeds the final shape of the patchy particle will be more compact compared to clusters of rigid spheres, since the soft spheres can be deformed by the capillary forces during reconfiguration.

We here employed a binary mixture of polystyrene spheres of 1.06 μm and 1.59 μm in diameter with cd = 10 and 1.6% v/v, respectively. This resulted in a size ratio of 1.5 and a crosslink density ratio of 6.3. If both sphere types would not deform during deformation, the shape of the reconfigured cluster would solely be determined by the size ratio between the particles, see Figure 5.2A. However, if the crosslink density of the larger spheres (cd=1.6% v/v) is insufficient to resist shape deformation induced by the capillary forces, the reconfigured shapes will be more compact (see Figure 5.2B).

Aggregates constructed from both colloid types were formed by exposing the binary mixture of charge-stabilized spheres to a 1M potassium chloride solution for several minutes. The aggregates obtained were of random shape and both components could be distinguished by size with bright field microscopy (see Figure 5.3A). The two seed particle types could also be recognized with confocal microscopy, which was possible since the 1.59 μm and 1.06 μm particles were provided with perylene and rhodamine dye, resulting in blue and red emitting particles, respectively. The confocal microscopy image in Figure 5.3B shows that the two seed types are uniformaly distributed over the aggregates.
After addition of organic solvent, the aggregates reconfigured into compact shapes of different sizes (Figure 5.3C). The reconfigured shapes were examined using high resolution SEM micrographs, where the two seed types could be distinguished by size. For patchy particles constructed from both seed particles different compositions and shapes were observed. The geometries of the

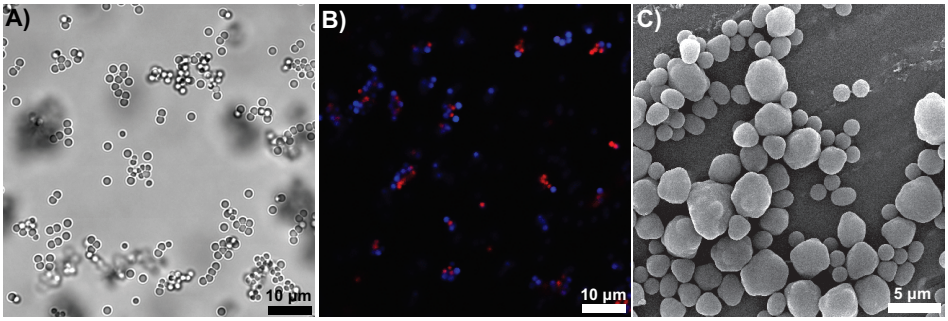


FIGURE 5.3: Applying the colloidal recycling method to a mixture of 1.06 μm polystyrene particles with cd = 10% v/v and 1.59 μm particles with cd = 1.6% v/v (size ratio of 1.5 and a crosslink density ratio of 6.3). A) Bright field microscopy image of randomly shaped aggregates after destabilization of the spheres. B) Confocal microscopy image of the aggregates with the 1.06 μm particles in red and the 1.6 μm seeds in blue. C) SEM micrograph of the reconfigured clusters obtained after reconfiguration and polymerization. Compact patchy shapes are formed of different sizes.

reconfigured clusters were set by both the 1.06 μm and the 1.59 μm spheres and depended on the total number of seeds in the cluster, N. For small patchy particles of N=2 this resulted in assymmetric dumbbells (Figure 5.4A) and aggregates of N=3 reconfigured into triangular shapes formed by two soft and one rigid seed or one soft and two rigid seeds (Figure 5.4B). Aggregates of N=4 yielded the tetrahedron shape (see Figure 5.4C for one permutation). Clusters of five spheres of any permutation reconfigured to triagular dipyramid structures (see Figure 5.4D for one permutation). For clusters of N>5 several three-dimensional shapes where observed where not all original seed particles could be unambiqiously identified from SEM micrographs (Figure 5.4E).

Reconstruction of the spherical seed particles (shown as overlayed on the bottom SEM micrographs in Figure 5.4) shows that the large spheres were partly deformed during reconfiguration while the smaller rigid particles remained spherical (see Figure 5.2). This is in agreement with our previous experiments where we found that the deformability of the seeds by capillary forces decreased with increasing crosslink density. Here, polystyrene spheres with cd = 10% v/v barely deformed.[154]
The geometries for clusters of N=2-5 are similar to those observed for identical spheres. Due to the difference in size and particle rigidity in the binary mixture a larger variety of shapes is observed compared to one-component systems. For colloidal clusters of binary mixtures with size ratio 1.5, formed using an emulsion based droplet evaporation technique, also geometries similar to one-component systems were observed.[156] Since Cho *et al*. used non-deformable spheres less

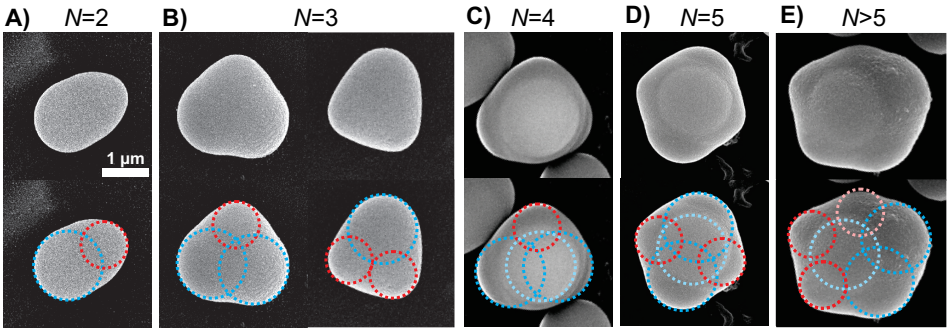


FIGURE 5.4: SEM micrographs of patchy particles constructed by 1.59 μm (cd=1.6% v/v) and 1.06 μm (cd=10% v/v) seed particles. Below the images a reconstruction of the spherical seed particles is shown. A) Asymmetric dumbbell constructed from one large and one small particle. B) The clusters of N=3 reconfigured to triangular shapes and consist of either two large and one small particle or one small and two large particles. C) Tetrahedron particle constructed by three large and one small sphere. D) Pentagonal dipyramid formed by three large and two small particles. E) Example of a cluster consisting of N>5 spheres. Reconstruction of the spherical seed particles indicates that the large spheres strongly deformed, whereas the smaller rigid particles maintaned their spherical sphape.

compact shapes were obtained. Besides the rigidity of the spheres another important difference with our results is the absence of the cluster-spanning droplet. With droplet evaporation techniques the cluster-spanning droplet is completely evaporated, while with the colloidal recycling method the organic droplet remains and is polymerized. The polystyrene spheres also have a preferred wetting angle with the droplet. These factors together with geometric constraints due to an increased contact area between deformed spheres influence the reconfiguration pathway. The patchy particles obtained at size ratio 1.5 have distinct and separated patches. Self-assembly of these complex particles could lead to novel structures.

5.3.2 Patchy particles with chemical and physical patchiness, size ratio 4.6

We examined the shapes obtained after reconfiguration of aggregates of binary mixtures with size ratio 4.6. This was achieved by applying the colloidal recycling method to a binary mixture of 0.23 μm (cd = 4% v/v) and 1.06 μm (cd=10% v/v) polystyrene particles. Since the crosslink density of both seed types was larger than 4% v/v we expect little deformation of the spheres during reconfiguration.[154]

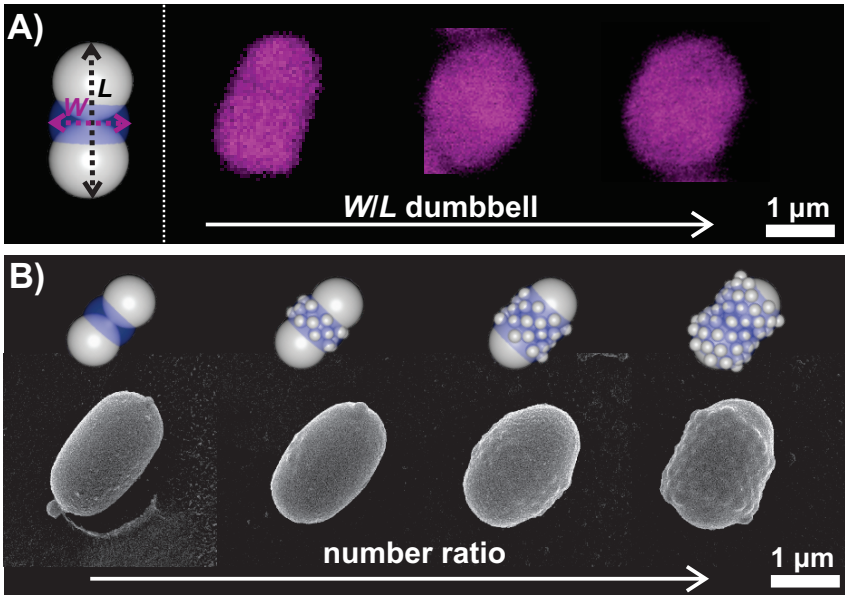


FIGURE 5.5: Dumbbell patchy particles consisting of two 1.06 μm spheres and various 0.23 μm spheres. A) Confocal microscopy images of dumbbell particles shaped from two 1.06 μm spheres with similar dumbbell lengths, but different dumbbell widths. B) SEM micrographs of dumbbells, where 0.23 μm spheres are positioned at the contact area between the large spheres. The width of the dumbbell increases with increasing number of 0.23 μm particles. At large number ratios the 0.23 μm particles arrange on an ordered lattice forming a 'jacket' around the dumbbell.

Aggregates of the 0.23 μm and 1.06 μm spheres were formed by exposing the binary mixture to a 1M potassium chloride solution for a total aggregation time of nine minutes. The composition of the aggregates could not be imaged with optical microscopy, since the 0.23 μm particles are at the diffraction limit of optical microscopy. The larger 1.06 μm spheres could be imaged in both bright field as well as confocal mode due to the rhodamine molecules incorporated in the colloids. Since the rhodamine was non-covalently bound to the 1.06 μm polystyrene particles, the dye-molecules could easily migrate to the organic solvent and smaller particles during reconfiguration. These migrated dye-molecules provided us with additional information on the shape of the reconfigured clusters.

Clusters of two 1.06 μm spheres formed dumbbells with similar dumbbell lengths but divergent widths, see Figure 5.5A. These results differ from one-component systems where uniform shapes were formed with a maximum polydispersity of

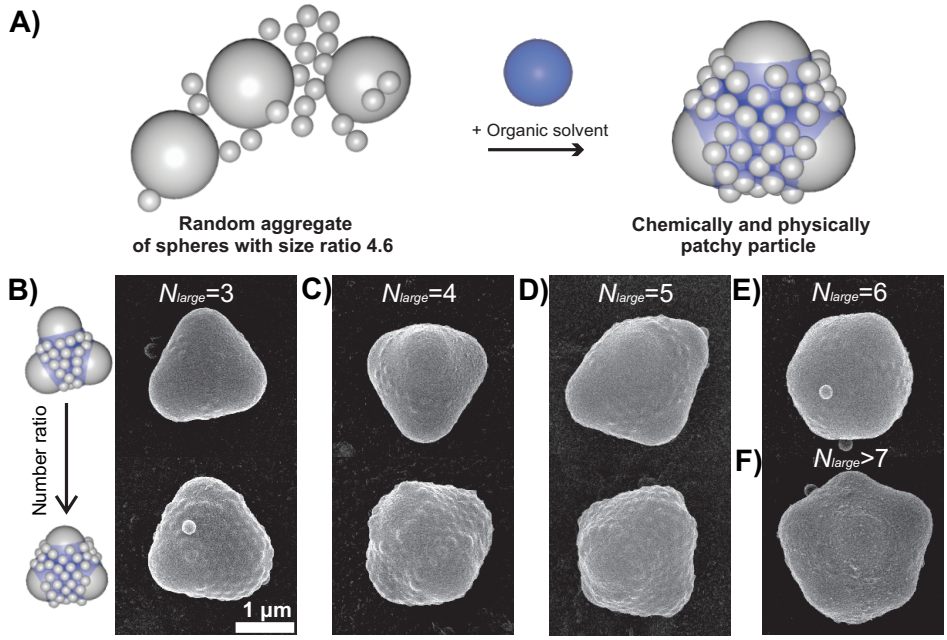


FIGURE 5.6: Chemically and physically patchy particles. A) Illustration of the reconfiguration of an aggregate consisting of spheres with size ratio 4.6. Reconfiguration is induced by the addition of organic solvent. The number of larger spheres, N_{large}, determines the geometry of the patchy particle resulting in the triangle at N_{large}=3, the tetrahedron at N_{large}=4, the triangular dipyramid at N_{large}=5 and the octahedron at N_{large}=6. The small particles position at the contact areas of the larger spheres and determine the final shape of the patchy particle. At large number ratios, the small particles arrange in an hexagonal pattern forming a 'jacket' around the cluster of 1.06 μm spheres. Since the protruding particles introduce surface roughness, the patchy particles own both chemical and physical patchiness.

6% in the length over width ratio (L/W) of dumbbells.[154] Analysis of high resolution SEM micrographs of dumbbell particles revealed that the small spheres all positioned close to the contact area between the larger spheres (see Figure 5.5B). At a given swelling ratio, the width of the dumbbells is therefore influenced by the number ratio between the small and large spheres, where the width increases with increasing number ratio. Large numbers of small particles arranged in a regular pattern forming a 'jacket' around the dumbbell. The patches originating from the small and the large spheres differ in both size and surface chemistry.
At size ratio 4.6, we found that the overall geometry of patchy particles of N>2 was determined solely by the number of 1.06 μm spheres, N_{large}. Similar to one-

component systems of rigid spheres, triangles were formed for N_{large}=3, tetrahedrons for N_{large}=4, the pentagonal dipyramid for N_{large}=5 and the octahedron for N_{large}=6 (Figure 5.6). The geometry of the larger spheres was not influenced by the smaller particles which accumulated at the contact areas between the larger spheres. Similar findings were obtained by Cho *et al*. for colloidal clusters of binary mixtures with size ratio's ≤ 3.[134,156] In our case, patchy particles are formed with both sphere types partly immersed in the cluster spanning droplet. The small spheres determined the exact shape of the patchy particles. At high number ratios, the small particles form an ordered hexagonal pattern at the center of the cluster of larger spheres. The patches of the large particles are especially well-pronounced on these 'jacketed' patchy particles. Additionally, the protruding part of the small particles introduce roughness on the surface of the polymerized droplet. This results in a difference in surface roughness between the patches and the body of the patchy particle, which can be used for depletion induced self-assembly.[29] These particles are therefore both chemically and physically patchy.

The patchy shapes obtained with the colloidal recycling method are not only determined by the size ratio between the particles, but also by the crosslink density and the wetting properties of the spheres. We were therefore able to form a variety of patchy particle shapes with distint patches.

5.4 Conclusions

The colloidal recycling method was used to form particles with distinct patches. This was achieved by employing binary mixtures of colloidal spheres of different size and particle rigidity. Various patchy shapes were formed, since all permutations were possible. At size ratio 1.5, the geometry of the reconfigured clusters was set by both the larger and the smaller particles. Since the larger spheres had a low crosslink density, these particles strongly deformed during reconfiguration. The resulting shapes were therefore more compact compared to clusters of rigid spheres. The geometries obtained were similar to one-component systems and to binary colloidal clusters formed via droplet evaporation methods.
Patchy particles with increased complexity were formed by mixing two types of rigid seed particles with size ratio 4.6. The shapes obtained have patches of different sizes and with different surface chemistry. The larger seeds determined the overall geometry and the small particles positioned at the contact areas between the larger spheres. At high number ratios, the small particles formed a 'jacket' around the clusters. The 'jacket' consisted of the polymerized droplet with the protruding part of the small spheres, which introduced a difference in surface roughness between the body and the patches. These advanced patchy particles are therefore both chemically and physically patchy and may act as complex building blocks for functional materials.

CHAPTER 6

ANISOTROPIC DISTORTIONS IN HEXAGONAL CRYSTALS AT FLUID INTERFACES

Abstract

Defects in colloidal crystals can be induced by a vacancy, interstitual, or by impurities and influence crystal properties such as the mechanical strength and orientation of the crystal. We here investigated how elongated particles distort the hexagonal order in a crystal of repulsive pMMA spheres at a fluid interface. The impurities are dumbbells constructed from two pMMA spheres, with different distances between the two spheres s_{DB}. Our study revealed that the number of nearest neighbors increased with s_{DB} from six to eight spheres. We analyzed both the orientation of the dumbbell with respect to the crystal orientation and the position of the surrounding spheres with respect to the dumbbell orientation. The preferred orientation of the dumbbell depended on the lattice spacing and s_{DB}. In crystals with large lattice spacings no preferred orientation was observed. At short lattice spacings dumbbells with seven and eight nearest neighbors preferentially aligned parallel to the crystal orientation whereas at six nearest neighbors a preferential orientation of 30° with the crystal orientation was measured. The repulsive interaction of the dumbbell with the surrounding spheres restricted the rotational motion of the dumbbell. Positional information of the surrounding spheres showed that all dumbbells anisotropically distorted the hexagonal order in the crystal and that the position of the neighboring spheres depended on the orientation of the dumbbell. Dumbbells with $s_{DB} = 1.03 \pm 0.19\ d$, where d is the diameter of the spheres, occupied one lattice site in the hexagonal crystal and distorted the positional order of the neighboring spheres only locally. Dumbbells with $s_{DB} = 1.27 \pm 0.14\ d$ were surrounded by seven nearest neighbors and distorted the translational order in the crystal by the insertion of two semi-infinite rows in the crystal. Dumbbells with $s_{DB} = 1.42 \pm 0.17\ d$ and eight nearest neighbors occupied two lattice sites and the hexagonal crystal was distorted only locally.

6.1 Introduction

The presence of defects is inevitable in colloidal crystals. Defects distort the structural order of colloids either locally by point defects such as vacancies or interstitials resulting in disclinations and dislocations, or by larger defects such as grain boundaries.[158] These imperfections can influence the mechanical strength of the crystal[159], change the crystal growth direction[160], enhance or deteriorate photonic properties[161,162] and induce melting[163]. The origin of a defect can either be a particle not positioned at a lattice site resulting in a point defect[164], curvature of the substrate inducing topological defects[37,165–168], or the interference of impurities or dopants[34].
Spherical impurities are observed to frustrate the crystal, inhibit crystal growth[34] and influence the segregation of grain boundaries[169]. By doping a crystal of spheres with dumbbells, consisting of two connected spheres, the dumbbells formed dislocation cages which influenced the dislocation dynamics.[38,39] Whereas in crystals of spheres the dislocation motion is unrestricted, the steric restriction of two connected spheres resulted in glassy dynamics. Anisotropic impurities could therefore be promising dopants to tune mechanical or physical properties of the crystal such as the crystallization dynamics and mechanical strength. Additionally, the influence of anisotropic impurities on crystals is relevant for understanding virus-capsid formation where anisotropically shaped defects are observed in immature virus particles.[170]

We studied how hexagonal crystals of highly repulsive spheres were distorted by dumbbell impurities of different dimensions. We formed colloidal crystals on a flat interface between an aqueous and an organic phase, to investigate both the structural order in the crystal as well as the dynamic behavior of the dumbbells with confocal microscopy. The dumbbells distorted the hexagonal order of the surrounding spheres anisotropically and the nature of the defects induced by the impurities depended on the distance between the two spheres forming the dumbbell, the orientation of the dumbbell and the degree of confinement at the interface. We also show that the anisotropic landscape around the dumbbell leads to a preferred dumbbell orientation at short lattice spacings.

6.2 Experimental Methods

Materials

Methacrylic acid (MA, 99.8% extra pure, stabilized), Cyclohexyl bromide (CHB, 99%, purified by filtering through activated alumina adsorbents), Glycerol (99+%), N,N-Dimethylethanolamine (99%) and dodecane (mixture of isomers) were purchased from Acros Organics. The cis-decahycronaphtalene (cis-decalin, 99%), octyl mercaptan($\geq$98.5%), ethanol (96%), ethylene glycol dimethacrylate (EGDM, 98%), methyl methacrylate (MM, 99%, contains $\leq$30 ppm MEHA as inhibitor), 2,2'-Azobis(2-methyl-propionitrile) (AIBN, $\geq$98%), N,N-Dimethylformamide ($\geq$99.8%) and rhodamine B isothiocyanate (RITC, mixed isomers) were purchased from Sigma-Aldrich. Exxson mobil chemical kindly provided Exxsol D120 ($\geq$98%) and 4-aminostyrene was purchased from Alfa Aesar. For stabilization of the pMMA spheres a poly(12-hydrostearic acid) graft polymer (PHS-g-pMMA, 45% solution in a 2:1 (w/w) ethyl acetate/butyl acetate mixture) was synthesized.[171,172] The water used was deionized using a Millipore Filtration System (MilliQ Gradient A10), resulting in a resistivity of 18.2 MΩ·cm.

Methods

Synthesis of core-shell pMMA spheres pMMA spheres of 2.00 ± 0.05 μm in diameter with a fluorescent core, a non-fluorescent shell (10 nm) and a crosslink density of 2% wt were synthesized according to a dispersion polymerization method developed R.P.A. Dullens *et al.*[171] and adjusted by M.T. Elesser *et al.*[172,173].

Preparation rhodamine aminostyrene To image the pMMA colloids with confocal microscopy rhodamine aminostyrene (RAS) was bound covalently to the pMMA particles during synthesis. This dye was prepared by dissolving 73.25 mg RITC in 9.77 g DMF, followed by the addition of 75 μL 4-aminostyrene. After 10 minutes of stirring the mixture was transferred to a 50 mL round bottom flask and connected to a rotation evaporator (Buchi rotavapor R-210). The reaction flask was placed in a preheated 40°C waterbath and stirred at 30 rpm at a 45° angle. The solvent was gradually removed from the reaction mixture by maintaining the pressure at 0.06 mbar for 3.5 days using an Edwards RV3 vacuum pump. The purple solid product (RAS) was stored at -20°C.

Preparation monomer solution To a 9.5 g solution of MM:MA (49:1) 0.0102 g of RAS dissolved in 0.310 g acetone was added. This mixture was placed in the ultrasonic bath for several minutes and vortexed for 1h. Subsequently, the mixture was filtrated using a 0.45 μm PTFE Whatman filter to remove undissolved dye, yielding the filtrated monomer solution.

Synthesis fluorescent pMMA cores The synthesis was performed in a round bottom reaction flask which was placed in a preheated oil bath (83°C), connected to a 16°C cooler and brought under a nitrogen atmosphere. To the reaction flask a mixture of 10.32 g of hexane:ExxsolD120 (2:1), the filtrated monomer solution, 0.103 g AIBN, 71.4 μL octyl mercaptan and 1.03 g PHS-g-pMMA was added under magnetic stirring at 280 rpm. After six minutes a blue glow appeared in the reaction mixture, indicating pMMA nuclei had formed. Immediately after this observation a crosslink solution containing 3.32 g hexane:ExxsolD120 (2:1) and 190 μL of EGDM was added gradually to the reaction mixture; 10 min at 20 μL/min followed by 28 min at 56 μL/min. After addition of the crosslink solution the reaction mixture was stirred for another 2h in the oil bath. The obtained pMMA cores were washed and transferred to dodecane.
Covalent binding of the PHS-g-pMMA stabilizer molecules to the colloids was achieved by a locking procedure. This procedure was also performed after the shell formation. Covalent binding was achieved by transferring the pMMA colloids in dodecane to a round bottom flask which was placed in a preheated oil bath (130°C), connected to a 16°C cooler and kept at a constant nitrogen atmosphere. The dispersion was magnetically stirred at 280 rpm and when the temperature of the dispersion reached 120°C DMAE (0.2 wt% with respect to the dispersion) was added. The reaction mixture was stirred for another 2h. The resulting pMMA cores were 1.80 ± 0.06 μm in diameter (see Figure 6.1A).

Shell growth A non-fluorescent shell was grown around the fluorescent pMMA cores to improve particle tracking in confocal microscopy images. The reaction was performed in a round bottom flask placed in a preheated oil bath (83°C), connected to a 16°C cooler while kept under nitrogen atmosphere. To this flask 8.42 g of pMMA cores in hexane:ExxsolD120 (1:1), 0.03368 g AIBN (2%wt with respect to monomer) and 0.113 g octyl mercaptan (4%wt with respect to momomer) were added while magnetically stirring at 300 rpm. After a few minutes of stirring a mixture containing 3.11 g hexane:ExxsolD120 (1:1), 2.83 g MM:MA (49:1), 0.0707 g EGDM, 0.02836 g AIBN (0.4%wt with respect to total syringe volume), 0.014 g octyl mercaptan and 0.014 g PHS-g-pMMA was slowly added over the course of 30 min at 273 μL/min. After addition the reaction was stirred for another hour in the oil bath before cooling down. The procedure to covalently bind the stabilizer molecules to the particles was repeated and the obtained core-shell particles were 2.00 ± 0.05 μm in diameter (Figure 6.1B and 6.1C).

Setup for a flat fluid interface A flat interface between two liquids was formed using a specially designed interface setup (Figure 6.2). The details of this setup are based on the design of the interface cell of Aveyard *et al.*[174] and have been further developed by D. ten Napel *et al.*[175]. Here, a aluminum-Teflon ring was inserted into a glass holder, the outer ring. Since aqueous solvents have a high

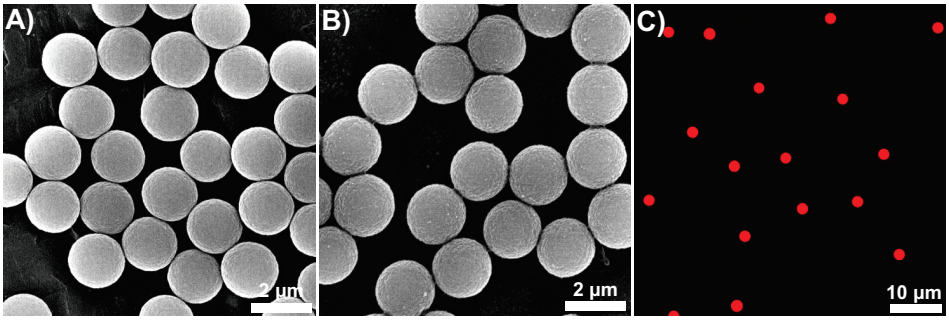


FIGURE 6.1: SEM micrographs of A) fluorescent pMMA cores of 1.80 ± 0.06 μm in diameter and B) pMMA core-shell particles of 2.00 ± 0.05 μm in diameter. C) Confocal microscopy image of the pMMA core-shell particles.

affinity for aluminum and organic solvents for Teflon, the interface between the two solvents aligned with the Teflon-aluminum transition in the ring. By adjusting the volumes of the two liquids a flat interface could be created at this transition. In our setup the outside of the ring consisted of aluminum, whereas the inside had an aluminum and a Teflon part. Small aluminum legs allowed the adjustment of the height of the aqueous liquid inside the ring. The aluminum-Teflon interface inside the ring was positioned at 1 mm from the bottom of the glass coverslip. To image the interface with confocal microscopy an 60x magnification objective (NA = 0.70), with a working distance of 2.6 - 1.8 mm was used. An illustration of the interface cell and a cross section of the setup are shown in Figure 6.2A and B, respectively.
To form a flat fluid interface 1 mL of glycerol:water (85:15 w/w) was added to the glass holder, followed by the placement of the aluminum-Teflon ring. Another 0.3-0.4 mL of glycerol:water (85:15 w/w) was added until the aluminum part on the inside of the ring was completely wetted. On top of the aqueous layer 0.3-0.4 mL of CHB:cis-decalin (70:30 w/w) was deposited forming a flat interface between the two liquid phases. Finally, 40 μL of a 0.08-0.20 wt% pMMA colloid dispersion in CHB:cis-decalin (70:30 w/w) was gently added on top of the organic layer. The setup was covered with a glass cover which was sealed with grease (Apiezon grease M) to close the system and avoid evaporation. The sample was imaged one to three days after preparation to allow the interface to saturate with particles.

Imaging and analysis The synthesized pMMA particles were imaged using a FEI nanoSEM scanning electron microscope (SEM) at 80 kV. The diameter of the pMMA cores and core-shell particles was determined by measuring the circumference of >100 particles in SEM micrographs with ImageJ.

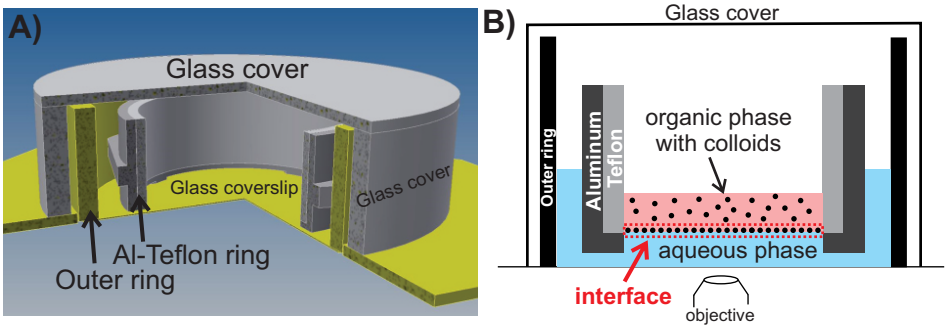


FIGURE 6.2: A) Illustration of the interface cell used to form a flat interface between an aqueous and an organic liquid. B) Cross section of the interface setup. The aqueous liquid has affinity for the aluminum part of the ring, while the organic liquid has affinity for the Teflon part. The interface will therefore be pinned at the transition between these two materials on the inside of the ring forming a flat interface. The interface is positioned at 1 mm from the bottom of the coverslip and the system is closed by a glass cover to avoid evaporation of the solvents.

The ordering of pMMA colloids at the flat interfaces was studied using a Nikon Eclipse Ti microscope. The microscope was equipped with an A1R confocal scan head and a CFI S Plan Fluor ELWD 60x C with a working distance of 2.6 - 1.8 mm and NA = 0.70. The RAS dyed cores of the pMMA spheres were excited with a laser wavelength of 561 nm and detected at 625 nm.
The coordinates and centers of mass of the particles in confocal images were determined using a Python implementation of the Crocker and Grier algorithm, TrackPy.[176,177] The anisotropic impurities were analyzed using a different implementation of this algoritm that accounts for the bias due to overlapping particle signals.[178] The crystal orientation α was measured manually by connecting the centers of mass of at least ten spheres along a crystal axis.

6.3 Results and Discussion

6.3.1 Ordering of repulsive spheres at a flat fluid interface

To determine the effect of anisotropic particles on a crystal of repulsive spheres at a fluid interface, we first analyzed the ordering of merely spheres. To exclude curvature effects on the motion and positioning of the particles in the crystal a special interface cell was used to yield a flat interface between CHB:cis-decalin (70:30 w/w) and glycerol:water (85:15 w/w) (see Figure 6.2). pMMA spheres of 2.00 ± 0.05 μm in diameter were dispersed in the organic liquid which was deposited on top of the aqueous phase. After an equilibration time of one to three

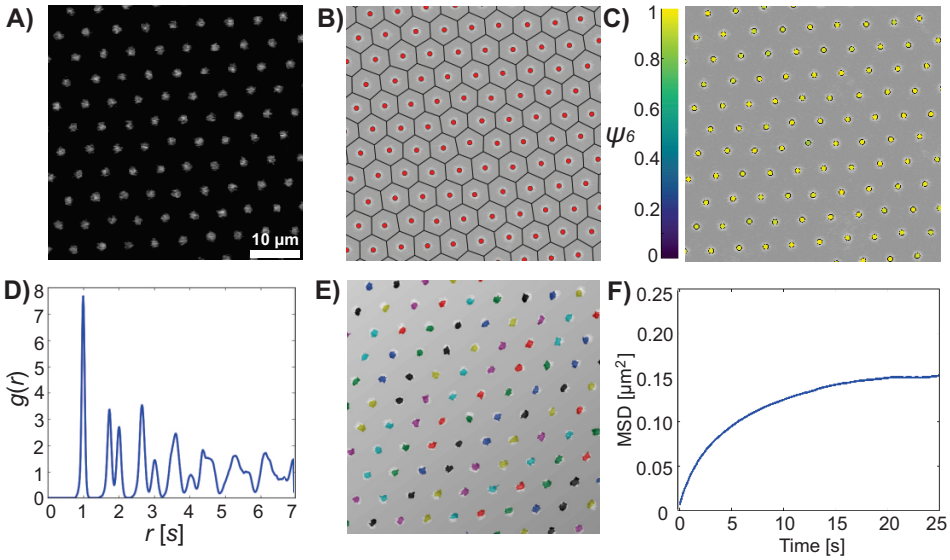


FIGURE 6.3: Ordering of repulsive pMMA spheres at a flat fluid interface. A) Confocal microscopy image of pMMA spheres of 2.00 ± 0.05 μm in diameter d bound to the interface between an CHB:cis-decalin (70:30 w/w) and a glycerol:water (85:15 w/w) phase. B) Voronoi diagram showing that all particles in (A) have six nearest neighbors and no disclinations are formed. C) The hexagonal bond order parameter, $|\psi_6|$, has values close to 1 for all particles, indicating that the spheres are ordered on an hexagonal lattice. D) The radial distribution function ($g(r)$) of the spheres collected from 1800 measurements in one minute. The peaks at large radial distances indicate that the hexagonal order ranges to distances of 7s, where s is the average lattice spacing in the crystal, $s = 2.73d$. The peak at 1s originates from the six NNs of the spheres. E) The trajectories that the colloids in (A) travelled in one minute (1800 measurements). The motion of the spheres is confined to a single lattice site in the crystal. F) The mean square displacement (MSD) of the spheres levels off at 20 s at 0.15 μm^2 confirming that the translational motion of the particles is restricted.

days spheres were observed both at the interface as well as in the upper organic phase. The non-adsorbed particles diffused in three dimensions, while the interfacially bound pMMA spheres moved in the two dimensions of the interfacial plane only. Interparticle distances of several times the diameter of the spheres were observed, induced by the strong Coulomb repulsions between the charged particles. The average interparticle distance between the spheres in bulk was at least two times larger compared to the interfacially bound spheres. This effect has been attributed to the presence of mirror charges originating from ions in the aqueous phase that screen the charge of the interfacially bound pMMA spheres, resulting in an additional Coulomb attraction[30,179,180].

The interfacially bound pMMA spheres positioned in a regular hexagonal pattern (see Figure 6.3A). The Voronoi diagram of this pattern shows that all particles are surrounded by six nearest neighbors (NNs), see Figure 6.3B. The local structural ordering of the crystal was analyzed by calculating the hexagonal bond order parameter ψ_6, which is defined as:

$$\psi_{6,j} = \frac{1}{N} \sum_{k=1}^{N} e^{6i\theta_{jk}}, \tag{6.1}$$

where N refers to the number of nearest neighbors of particle j and θ_{jk} is the angle between a fixed reference axis and the vector between particle j and neighbor particle k. The absolute value of ψ_6 is an indication of the local hexagonal crystallinity and ranges from 0 to 1, with $|\psi_6|$=1 for perfect hexagonal symmetry. The spheres at the fluid interface have $|\psi_6|$-values close to 1 indicating that the spheres arrange on a hexagonal lattice, see Figure 6.3C.
Positional information was obtained from the radial distibution function, which is defined as:

$$g(r) = \rho \cdot 2\pi r dr \tag{6.2}$$

where ρ is the average particle density in a $2\pi r$ shell with shell thickness dr at a distance r from the center of mass (COM) of the particles. The $g(r)$ shown in Figure 6.3D is constructed from the particle positions extracted from 1800 measurements collected over one minute. Peaks in $g(r)$ are observed up to a distance r of at least seven times the average interparticle distance s between the spheres. Although the spheres are free to diffuse at the interface, the trajectories of the spheres (Figure 6.3E) display that this translational motion is restricted to a lattice site. This is confirmed by the mean square displacement (MSD) of the spheres over time, Figure 6.3F, where the MSD levels off around 20 s at 0.15 μm^2. The degree of confinement is determined by the range of the repulsive and attractive Coulomb forces and depends on the colloid density at the interface.[174,181]

6.3.2 Impurities at a flat fluid interface

Besides individual spheres, impurities were also found at the fluid interface. We classified these impurities into three different classes. The first class includes spherical objects with sizes significantly smaller (Figure 6.4A) or larger (Figure 6.4B) than the diameter, d, of the particles. These objects are side products formed during the synthesis of the pMMA spheres. The effect of the large spherical impurities on the crystal growth of colloidal spheres was studied by Villeneuve *et al.* who found that impurities induce the formation of grain boundaries and inhibit crystal growth.[34] The second type of impurities are circular patterns of spheres with short interparticle distances (Figure 6.4C). These spherical shells are cross-sections of likely aqueous droplets stabilized by colloids in the organic phase

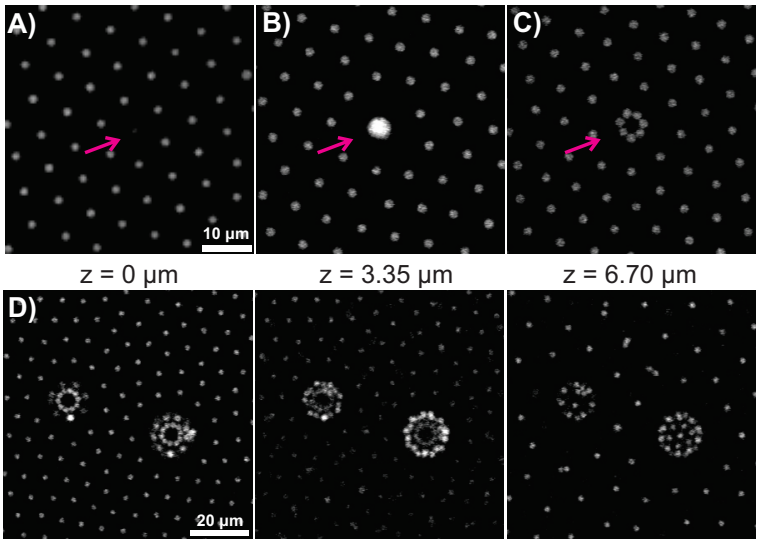


FIGURE 6.4: Confocal microscopy images of spherical and circular impurities observed at an organic-aqueous fluid interface. Spherical particles with a diameter significantly smaller (A) or larger (B) than the average diameter of the spheres. C) Circular structures of particles with short interparticle distances. These patterns are cross-sections of droplets stabilized by pMMA spheres in the organic phase as shown in (D), where z corresponds to the height of the plane in the third dimension with z=0 μm at the interface.

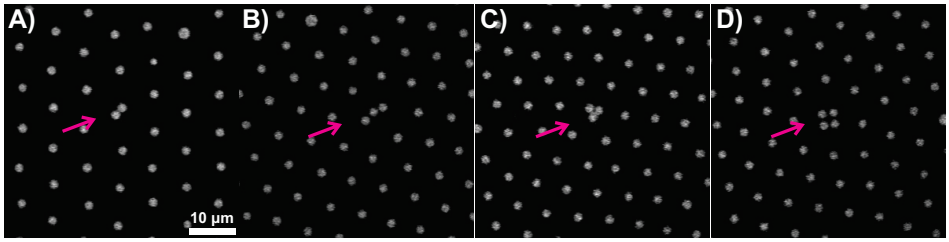


FIGURE 6.5: Confocal microscopy images of anisotropic impurities observed in the two-dimensional crystal of hexagonally ordered repulsive pMMA spheres at the fluid interface. C-F) Anisotropic defects assembled by several spheres such as; chain-like structures(C), dumbbells(D), triangles(E) and squares(F).

(Figure 6.4D). The number of these defects increased with time and temperature, probably due to evaporation and condensation within the interface cell.
In this study we are mostly interested in the third class of impurities; anisotropic mesostructures formed by the assembly of individual spheres with interparticle distances « s. Dumbbell shapes were formed by two spheres (Figure 6.5A), but

different shapes were observed for clusters constructed by three or more particles. For clusters of three particles chain-like structures (Figure 6.5B) were found as well as well-defined triangles (Figure 6.5C). Also for larger clusters compact, such as the square for four spheres (Figure 6.5D), as well as elongated shapes were observed. Similar anisotropically shaped clusters were observed of polystyrene spheres at water-air interfaces[182,183] and of pMMA spheres in bulk after centrifugation[184] and at aqueous-organic interfaces[185].
The interaction of pMMA spheres at an aqueous-organic interface was described by Leunissen *et al.*[28] and Kelleher *et al.*.[179,181] They showed that the net interaction between pMMA spheres bound to an aqueous-organic interface is the sum of Coulomb repulsions originating from the spheres' surface charge and Coulomb attractions due to interaction of the particles with the mirror charges of the neighboring spheres.[28,179,181] Since high wetting angles of the pMMA colloids with the aqueous phase were measured, the system could be described by spheres with charge q arranged on a conducting medium, which is the aqueous phase. This results in a dipolar force between pairs of interfacially bound spheres with pairwise additive interactions. The net interaction of two such particles can therefore be approximated by a pair potential of the form[181],

$$U(r) \simeq \frac{A}{r^3}, \tag{6.3}$$

where $A = p^2/8\pi\epsilon$, with ϵ the dielectric constant of the oil and $p = qd$ the magnitude of the electric dipole moment of the particles and r the interparticle distance. Interestingly, this interaction profile does not allow the formation of the observed mesostructures with much shorter interparticle distances. Other phenomena or additional interfacial forces have to play a role. In the next section we analyse interfacially bound dumbbells and use these findings to speculate on the origin of the anisotropic impurities.

6.3.3 Interfacially bound dumbbells

To study the effect of the anisotropy of impurities on the hexagonal order of spheres, we analyzed the distortion induced by elongated dumbbell shapes. The interfacially bound dumbbells were characterized by their position at the interface and their dimensions. Over 95% of the dumbbells aligned with their long axis parallel to the interfacial plane. We expected preferential wetting of the particles by the organic liquid, since Kelleher *et al.* measured contact angles close to 180° for pMMA spheres at an interface between aqueous 70 wt% glycerol solution (10 mM NaCl) and an organic phase consisting of CHB, hexane, and dodecane (5:3:2 v/v). Nevertheless, we observed that the motion of the anisotropic particles was restricted to the two dimensions of the interfacial plane, confirming

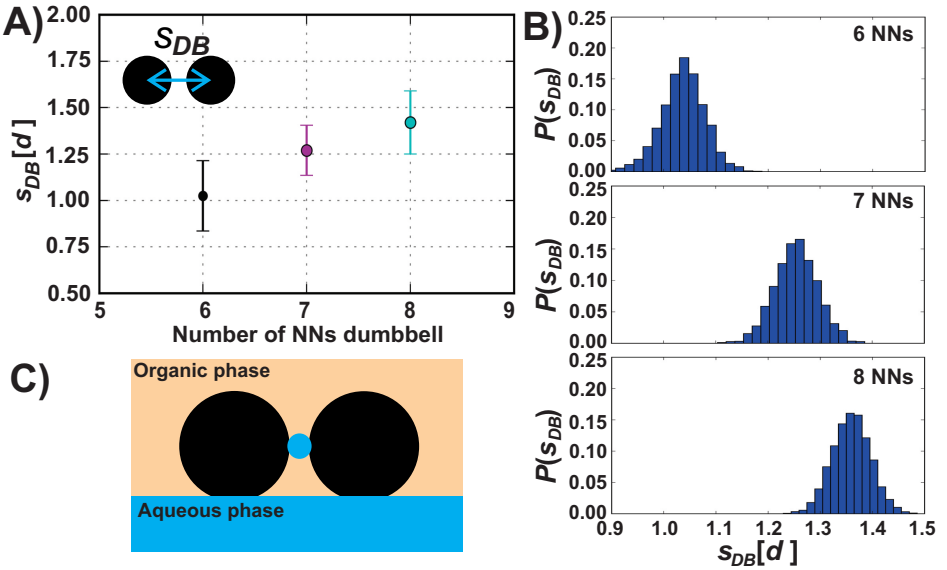


FIGURE 6.6: The intradumbbell distance (s_{DB}) and the number of nearest neighbors (NNs) of interfacially bound dumbbells. The diameter of the spheres, d = 2.00 ± 0.05 μm. A) s_{DB} of dumbbells with six, seven or eight NNs. The number of NNs increases with the distance between the two spheres of the dumbbell. s_{DB} was determined for >225 different dumbbells. B) s_{DB} of individual dumbbells with six, seven or eight NNs, calculated from > 3100 measurements collected over several minutes. The pixelsize is 0.07-0.10d. Since the standard deviations measured in s_{DB} are close to the pixelsize, s_{DB} is essentially constant for individual dumbbells. C) Illustration of a dumbbell at an organic-aqueous interface formed by a small aqueous droplet connecting two spheres.

that the colloids were interfacially bound. In our analysis, dumbbells with their long axis aligned parallel to interfacial plane were examined only.
We found that the distance between the two spheres forming the dumbbell, which we from here on refer to as the intradumbbell distance s_{DB}, differed per particle. Furthermore, dumbbells with six, seven or eight NNs were observed. Analysis of s_{DB} and the number of NNs of >225 dumbbells revealed a relation between the two, where the number of NNs increased with increasing s_{DB} (Figure 6.6A). Figure 6.6B shows s_{DB} of individual dumbbells with six, seven or eight NNs from at least 3100 measurements collected in several minutes. s_{DB} deviates at max 0.1d from the average s_{DB} value, which is similar to the pixelsize and likely caused by a tracking error. We therefore assume that s_{DB} is fixed for each dumbbell.
These findings allow us to speculate on the origin of the formation of dumbbells and larger structures at an organic-aqueous interface. It was suggested that residual van der Waals forces between the spheres could cause attraction.[185] If van der

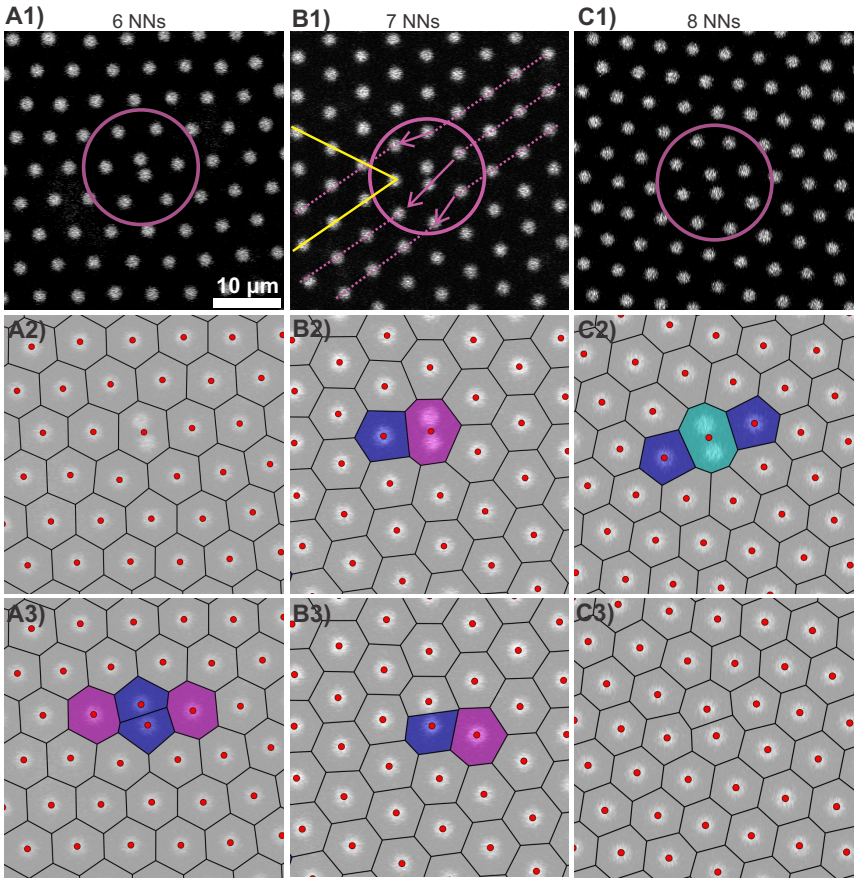


FIGURE 6.7: Dislocations induced by dumbbells with six, seven and eight NNs. Confocal microscopy images of dumbbells with six (A1), seven (B1) and eight (C1) NNs. In B1) the line dislocation is visualized with by the yellow lines. Corresponding Voronoi diagrams of the microscopy images in A1-C1. The dumbbell is considered as one particle in A2-C2 and as two individual spheres in A3-C3. The Voronoi cells are colored according to the coordination number, z_i, of the colloids; purple for z_i=5, grey for z_i=6, magenta for z_i=7 and turquoise for z_i=8. A dumbbell with six NNs substitutes one lattice position in the hexagonal crystal without the formation of dislocations (A2 and A3). At seven NNs a five-and-seven disclination pair is formed resulting in the insertion of two semi-infinite rows in the hexagonal crystal (B2 and B3). At eight NNs the dumbbell substitutes two lattice sites in the hexagonal crystal.

Waals forces between the spheres would induce the formation of dumbbells, s_{DB} would approximately be equal to the diameter of the spheres. Since we found

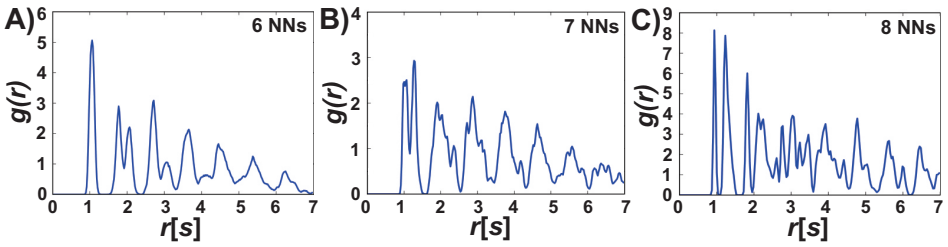


FIGURE 6.8: Radial distribution functions of crystals around typical dumbbells with A) six, B) seven and C) eight neighbors with the COM of the dumbbell at r=0. Constructed from at least 3100 measurements collected over several minutes.

differences in s_{DB} much larger than the polydispersity of the spheres, residual van der Waals forces do not explain the formation of the clusters. Distortions of the interface induced by surface roughness could also induce attraction[186], but it is unlikely that this would result in dumbbells with different s_{DB}. A plausible explanation is the interference of interfacial contaminations[183]. Since we observed larger droplets covered with spheres, it is likely that smaller droplets are also present at the interface. Impurities with sizes close to or smaller than the diffraction limit of optical microscopy, such as droplets or nanobubbles[187–189], could connect spheres to form larger structures, as illustrated in Figure 6.6C. This explanation is also in agreement with the fixed s_{DB} for individual dumbbells, but deviating values for s_{DB} of different dumbbells.

Confocal microscopy images of typical interfacially bound dumbbells with six, seven or eight NNs are shown in Figure 6.7A1, 6.7B1 and 6.7C1, respectively. By performing Voronoi tesselations on these images the disclinations and dislocations induced by the different dumbbells were visualized. We show two Voronoi diagrams: one where the dumbbell is treated as a single particle and one where the dumbbell is viewed as two individual spheres.
When the dumbbell is viewed as one particle, the Voronoi diagram of a typical dumbbell with six NNs shows that all particles have the same coordination number, z_i=6 (Figure 6.7A2). The Voronoi diagram obtained when the dumbbell is taken as two individual spheres reveals a dislocation pair, with z_i=5 at the spheres forming the dumbbell and z_i=7 at two of the NNs (Figure 6.7A3). This indicates that the dumbbell substitutes a single lattice site in the hexagonal crystal without long-range distortions of the orientational and translational order. A five-and-seven coordinated disclination pair is introduced for the dumbbell with seven NNs, see Figure 6.7B2 and B3. The isolated dislocation distorts the translational order in the hexagonal crystal by the insertion of two semi-infinite rows in the crystal, as illustrated by the yellow lines in the corresponding confocal image in Figure 6.7B1. At eight NNs a z_i=8 is located at the dumbbell and two of

the NNs have z_i=5, which is an unusual dislocation (Figure 6.7C2). The Voronoi diagram of the two separate spheres reveals that the dumbbell substitutes two lattice positions in the hexagonal crystal, without long-ranged distortions of the crystal (Figure 6.7C3). We expect that the number of lattice sites in the hexagonal crystal occupied by elongated impurites will increase with the length of the particle. For large s_{DB} dumbbells will act as separate spheres, but linear impurities constructed by more than two spheres, such as chains, could provide this information.

Positional information of the spheres surrounding the dumbbell was obtained from $g(r)$ with the COM of the dumbbell as origin. Peaks in $g(r)$ are observed to a distance r of at least seven times the lattice spacing s for dumbbells with six, seven as well as eight NNs, see Figure 6.8. This indicates that local order is maintained for the spheres around the dumbbells. Interestingly, the shape of the radial distribution function strongly depends on the number of NNs. The radial distribution function of the dumbbell with six NNs (Figure 6.8A) is largely in agreement with $g(r)$ obtained for spheres indicating that overall the hexagonal order of the crystal was conserved (Figure 6.3D). Only small differences are found in the width and position of the peaks. For example, the peak of the NNs, at $r = 1s$ for spheres, is broader and slightly shifted to a larger distance r. At seven NNs the location of the peaks in the $g(r)$ (Figure 6.8B) deviate from $g(r)$ of spheres. Whereas all NNs are positioned at $r = 1s$ for spheres, the seven NNs are observed at different distances r from the dumbbell, resulting in a partly splitted peak around r=1s. At eight NNs the peak at $r = 1s$ has splitted completely into two separate peaks (Figure 6.8C). These findings denote that the distortion of the hexagonal order by dumbbells depends on the length of the dumbbell, s_{DB}. In the next sections we took the anisotropy of the dumbbell in our analysis into account to investigate the dynamics of dumbbells with six, seven and eight NNs and their effect on the surrounding crystal, separately.

6.3.4 Dumbbell orientation and crystal distortion

Analysis approach

To study the effect of dumbbell impurities on a hexagonal crystal, the anisotropy of the dumbbell has to be accounted for. We measured both the orientation of the dumbbell with respect to the crystal orientation and the position of the surrounding spheres with respect to the dumbbell orientation. On a two-dimensional hexagonal lattice different axes of reflection symmetry are present. In Figure 6.9A we illustrated the crystal orientation axes which make angles with $\vec{a}_1$ of 0, $\pi/3$ and $2\pi/3$ (green lines) or $\pi/6$, $\pi/2$ and $5\pi/6$ (dotted purple lines). We defined the dumbbell orientation as the angle β, between the long dumbbell axis and the

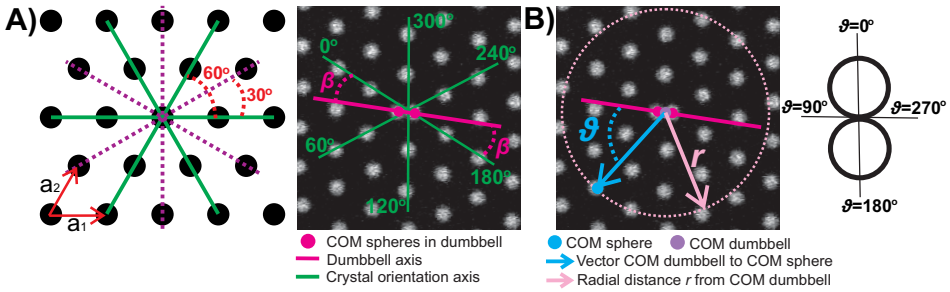


FIGURE 6.9: Illustration of the parameters used to determine the orientation of dumbbells with respect to the crystal orientation and the position of the spheres in the surrounding crystal with respect to the dumbbell. A) Different axes of reflection symmetry are present on a two-dimensional hexagonal lattice. The dumbbell orientation was defined as the angle β between the dumbbell axis and the crystal orientation axes in green. The six-fold symmetry in an hexagonal crystal allowed us to mirror all data of β into the range $\beta\epsilon[0°, 30°]$. Additionally, the average interparticle distance between the spheres in the crystal, s, was also included in the analysis. B) The position of the spheres was described by the distance r between the COM of the sphere and the COM of the dumbbell and the angle ϑ between the dumbbell axis and the vector of the COM of the dumbbell to the COM of the sphere.

crystal orientation axis in green (Figure 6.9A). A preference for a certain value of β would indicate an anisotropic energy landscape. The degree of confinement of the dumbbell also depends on the average lattice spacing s in the hexagonal crystal and the dimensions of the dumbbell and we therefore investigated.
To determine how dumbbells distort the hexagonal order in the crystal, we measured the position of the surrounding spheres with respect to the dumbbell axis. The position of spheres was defined by the radial distance r between the COM of the dumbbell and the COM of the sphere, and the angle ϑ between the vector from the dumbbell to the sphere and the dumbbell axis (Figure 6.9B). Spheres ordered on a perfect hexagonal lattice have equal interparticle distances, and angles of 60° between the vectors with their six NNs. If dumbbell impurities distort the hexagonal order of the surrounding spheres, the neighboring spheres will position at different values of r as a function of ϑ at a given dumbbell orientation β. These parameters are therefore required to determine the distortion of the hexagonal order by dumbbells.

Dumbbell orientation in crystals with different lattice spacings

The orientation of dumbbells in crystals with different lattice spacings s was measured to determine the influence of particle confinement on the motion and position of the dumbbells. Trajectories of dumbbells with six NNs, travelled over

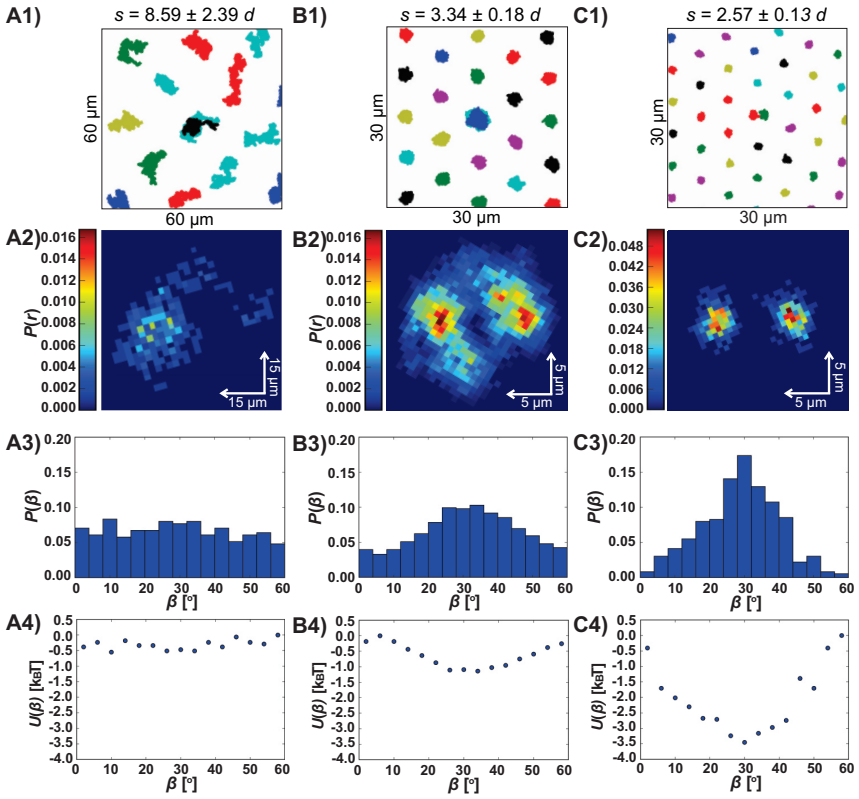


FIGURE 6.10: Trajectories and preferred orientation of individual dumbbells with six NNs in crystals with different s. (A1-A4) $s = 8.59 \pm 2.39d$ (300 measurements in 15 minutes), (B1-B4) $s = 3.34 \pm 0.18d$ (4500 measurements in 15 minutes), and (C1-C4) $s = 2.57 \pm 0.13d$ (360 measurements in 6 minutes). A1-C1) Trajectories of dumbbells and surrounding spheres. At decreasing s the particles are increasingly confined to a lattice position. A2-C2) Probability density plots, $P(r)$, of the position of the dumbbells. At $s = 8.59 \pm 2.39d$ the dumbbell rotated without restrictions and only slight restrictions in the translational motion were observed. At $s = 3.34 \pm 0.18d$, the translational motion of the dumbbell was restricted to one lattice site, but full dumbbell rotation was still allowed. At $s = 2.57 \pm 0.13d$ both the translation and rotation of the dumbbell were resticted. A3-C3) The probability for the dumbbell to orient at a certain value of β, $P(\beta)$, where we combined all data to $\beta\epsilon[0°, 60°]$. A4-C4) The confinement energy $U(\beta)$ corresponding to $P(\beta)$. In a highly fluidic crystal, $s = 8.59 \pm 2.39d$, no preferred dumbbell orientation was observed. At $s = 3.34 \pm 0.18d$ $P(\beta)$ was largest at $\beta = 30°$ corresponding to an confinement energy of -1.1 k_BT. Highly confined dumbbells, $s = 2.57 \pm 0.13d$, preferentially oriented at $\beta = 30°$ with an confinement energy of -3.5 k_BT.

several minutes in crystals with s = 8.59 $\pm$ 2.39d, s = 3.34 $\pm$ 0.18d and s = 2.57 $\pm$ 0.13d, are shown in Figure 6.10A1, 6.10B1 and 6.10C1, respectively. The area covered by the dumbbell and the surrounding spheres decreased drastically with decreasing s. The probability density plot of the position of the dumbbell, $P(r)$, in a crystal with s = 8.59 $\pm$ 2.39d shows that the confinement of the dumbbell in the crystal was low with no restrictions in the rotational motion and some restrictions in the translational motion (Figure 6.10A2). At s = 3.34 $\pm$ 0.18d the dumbbell was confined to a lattice position, but full rotation around the COM of the dumbbell was still observed (Figure 6.10B2). At s = 2.57 $\pm$ 0.13d the confinement of the particles increased further leading to large restrictions in both the translational and rotational motion of the dumbbell (Figure 6.10C2).
Due to the anisotropy of the dumbbell we expected that restrictions in the rotational motion would lead to a preference for a certain orientation of the dumbbell with respect to the crystal. We measured the dumbbell orientation, defined by β (Figure 6.9A), for individual dumbbells over time in crystals with different s. At s = 8.59 $\pm$ 2.39d the crystal was highly fluidic and the probability for the dumbbell to orient at a certain value of β, $P(\beta)$, was uniform for all β (Figure 6.10A3). By decreasing s to 3.34 $\pm$ 0.18d a non-uniform distribution in $P(\beta)$ was measured with the highest probability at $\beta = 30^\circ$ and the lowest at $\beta = 0^\circ$ and 60° (Figure 6.10B3). In crystals with s = 2.57 $\pm$ 0.13d the preference for $\beta = 30^\circ$ became even more significant (Figure 6.10C3).

Using $P(\beta)$ we calculated the confinement potential of the dumbbells, $U(\beta)$, via the Boltzmann distribution:

$$U(\beta) = U_0 - k_B T \ln P(\beta) \tag{6.4}$$

where k_B is the Boltzmann constant and T the temperature. The energy U is determined with respect to a reference value U_0, which we set at the maximum measured value of U. In Figure 6.10A4-C4 the energy profiles calculated from the probability functions in Figure 6.10A3-C3 are shown, respectively. At large s, 8.59 $\pm$ 2.39d, the confinement energy was independent of β. In more dense crystals, s = 3.34 $\pm$ 0.18d an energy difference of -1.1 $k_B T$ is observed between $\beta = 30^\circ$ and $\beta = 0^\circ$ or 60°. The confinement energy increased to -3.5 $k_B T$ when the lattice spacing in the crystal was increased to s = 2.57 $\pm$ 0.13d.

Besides analysing individual dumbbells in time we also determined $P(\beta)$ from an ensemble of different dumbbells with six NNs. Analysis of 150 confocal microscopy images of different dumbbells with six NNs in crystals with s = 3.59 $\pm$ 0.29d, showed no significant preference for β (Figure 6.11A). In more compact crystals with s = 2.64 $\pm$ 0.09d, a preferred orientation of $\beta = 15^\circ$-30° was observed from analysis of 100 different dumbbells (Figure 6.11B). These results are in agreement with the measurements of individual dumbbells, where a preference for β

= 30° was found as short s.

Our results show that dumbbells with six NNs become more confined to $\beta = 30°$ with decreasing lattice spacing s due to restrictions in the rotational motion. This can be understood by examining the energy landscape around the dumbbell in the hexagonal crystal of spheres. We plotted the energy landscape using the pair potential of individual spheres assuming pairwise additivity, see Equation 6.3. To calculate the pair potential the particle charge q is required. For pMMA spheres of 2.6 μm in diameter dispersed in CHB:hexane:dodecane (5:3:2 v/v) Kelleher *et al.* measured a charge of 530-590e, with e as the elementary charge.[179] Using electrophoresis, Leunissen *et al.* measured a charge of 450e for pMMA colloids of 2.16 μm in diameter in density-matched CHB:cis-decalin.[28] Since our colloids are synthesized according to the same synthetic method[173] and a comparable interface was used, we assumed similar values for q. The dielectric constant of our organic phase, CHB:cis-decalin (70:30 w/w), is 5.6.
We plotted the potential energy, $U(r)$, for a dumbbell particle and six hexagonally ordered spheres. The energy profile around the dumbbell is anisotropic as expected, see Figure 6.12A. Although the energy profile of the individual spheres is isotropic, the potential energy landscape created by the six particles is anisotropic (Figure 6.12B). At equal distance r from the center particle the potential energy is lowest in the direction in between the spheres and highest in the direction of the

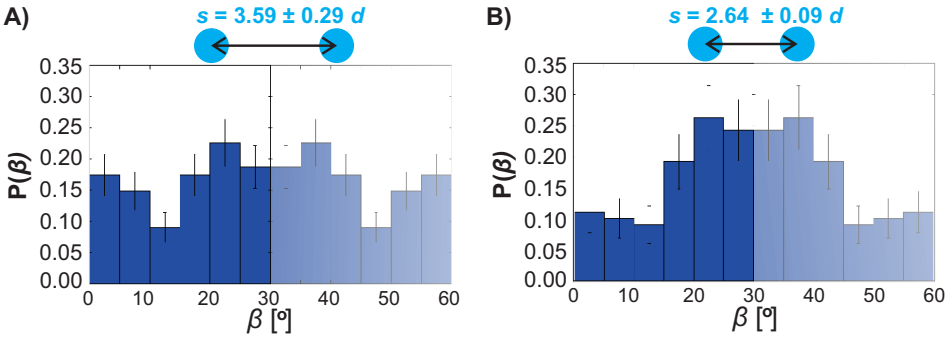


FIGURE 6.11: Dumbbell orientations of an ensemble of dumbbells with six NNs in crystals with different lattice spacing s obtained from confocal microscopy images. β was measured as the angle between the dumbbell axis and the crystal orientation axis closest to the dumbbell axis, therefore $\beta\epsilon[0°, 30°]$. Due to symmetry in the hexagonal crystal we expect the values for $\beta\epsilon[0°, 30°]$ to be symmetric to $\beta\epsilon[60°, 30°]$, respectively. The probability to find a dumbbell with a certain value of β, $P(\beta)$, in crystals with A) $s = 3.59 \pm 0.29d$, where no significant preference in β is observed from analysis of 150 different dumbbells, and at B) $s = 2.64 \pm 0.09d$, where dumbbells preferably oriented at β-values of 15°-30°. 100 different dumbbells were analyzed.

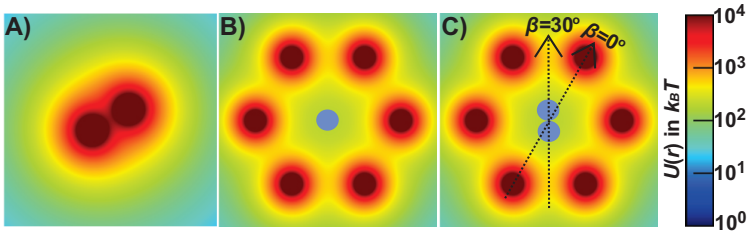


FIGURE 6.12: Potential energy profile around A) a dumbbell and B) six hexagonally ordered spheres. C) Due to the anisotropic energy profile around the dumbbell and inside the hexagon, it is energetically favorable for the dumbbell to orient at $\beta = 30°$.

spheres. Since the dumbbell has an anisotropic interaction itself, the dumbbell experiences the least repulsion at $\beta = 30°$, see Figure 6.12C.

Crystal distortion by dumbbells with six NNs

At short lattice spacings the energy landscape around dumbbells with six NNs is not uniform, which leads to a preferred orientation of the dumbbell. In turn, the anisotropy of the dumbbell would also affect the position of the surroundig spheres in the hexagonal crystal. Although no dislocations were formed by dumbbells with $s_{DB} = 1.03 \pm 0.19d$ and six NNs, small differences were observed in the position and width of the peaks in $g(r)$ for a dumbbell with six NNs in a crystal with $s = 3.34 \pm 0.18d$ (Figure 6.8A), compared to $g(r)$ for hexagonally ordered spheres (Figure 6.3D). This indicates that dumbbells with six NNs in crystals with short lattice spacings change the hexagonal order in the crystal locally. To investigate whether the distance r at which the neighboring spheres were positioned was related to the anisotropy of the dumbbell, we included the angle between the dumbbell axis and the vector of the dumbbell to any neighboring sphere, ϑ, in our analysis (see Figure 6.9B).
We identified and quantified any anisotropic distortion of the crystal by plotting $g(r)$ for restricted angular ranges of ϑ, by defining a restricted angular radial distribution function:

$$g_\vartheta(r) = \rho_\vartheta \cdot \delta\rho r dr, \tag{6.5}$$

where ρ_ϑ is the average particle density in the angular range $[\vartheta \pm \frac{\delta\vartheta}{2}]$ in a $\rho_\vartheta \cdot \delta\rho r dr$ area. We plotted $g_\vartheta(r)$ separatly for $\vartheta = 0°$, 15°, 30°....360° $\pm \frac{\delta\vartheta}{2}$, with $\delta\vartheta = 15°$, covering the complete radial distribution in 24 intervals of 15°. In Figure 6.13 four $g_\vartheta(r)$ graphs are shown, containing positional information of spheres surrounding the dumbbell at angles $\vartheta\epsilon[0° , 90°]$, [90°, 180°], [180°, 270°] and [270°, 360°], respectively. The four $g_\vartheta(r)$-plots show peaks at similar distances r, pointing to symmetric behavior of the spheres in the four quadrants around the dumbbell

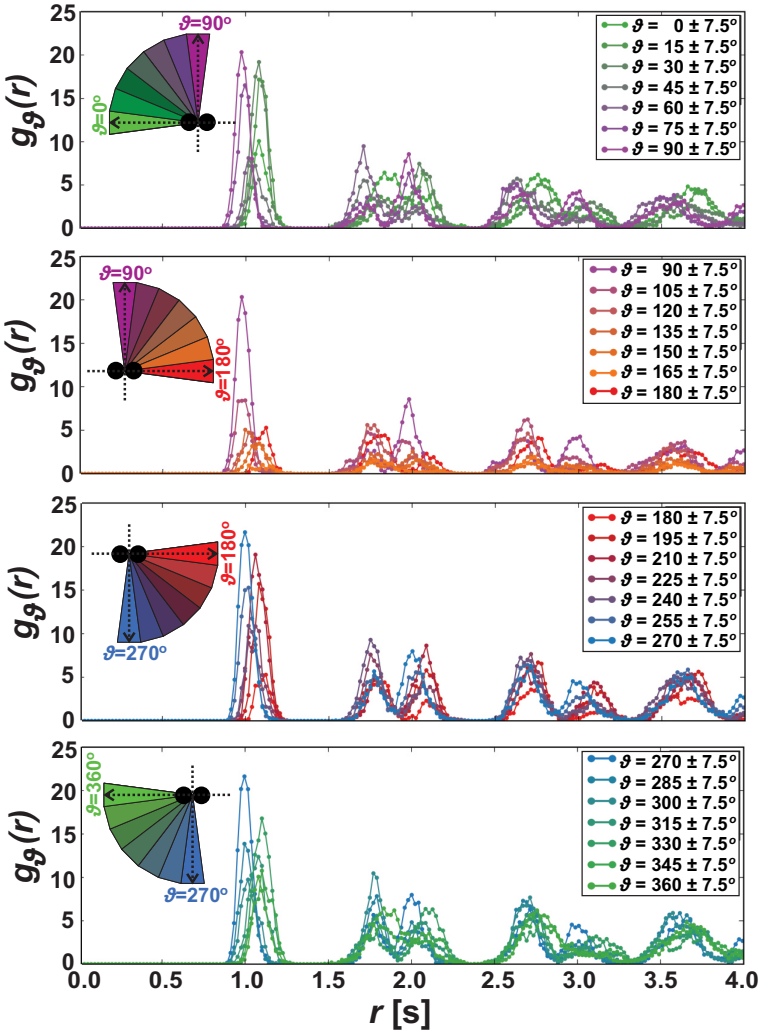
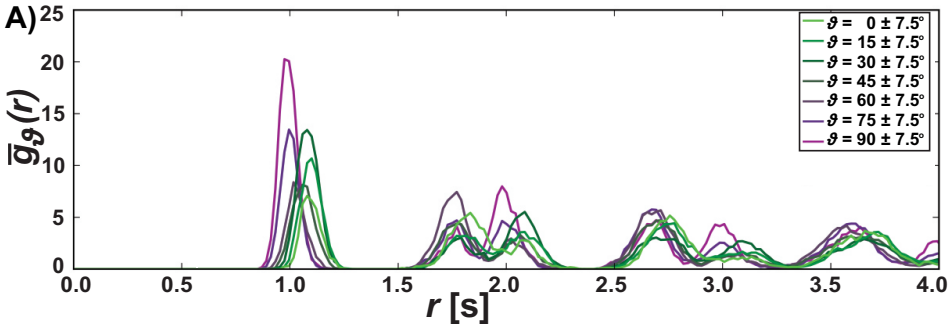
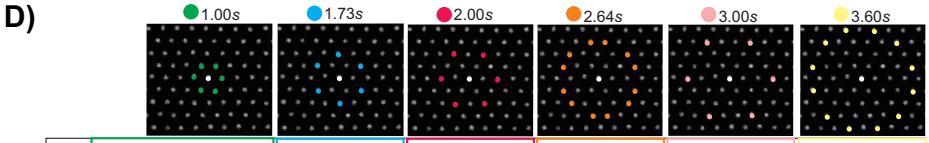


FIGURE 6.13: Restricted angular radial distribution function, $g_\vartheta(r)$, of a dumbbell with six NNs in a crystal with $s = 3.34 \pm 0.18d$, where d is the diameter of the spheres. $g_\vartheta(r)$ was obtained from 4500 measurements collected over 15 minutes with $r = 0$ at the COM of a dumbbell. Four $g_\vartheta(r)$ graphs are shown with positional data of spheres at $\vartheta\epsilon[0°, 90°]$, [90°, 180°], [180°, 270°] and [270°, 360°], respectively. Peaks in the four graphs are observed at similar distances r, pointing to symmetric behavior of the spheres in the four quadrants around the dumbbell.





ϑ [°]	W_{DB} [s]	r_{DB} [s]	Δ_{hex_1s} [s]	r_{DB} [s]	$\Delta_{hex_1.73s}$ [s]	r_{DB} [s]	Δ_{hex_2s} [s]	r_{DB} [s]	$\Delta_{hex_2.64s}$ [s]	r_{DB} [s]	Δ_{hex_3s} [s]	r_{DB} [s]	$\Delta_{hex_3.60s}$ [s]
0	0.11	1.10	+10%	1.83	+ 6%	2.10	+ 5%	2.74	+ 4%	-	-	3.61	0%
15	0.13	1.10	+10%	1.81	+ 5%	2.10	+ 5%	2.74	+ 4%	-	-	3.64	+ 1%
30	0.13	1.09	+ 9%	1.79	+ 3%	2.09	+ 5%	2.71	+ 2%	3.09	+ 3%	3.66	+ 2%
45	0.13	1.06	+ 6%	1.77	+ 2%	2.05	+ 3%	2.71	+ 2%	3.06	+ 2%	3.63	+ 1%
60	0.10	1.02	+ 2%	1.76	+ 2%	2.04	+ 2%	2.67	+ 1%	3.04	+ 1%	3.58	- 1%
75	0.10	1.00	0%	1.76	+ 2%	2.00	0%	2.67	+ 1%	3.00	0%	3.59	0%
90	0.10	0.99	- 1%	1.76	+ 2%	1.99	- 1%	2.67	+ 1%	3.00	0%	3.59	0%

FIGURE 6.14: Anisotropic crystal distortion by dumbbells with six NNs. A) The averaged $g_\vartheta(r)$, $\bar{g}_\vartheta(r)$, obtained by combining all positional data of the spheres into the range $\vartheta\epsilon[0°, 90°]$. The distance r at which a neighboring sphere is positioned decreases with increasing ϑ. ϑ is related to the dumbbell orientation β, for example the NNs position at B) $\vartheta \simeq 0°$ and 60° for $\beta = 0°$ and at C) $\vartheta \simeq 30°$ and 90° for $\beta = 30°$. D) Comparison of the observed peak positions to the expected peak positions for neighboring spheres in an hexagonal crystal, r_{hex} = 1.00, 1.73, 2.00, 2.64, 3.00 and 3.60s. For the NNs of the dumbbell deviations of -1 to +10% were measured compared to r_{hex}. For the next NNs deviations of -1 to +6% were found and the differences decrease further with r. Compared to r_{hex} = 3.60s differences of 1 or 2% were found, indicating that the hexagonal order in the crystal had almost completely restored. Therefore, the hexagonal order was only locally anisotropically distorted and dumbbells with six NNs occupied one lattice position in the hexgonal crystal.

(Figure 6.9B).
This four-fold symmetry allowed us to combine and average the data into an effective angular range of $\vartheta\epsilon[0^\circ , 90^\circ]$. From this effective angular range we calculated an averaged $\bar{g}_\vartheta(r)$ (see Figure 6.14A). A relation between ϑ and r can be observed, where the distance r at which a nearest neighbor is located decreases with increasing ϑ. NNs at $\vartheta = 90^\circ$ were positioned closer to the COM of the dumbbell compared to NNs positioned in line with the dumbbell axis at $\vartheta = 0^\circ$, resulting in an anisotropic distortion of the hexagonal order locally around the dumbbell.
Interestingly, the first peak for all values of ϑ slightly shifts around $r = 1s$, which indicates that the dumbbell rotated in time affecting the position of the surrounding spheres in turn. The effect of β on ϑ is illustrated in Figure 6.14B and 6.14C by overlaying the position of the spheres found in confocal microscopy images with a schematic of ϑ, corresponding to the colors used in the Figure 6.14A. When the dumbbell is aligned with the crystal orientation, $\beta = 0^\circ$, the NNs position at $\vartheta \simeq 0^\circ$ and 60° (Figure 6.14B). For a dumbbell oriented at $\beta = 30^\circ$ the six NNs are located at $\vartheta \simeq 30^\circ$ and 90° (Figure 6.14C).

Voronoi tesselations indicated that dumbbells with six NNs occupied one lattice site in the hexagonal crystal (see Figure 6.7A2 and 6.7A3). To quantify the anisotropic distortion of the hexagonal crystal we therefore compared the position of the neighboring spheres to expected values for neighborings spheres in an hexagonal crystal with lattice spacing s, r_{hex} = 1.00, 1.73, 2.00, 2.64, 3.00, 3.46 and 3.60s (Figure 6.14D). The NNs around the dumbbell were positioned at r = 0.99s to 1.10s, with the shortest distance r for spheres at $\vartheta = 90^\circ$ and the largest distance r for spheres at $\vartheta = 0^\circ$. These distances deviate by -1 to +10% from the expected value, $r_{hex} = 1s$, for NNs in a hexagonal crystal. The full width at half maximum of the peaks w_{DB} originating from the NNs is similar for all ϑ-values, indicating that all NNs had similar freedom of motion. In the hexagonal crystal, neighboring spheres in the second ring are expected at r_{hex} = 1.73 and 2.00s. The second NNs of the dumbbell located at distances r deviating by -1 to +6% from the expected values for the hexagonal crystal. The differences in the position of the neighboring spheres decreased with increasing distance r. Compared to r_{hex} = 3.60s small deviations, 1 to +2%, were observed which indicates that the hexagonal order had almost completely restored. This means that dumbbells with six NNs occupy one lattice position in the crystal and distort the hexagonal order only locally.

Crystal distortion by dumbbells with seven NNs

Dumbbells with $s_{DB} = 1.27 \pm 0.14d$ were typically surrounded by seven NNs, which introduced an isolated dislocation characterized by the insertion of two

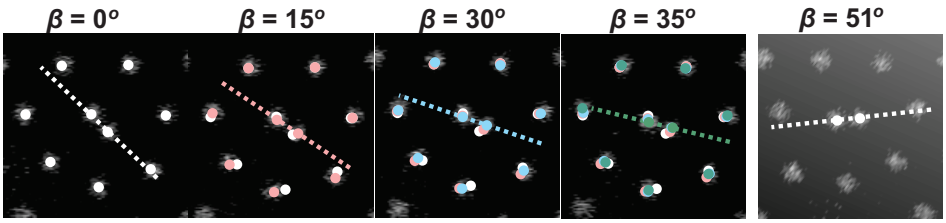


FIGURE 6.15: Confocal microscopy images of a dumbbell with seven NNs rotating in a crystal with $s = 2.67 \pm 0.17d$. At $\beta = 0°$ the dumbbell is aligned with the crystal orientation. Rotation of the dumbbell to $\beta = 15°$ resulted in the displacement of the four NNs on the line dislocation side of the dumbbell. Rotation to β=30° and subsequently 35° induced the displacement of all particles. Although not observed at this lattice spacing, it is expected that at $\beta = 51°$ a similar situation to $\beta = 0°$ will occur, since 360/7=51°.

semi-infinite rows in the hexagonal crystal (see Figure 6.6B1). Isolated dislocations change the translational order in the long range and the orientational order locally. The dumbbell orientation was therefore determined with respect to the crystal orientation measured at sigficant distance from the dumbbell.
The introduction of two halfrows in the crystal lead to an asymmetry in the surrounding crystal between the two sides of the dumbbell axis. Confocal microscopy images of a rotating dumbbell with seven NNs at different points in time are shown in Figure 6.15. In contrast to dumbbells with six and eight NNs, the crystal orientation is not a symmetry axis for the neighboring spheres, as can be observed at $\beta = 0°$. When the dumbbell rotated to $\beta = 15°$ the NNs on the side of the dumbbell axis with the line dislocations were observed to change position. Upon further rotation to $\beta = 30°$ and 35° the other NNs also slightly changed position to adapt to the orientation of the dumbbell. At $\beta = 51°$ we expect a situation equal to $\beta = 0°$, since 360/7 = 51. Rotation to $\beta = 51°$ was not observed for this dumbbell, which points to an energy barrier at this lattice spacing, $s = 2.67 \pm 0.17d$, that restricted the rotational motion of the dumbbell.

For a dumbbell with seven NNs in a crystal with $s = 2.22 \pm 0.11d$ restrictions in both the translational and rotational motion were observed from the trajectories of the particles and the probability density plot of the position of the dumbbell $P(r)$ (Figure 6.16A). The strongly confined dumbbell oriented at -22° < β < 22° only (see Figure 6.16B) and preferentially aligned parallel to the crystal orientation axis, $\beta = 0°$. The confinement potential of the dumbbell $U(\beta)$, calculated using $P(\beta)$, showed a confinement energy of -5 k_BT at $\beta = 0°$ (Figure 6.16C). Analysis of 34 individual dumbbells with seven NNs yielded a similar result; an average β-value of 6.5 ± 4.7°.
To explain why dumbbells with seven NNs preferably align parallel to the crystal

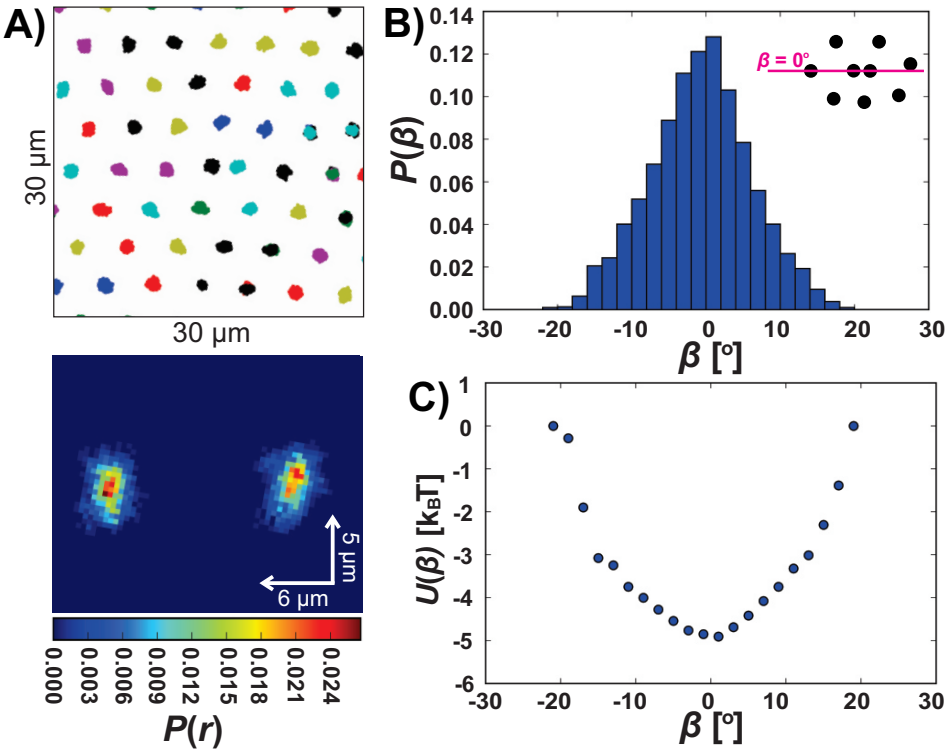


FIGURE 6.16: Trajectories and preferred orientation of a dumbbell with seven NNs in a crystal with $s = 2.22 \pm 0.11d$, obtained from 3162 measurements collected in 6.4 minutes. A) The trajectories (top) of a dumbbell with seven NNs and the surrounding spheres and the probability density plot of the position of the dumbbell $P(r)$ (bottom). The dumbbell was largely confined in the crystal and the translational and rotational motion were restricted. B) $P(\beta)$, dumbbell orientations of -22° < β < 22° were measured with the highest probabilty at $\beta = 0°$. C) The confinement potential $U(\beta)$ calculated from $P(\beta)$ shows a confinement energy of -5k_BT at $\beta = 0°$.

orientation, we refer to the behavior of isolated dislocations in hexagonal crystals. An isolated dislocation directs parallel to the Burgers vector originating from the two halfrows inserted in the crystal.[190] The Burgers vector can be determined by drawing a closed circuit, a Burgers circuit, around a fixed point in a crystal. A Burgers circuit around a dumbbell with seven NNs is drawn in Figure 6.17A. By applying the same circuit to an hexagonal crystal of spheres the circuit is not closed and the Burgers vector is the vector connecting the start and finish point of the circuit (Figure 6.17B). This vector is directed parallel to the crystal orientation and always perpendicular to an isolated dislocation, as shown in the Voronoi

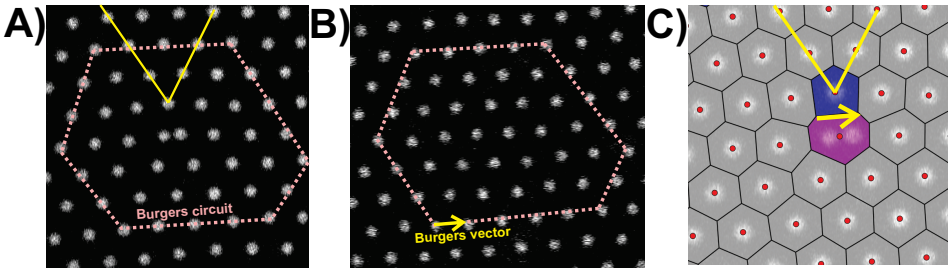
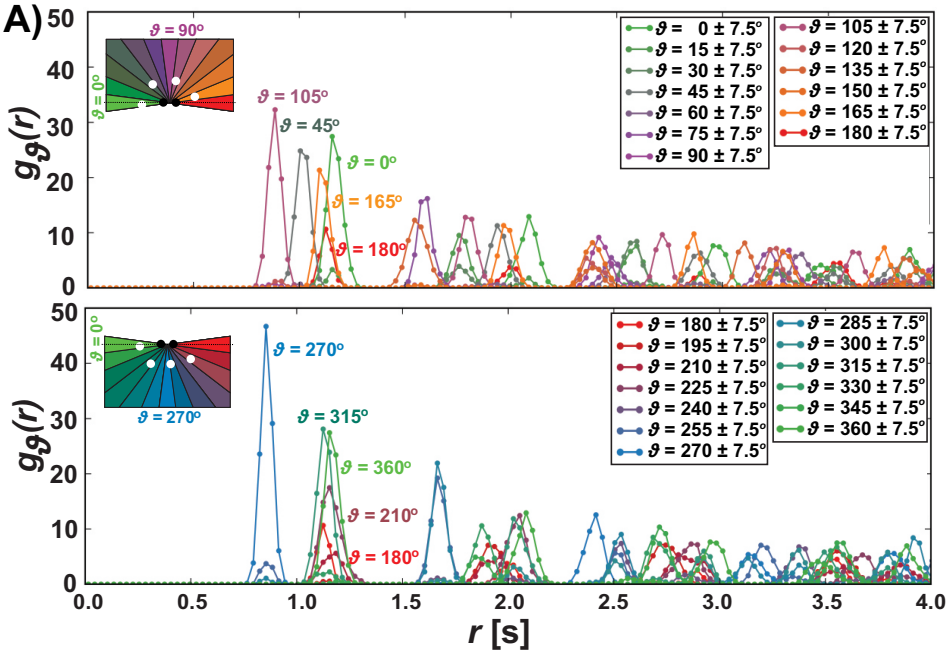


FIGURE 6.17: The Burgers circuit and Burgers vector in a hexagonal crystal with an isolated dislocation originating from a dumbbell with seven NNs. A) A closed Burgers circuit drawn (dotted line) around the dumbbell. The two inserted semi-infinite rows are indicated by the yellow lines. B) The Burgers circuit of (A) applied to a hexagonal crystal of spheres. The circuit is closed by the Burgers vector which connects the start and finish point of the Burgers circuit. The direction of the Burgers vector is equal to the crystal orientation. C) Voronoi diagram of a dumbbell with seven NNs with the Burgers vector illustrated perpendicular to the isolated dislocation.

diagram of the dumbbell in Figure 6.17C. Dumbbells with seven NNs therefore preferably orient at $\beta = 0°$.

To analyse the position of the neighboring spheres we calculated $g_\vartheta(r)$ for a dumbbell with seven NNs in a crystal with $s = 2.33 \pm 0.12d$. $g_\vartheta(r)$ was plotted separately for $\vartheta\epsilon[0°, 180°]$ and $\vartheta\epsilon[180°, 360°]$, see Figure 6.18A. On one side of the dumbbell axis, $\vartheta\epsilon[0°, 180°]$, strong peaks of NNs were observed at $\vartheta = 0$, 45, 105 and $165 \pm 7.5°$ (top graph in Figure 6.18A). Depending on the orientation of the dumbbell the nearest neighbor located at $\vartheta = 165 \pm 7.5°$ could also be found at $\vartheta = 180 \pm 7.5°$. On the other side of the dumbbell axis, $\vartheta\epsilon[180°, 360°]$, the NNs positioned at ϑ = 210, 270, 315 and $360 \pm 7.5°$ (bottom graph in Figure 6.18A). The location of the NNs is illustrated in the top left of the graphs. Peaks in $g_\vartheta(r)$ of NNs positioned at other ϑ-values were small or absent, which again points to the restrictions in the rotational freedom of the dumbbell.
The full width at half maximum of the peaks in $g_\vartheta(r)$ originating from the NNs, w_{NNs}, was similar for most NNs (Figure 6.18B). w_{NNs} of the nearest neighbor at $\vartheta = 210°$ was largest which is in agreement with qualitative observations for a dumbbell rotating in time, see Figure 6.15. The NNs were located at distances r = 0.86s to 1.17s, which is a difference of 36%. The NNs at $\vartheta = 105°$ and 270° were positioned at r = 0.86s and 0.89s, respectively, while the NNs at ϑ = 0, 165, 210 and $315 \pm 7.5°$ were found at distances r ranging from 1.11s to 1.17s. Only the nearest neighbor located at $\vartheta = 45°$ was positioned at the expected lattice position for NNs in a hexagonal crystal, r = 1.02s. These findings explain the semi-splitted peak observed in the $g(r)$ for the NNs of a dumbbell with seven NNs shown



B)

ϑ [°]	w_{NNs} [s]	r_{NNs} [s]
0	0.09	1.17
45	0.08	1.02
105	0.08	0.89
165	0.08	1.11
210	0.11	1.16
270	0.08	0.86
315	0.09	1.14

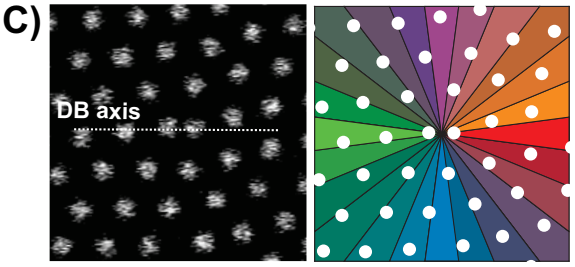


FIGURE 6.18: Positional information of spheres surrounding a typical dumbbell with seven NNs in a hexagonal crystal with $s = 2.33 \pm 0.12d$ calculated from 5440 measurements collected over three minutes. A) Restricted angular radial distribution functions $g_\vartheta(r)$ covering both sides of the dumbbell axis, $\vartheta\epsilon[0°, 180°]$ (top) and $\vartheta\epsilon[180°, 360°]$ (bottom). No symmetry is observed in the position of the surrounding spheres. B) The full width at half maximum of peaks in $g_\vartheta(r)$ originating from the NNs, w_{NNs}, is largest for the nearest neighbor positioned at $\vartheta = 210°$. The distance r at which the NNs position deviates from $r = 0.86s$ to $1.17s$. C) Confocal microscopy image of a dumbbell with seven NNs and an illustration of the ϑ-values of the spheres surrounding the dumbbell.

in Figure 6.8B. A confocal microscopy image of a dumbbell with seven NNs is shown in Figure 6.18 with the positions of the spheres overlaying an illustration

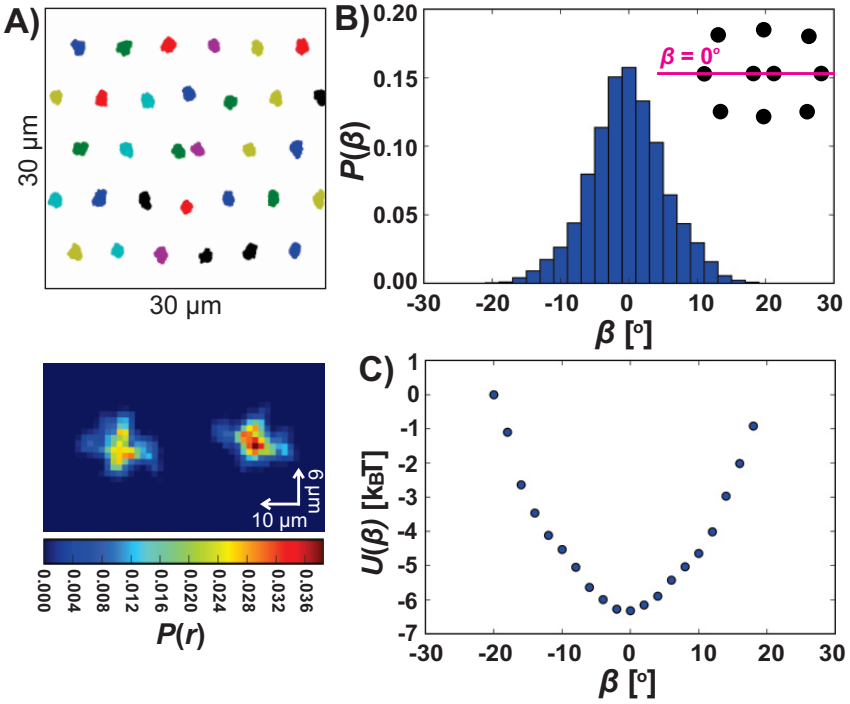


FIGURE 6.19: Trajectories and preffered orientation of a typical dumbbell with eight NNs in a crystal with $s = 3.20 \pm 0.15d$ calculated from 7090 measurments collected in two minutes. A) Trajectories of the dumbbell and the surrounding spheres (top) and the probability density plot of the position of the dumbbell $P(r)$ (bottom). Both the translational and rotational motion of the dumbbell were restricted. The limited translational motion was directed perpendicular or parallel to the crystal orientation axis, resulting in a cross-profile in $P(r)$. B) $P(\beta)$, dumbbell orientations of -22° < β < 22° were measured where the dumbbell preferentially oriented parallel to the crystal orientation axis, at $\beta = 0°$. C) The confinement potential $U(\beta)$ calculated from $P(\beta)$ shows a strong confinement energy of -7 k_BT at $\beta = 0°$.

of the ϑ-values of the neighboring spheres to visualize the asymmetry in the crystal around a dumbbell with seven NNs.

Crystal distortion by dumbbells with eight NNs

Dumbbells with large intradumbbell distances, $s_{DB} = 1.42 \pm 0.17d$, were often surrounded by eight NNs. We analysed the orientation of a typical dumbbell with eight NNs in a crystal with $s = 3.20 \pm 0.15d$. The trajectories of the dumbbell and the surrounding spheres travelled over several minutes show that the parti-

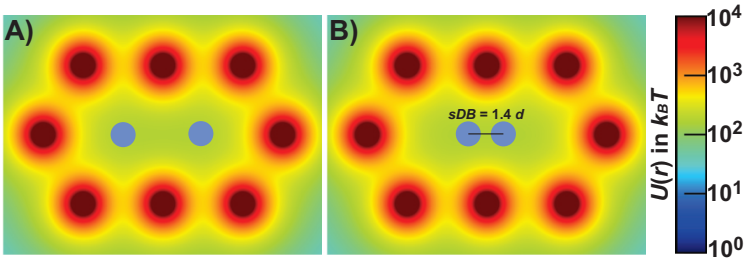


FIGURE 6.20: The potential energy landscape A) of eight neighboring spheres on two hexagonal lattice positions and B) around a dumbbell with s_{DB} = 1.4d occupying two lattice sites.

cles were confined to their lattice position in the crystal (Figure 6.19A top). In the probability density plot of the position of the dumbbell, $P(r)$, the limited translational motion of the dumbbell was only directed parallel and perpendicular to the crystal orientation axis (Figure 6.19A bottom).
Analysis of the dumbbell orientation revealed that the dumbbell oriented at -22° < β < 22°, with a high probability to orient parallel to the crystal orientation, at β = 0°, see Figure 6.19B. The confinement potential calculated from $P(\beta)$ shows strong confinement of the dumbbell at β = 0° with a confinement energy of -7 k_BT (Figure 6.19C). Rotation of the dumbbell likely requires large distortions in the surrounding crystal, which is energetically unfavorable. Similar results were obtained by analysis of single confocal microscopy images of 22 different dumbbells with eight NNs, β = 3.6 ± 2.5°.

In $g(r)$ of a dumbbell with eight NNs two separate peaks were observed around r = 1s, which points to large differences in the distance r at which the eight NNs are positioned (Figure 6.8). To include the anisotropy of the dumbbell in our analysis we calculated the $g_\vartheta(r)$ of a typical dumbbell with eight NNs, for $\vartheta\epsilon$[0°, 90°], [90°, 180°], [180°, 270°] and [270°, 360°], separately (see Figure 6.21). The four $g_\vartheta(r)$ graphs show peaks at similar positions and this symmetric behavior in the position of the spheres allowed us to combine and average the positional data into an effective angular range of $\vartheta\epsilon$[0°, 90°]. In the resulting $\bar{g}_\vartheta(r)$ large differences were observed in the peak positions of the NNs (see Figure 6.22A). The peaks originating from NNs located at ϑ = 75° and 90° were completely separated from the peaks originating from NNs at ϑ = 0° to 60°. The distance r at which the NNs at ϑ = 45° and 0° were positioned differ by 29% and 45%, respectively, from the distance r where the NNs at ϑ = 90° were found. This explains the presence of the two peaks around r = 1s in the $g(r)$ for a dumbbell with eight NNs (Figure 6.8).
A confocal microscopy image of a dumbbell with eight NNs is shown in Figure 6.22B with an illustration of the ϑ-values of the surrounding spheres. Voronoi

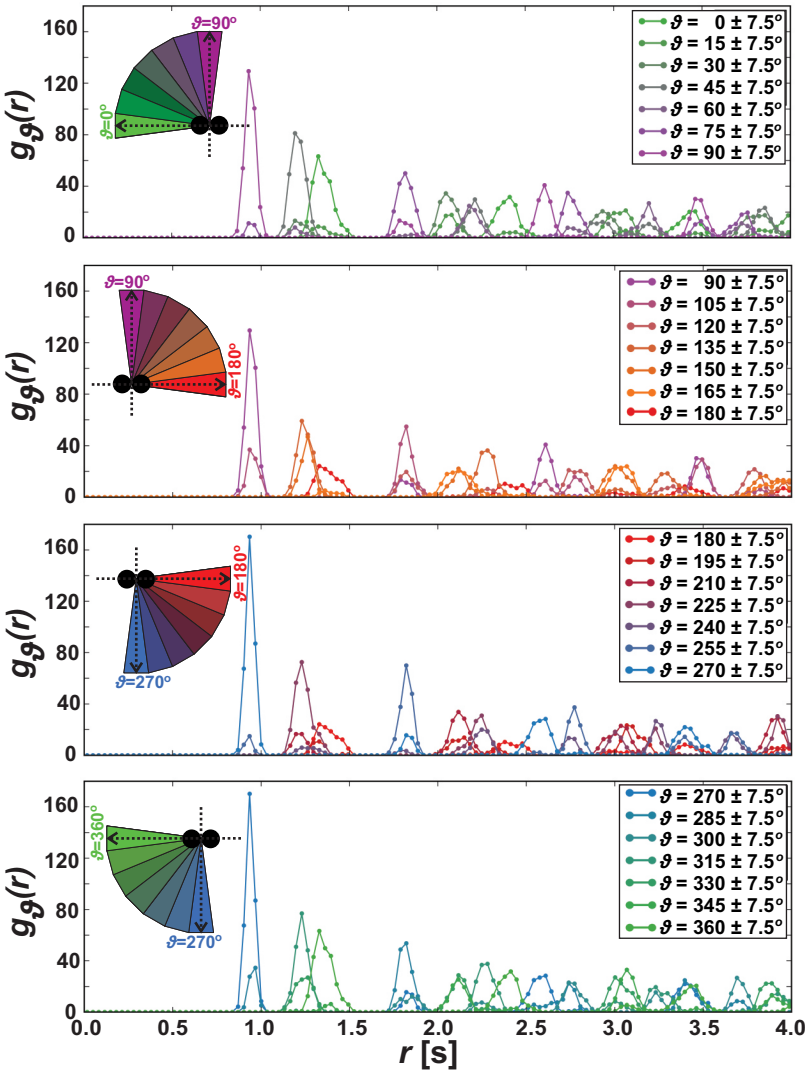
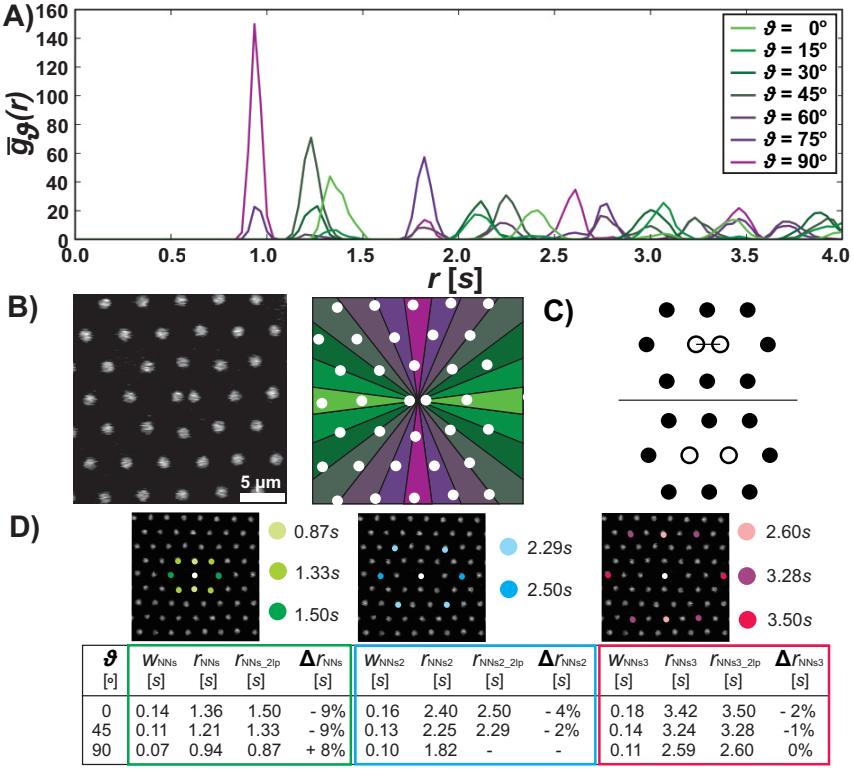


FIGURE 6.21: Restricted angular radial distribution functions $g_\vartheta(r)$ of a typical dumbbell with eight NNs in a crystal with $s = 3.20 \pm 0.15d$, obtained from 7090 measurements in two minutes. The four $g_\vartheta(r)$ graphs contain positional information of spheres surrounding the dumbbell at $\vartheta\epsilon[0°, 90°]$, $[90°, 180°]$, $[180°, 270°]$ and $[270°, 360°]$, respectively. Peaks are observed at similar distances r in the four graphs, pointing to symmetric behavior of the spheres in the four quadrants around the dumbbell.



ϑ [°]	w_{NNs} [s]	r_{NNs} [s]	r_{NNs_2lp} [s]	Δr_{NNs} [s]	w_{NNs2} [s]	r_{NNs2} [s]	r_{NNs2_2lp} [s]	Δr_{NNs2} [s]	w_{NNs3} [s]	r_{NNs3} [s]	r_{NNs3_2lp} [s]	Δr_{NNs3} [s]
0	0.14	1.36	1.50	- 9%	0.16	2.40	2.50	- 4%	0.18	3.42	3.50	- 2%
45	0.11	1.21	1.33	- 9%	0.13	2.25	2.29	- 2%	0.14	3.24	3.28	-1%
90	0.07	0.94	0.87	+ 8%	0.10	1.82	-	-	0.11	2.59	2.60	0%

FIGURE 6.22: Crystal distortion by dumbbells with eight NNs. A) $\bar{g}_\vartheta(r)$ of a dumbbell with eight NNs with all positional data of the surrounding spheres projected to $\vartheta\epsilon[0°, 90°]$. The distance r at which the spheres positioned largely depended on ϑ and the NNs were predominantly located at ϑ = 0°, 45° and 90°. B) Confocal microscopy image of a dumbbell oriented at $\beta = 0°$ with an illustration of the ϑ-values of the surrounding spheres. C) Illustration of an hexagonal crystal where the dumbbell occupies two lattice positions. D) Comparison of the positions of spheres around the dumbbell to the positions expected around a sphere occupying two lattice sites in a hexagonal crystal. The positions of the NNs around the dumbbell differed by -9 to +8% from the expected positions, r = 0.87s, 1.33s and 1.50s. In the second row of neighboring spheres, NNs2, deviations of -2 to -4% were found. In the third ring of neighboring spheres, NNs3, deviations of -1 and -2 % were measured, indicating that the hexagonal order has almost completely restored at this distance. Dumbbells with eight NNs occupy two lattice sites in the hexagonal crystal and distort the order only locally. The full width half maximum of the peaks originating from the neighboring spheres around the dumbbell, w_{NNs}, w_{NNs2} and w_{NNs3}, decreased with increasing ϑ.

diagrams indicated that dumbbells with eight NNs occupied two lattice sites in a hexagonal crystal (Figure 6.7C2, 6.7C3 and 6.22C). We therefore compared the positions of the neighboring spheres with the expected lattice positions of the neighbors of a sphere occupying two lattice sites (Figure 6.22D). Since in $\bar{g}_\vartheta(r)$ the peaks at $\vartheta = 0^\circ$, 45° and 90° were most pronounced, we only compared the positions of neighboring spheres at these ϑ-values. The full width half maximum of the peaks originating from the neighboring spheres around the dumbbell, w_{NNs}, w_{NNs2} and w_{NNs3}, decreased with increasing ϑ. This indicates that the confinement of the surrounding spheres decreased with increasing ϑ. For the NNs differences of -9 to +8% in the distance r at which the spheres were located were observed compared to the values expected. The deviations quickly decreased with increasing distance r. In the third row of NNs, NNs3, differences of only -1 and -2% were measured compared to the expected values which indicated that the hexagonal order had almost completely restored. Dumbbells with eight NNs evidently occupied two lattice sites in the hexagonal crystal and distort the crystal only locally.

6.4 Further Discussion

We showed that dumbbells with s_{DB}-values close to the diameter of the particles were surrounded by six NNs and that the number of NNs increased to seven and eight with the intradumbbell distance s_{DB}. All dumbbells distorted the hexagonal order of the surrounding spheres, either locally or over long distances. The preferred orientation of the dumbbells with respect to the crystal orientation depended on the number of NNs and the lattice spacing s. At short lattice spacings dumbbells with six NNs favored $\beta = 30^\circ$, whereas dumbbells with seven or eight NNs preferentially oriented at $\beta = 0^\circ$. The energy cost for the dumbbell to rotate in the crystal increased with s_{DB} and with increasing confinement. Dumbbells with six NNs have relatively more rotational freedom compared to dumbbells with seven or eight NNs at similar lattice spacings. The surroundings of dumbbells with six NNs are highly symmetric, while an strongly anisotropic environment was observed for dumbbells with seven and eight NNs. The energy cost for rotation is therefore larger for dumbbells with seven and eight NNs compared to dumbbells with six NNs.

Since dumbbells distort the hexagonal order is it likely that pairs of dumbbells interact at short distances. In Figure 6.23A-C confocal microscopy images are shown of dumbbells as NNs. Two dumbbells with short s_{DB} aligned parallel, were observed to occupy two lattice sites in the crystal (Figure 6.23A). Three lattice sites were occupied by two dumbells aligned parallel, but in sequence (Figure 6.23B). Dumbbells could also align perpedicular as illustrated in Figure 6.23C. The preferred situation probably depends on the lattice spacing s and s_{DB} of

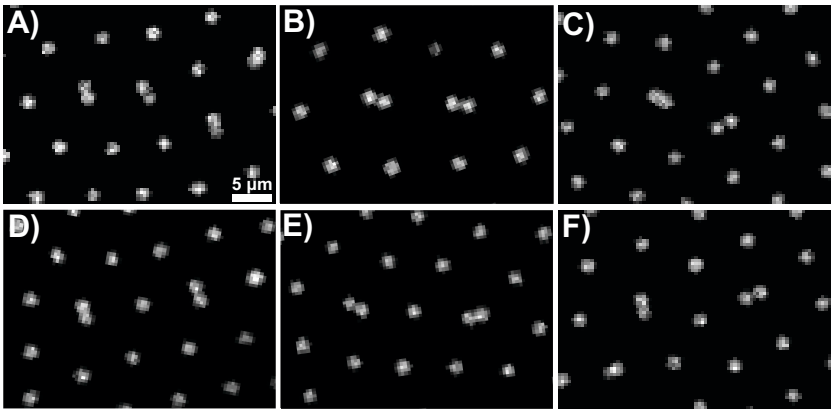


FIGURE 6.23: Orientations of neighboring dumbbells (A-C) and dumbbells separated by one crystal row (D-F). The dumbbells oriented parallel or perpendicular. Two neighboring dumbbells could occupy two (A) or three (B) lattice positions in the hexagonal crystal depending on their orientation with respect to each other and s_{DB}.

the dumbbells. Similar orientations were also observed for dumbbells separated by one crystal row of particles, Figure 6.23D-F. Further research on neighboring dumbbells should provide information on the interaction between dumbbells and their effect on the hexagonal order in the crystal. Investigation of the effect of other anisotropic impurities such as chains, triangular and square shapes (Figure 6.5) on the hexagonal order could also provide additional information.

6.5 Conclusions

We studied how repulsive pMMA spheres and anisotropic impurities arranged at a flat fluid interface between a glycerol:water (85:15) and CHB:cis-decalin (70:30) phase. Spheres ordered on a hexagonal lattice where their motion was restricted to one lattice site at short lattice spacings. At the fluid interface three types of impurities were observed in the crystal: (1) spherical objects significantly smaller or larger with respect to the particle diameter, (2) colloid stabilized droplets of the aqueous phase in the organic phase and (3) anisotropic clusters of spheres. Analysis of anisotropic clusters formed by two spheres, dumbbells, showed that the distance between the two spheres, the intradumbbell distance s_{DB}, differed per dumbbell. As s_{DB} increased the number of nearest neighbors also increased from six to a maximum of eight. We speculated that the formation of the anisotropic clusters originated from small aqueous droplets between the spheres forming the dumbbell.

The orientation of the dumbbells with respect to the hexagonal crystal depended on s_{DB} and the lattice spacing. At short lattice spacings the rotational and translation motion of the dumbbells was restricted and a preferred orientation of the dumbbell axis with respect to the crystal orientation was found. Dumbbells with six nearest neighbors preferably oriented at 30° with respect to the crystal direction and occupied one lattice site in the hexagonal crystal. The position of the surrounding spheres depended on the dumbbell orientation and the hexagonal order was locally anisotropically distorted. Dumbbells with seven nearest neighbors distorted the translational order in the crystal over long ranges by the introduction of an isolation dislocation and preferably oriented parallel to the crystal orientation. At larger s_{DB} dumbbells were surrounded by eight nearest neighbors occupying two lattice sites in the hexagonal crystal. The rotational motion of these dumbbells was strongly restricted and the dumbbells preferentially oriented in line with the crystal orientation. The confinement potential of the dumbbells and the surrounding spheres showed confinement energies up to -7 k_BT. The anisotropic energy landscape around the dumbbells originated from the repulsion between the two spheres forming the dumbbell and the surrounding spheres in the crystal.
Our results emphasize that the distortion of anisotropic impurities differ from isotropic impurities, which will likely also affect the physical properties of colloidal crystals. We therefore encourage future studies on the affect of anisotropic impurities on crystals.

Summary

In the *Summary* I will explain to a general public what I've studied in the past four years, how I studied this and why this research is important. Science is something you do together, so with 'I' I also refer to my supervisor, colleaques and the students that contributed to the research presented in this thesis. First, I will shortly introduce the scientific field of colloidal matter followed by a specific explanation of the research I've performed during my PhD. Finally, I'll summarize all my results creatively in a single illustration.

During my PhD-research I studied the behavior of micron-sized particles, so-called colloids. Colloids are not visible by eye since their dimensions are 100-10000 times smaller than the thickness of a hair. To visualize these particles we use instruments such as light and electron microscopes. To measure properties such as the electrical charge of the particles and the visco-elasticity of colloidal suspensions we use analytical methodes such as dynamic light scattering and rheometry.
When scientists study the 'behavior' of materials and particles they investigate the chemical and physical properties of the material. What shape does the particle have? What is the density? Size? Which molecules are present at the surface of the material? And how does the particle respond to its environment? How do particles interact between themselves and can we use this to assemble them into larger structures? All these questions and answers are required to understand why a system 'behaves' in a certain way.

And why do we study colloids? Without many of you realizing it colloids are abundantly present in our daily life. We drink and eat them, we put them on our skin and hair as creams or on the wall in paint. The colloids determine to a great extent the properties of a product. For example, the fatty colloids in milk give milk it's white appearence and the colloids in toothpaste make sure the paste only comes out when you push on the tube. Colloids are therefore crucial components in so-called 'soft materials'.
Insight and understanding of the properties of colloids is required to develop new materials with desired properties such as resistance to extreme force. Scientist are

nowadays very interested in the development of 'smart' materials, materials that respond and adapt to their environment. An example is a temperature sensitive material. A capsule of this material could be programmed to controllably open and close to deliver a medicine locally in the human body. To develop these materials a fundamental understanding of the building blocks is crucial. With my PhD research I've added a small piece to the scientific puzzle of this fundamental knowledge.

The title of my thesis **'Assembling Anisotropic Colloidal Building Blocks'** reveals what my piece of the puzzle is about. As explained, colloids can be used as building blocks for complex materials and structures and **'Colloidal Building Blocks'** refers to this. The building blocks can have different sizes and shapes and everything non-spherical is referred to as **'Anisotropic'**. The colloidal building blocks can be assembled into larger structures, hence the term **'Assembling'**.

In **Chapter 2** I've developed a way to make colloidal building blocks of different shapes and with different surface roughness. In science, the fabrication of molecules or colloids is called *synthesis*. The shape of the colloids was tuned by changing the volume of spheres during synthesis. By first increasing the volume by swelling, followed by decreasing the volume the shell around the spheres collapsed forming one or more dents. The resulting shape is comparable to a collapsed football. The surface roughness on the particles was controlled by adding an additional chemical component, hydroquinone, during the synthesis. Without hydroquinone small nanoparticles were formed that adhered to the larger colloidal spheres introducing surface roughness. By adding hydroquinone the formation of the nanoparticles was surpressed resulting in semi-rough and smooth spheres. Smooth and rough spheres give rise to different properties in suspension. A creme with rough particles is for example less easily spread compared to a creme with smooth particles.

In **Chapter 3** a new method, the *Colloidal Recycling method*, is presented to assemble simple spheres into clusters with complex shapes. The cluster shapes are anisotropic and depend on the number of spheres forming the clusters. The Colloidal Recycling method involves two steps. In the first step spheres are made attractive, sticky, resulting in random clusters of spheres upon collision. In the second step an additional liquid is added with affinity for the colloids. The liquid deposits as small droplets at the contact areas between the spheres in the clusters and acts as lubricating oil between the spheres. The spheres can now slide and/or roll over one another and by merging of the small droplets into one cluster-spanning droplet the clusters reconfigure into compact shapes. Parts of the spheres are protruding from the cluster-spanning droplet and these parts are called patches, areas of a particles that can be made attractive. These clusters are

therefore referred to as *patchy particles*. The Colloidal Recycling method is unique since large quantities can be synthesized and the type of colloid and swelling material is highly variable. This offers the opportunity to assemble a diverse range of patchy particles. The assembled patchy particles are interesting as larger, more complex, building blocks to fabricate macro-structures.

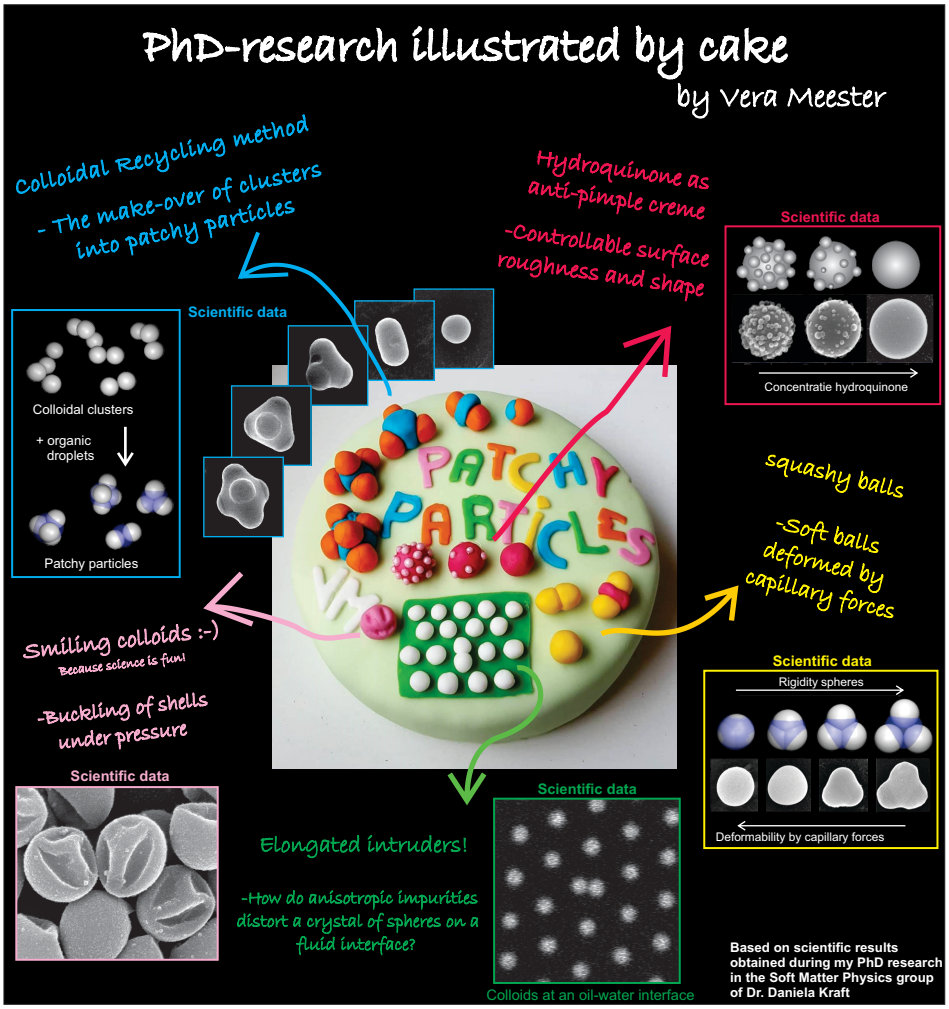
In **Chapter 4** I explore the *Colloidal Recycling method* by investigating the effect of the small droplets between the two spheres on the shape of the original spheres and the geometry of the reconfigured cluster. Droplets prefer a spherical shape, since this minimizes the contact area of the liquid droplet with the environment. On the other hand, the spheres try to spread the droplet on their surfaces which would deform the droplet. Our results indicated that a balance is found, where the capillary forces originating from the droplet are strong enough to deform spheres. Soft spheres are so strongly deformed by these forces that the clusters completely merge into one large ball. Rigid spheres deform less resulting in anisotropically shaped patchy particles. We showed that we can use the rigidness of the spheres to control the shape of the final patchy particle.

In **Chapter 5** the knowledge of Chapter 3 and 4 are combined to obtain patchy particles of complex shapes. This was achieved by applying the Colloidal Recycling method to mixtures of spheres with different size and rigidity. By combining soft and rigid spheres unique shapes were obtained where the soft spheres had deformed while the rigid spheres were not. The shape of the reconfigured clusters also depended on the size ratio between the spheres. Spheres of 1 micrometer and 0.23 micrometer, a size ratio of 4.6, formed structures where the larger spheres determined the geometry of the cluster while the small spheres positioned at the contact areas of the larger spheres. The small spheres therefore formed a 'jacket' around the cluster. The 'jacket' introduced surface roughness to the clusters which offers additional opportunities for the self-assembly of these patchy particles into larger structures.

In **Chapter 6** I studied how highly repulsive spheres ordered at an interface between water and oil. Similar to soap molecules, surfactants, colloids attach to water-oil interfaces. At the interface the colloids form ordered patterns, so-called *colloidal crystals*. The spheres were all surrounded by 6 other spheres, which we call hexagonal ordering. We, however, purposely distorted the hexagonal order by introducing elongated impurities, dumbbells, in the hexagonal crystal. The *crystal defects* induced by these distortions depended on the length of the dumbbells. For high particle densities at the interface, the dumbbells could not move anymore, the translational and rotational motion was restricted, and the orientation of the dumbbells in this confined space also depended on the length of the dumbbell. These impurities can be used to change the properties of colloidal crys-

tals such as the mechanical strength. The results provide insight in the formation of defects formed by anisotropic impurities in crystals, which is also observed in biological systems such as virus capsids.

Finally, I've illustrated my PhD research in a creative way, using a cake:



Samenvatting

In de *Samenvatting voor Iedereen* leg ik aan een breed publiek uit wat ik heb onderzocht in de afgelopen vier jaar, hoe ik dat gedaan heb en waarom het belangrijk is. Wetenschap doe je nooit alleen dus met 'ik' refereer ik ook aan mijn begeleider, collega's en de studenten die hebben bijgedragen aan het werk gepresenteerd in deze thesis. Eerst zal ik een korte introductie geven van het vakgebied gevolgd door een specifieke uitleg van het onderzoek dat ik heb verricht. Als laatste vat ik deze thesis op creatieve manier samen in een enkele illustratie.

Mijn promotie-onderzoek was gericht op het bestuderen van het 'gedrag' van micron-grootte deeltjes, zogenaamde colloiden. Ter vergelijking: colloiden zijn 100-10000 keer kleiner dan de dikte van een haar, waardoor ze niet met het blote oog te zien zijn. Om colloiden zichtbaar te maken gebruiken wij apparaten zoals een lichtmicroscoop of een elektronenmicroscoop. Andere eigenschappen van deze deeltjes zoals de elektrische lading en de visco-elasticiteit (bijvoorbeeld de gel-achtigheid) van een vloeistof met colloiden, kunnen we meten met analytische meetmethoden zoals dynamische lichtverstrooiing en rheometrie.
Als wetenschappers kijken naar het 'gedrag' van materialen of deeltjes dan bestuderen ze de chemische en fysische eigenschappen van een stof. Wat voor vorm heeft het deeltje? Wat voor dichtheid? Grootte? Wat voor moleculen zitten er aan de buitenkant van het deeltje? En hoe reageert het deeltje op zijn omgeving? Welke interactie hebben zij met elkaar en kunnen we dit gebruiken om andere structuren te bouwen? Al deze antwoorden zijn nodig om te begrijpen waarom een systeem zich op een bepaalde manier 'gedraagt'.

En waarom doen we onderzoek naar colloiden? Zonder dat u het wellicht weet komt u colloiden overal in uw dagelijks leven tegen. U eet of drinkt ze op, smeert ze op uw gezicht of haar in cremes, of smeert ze op de muur als verf. De colloiden bepalen voor een groot deel de eigenschappen van een product. Het zijn de vet-colloiden in melk die de melk wit maken, de colloiden in je dagcreme die de creme smeerbaar maken en de colloiden in je tandpasta die zorgen dat je tandpasta pas uit de tube loopt als je er druk op uitoefent. Colloiden zijn dus cruciale componenten in zogenoemde 'zachte materialen'.

Inzicht in en het begrijpen van de eigenschappen van colloiden is nodig om nieuwe materialen te ontwikkelen die bijvoorbeeld veel druk aankunnen of juist erg zacht zijn. Ook wordt er binnen de wetenschap gezocht naar 'slimme' materialen; materialen die reageren en anticiperen op hun omgeving. Een voorbeeld is een materiaal dat uitzet bij temperatuursverhoging. Een capsule van dit materiaal zou dan op commando open en dicht kunnen gaan, waardoor het een medicijn lokaal zou kunnen toedienen in het lichaam. Om deze materialen te kunnen maken is allereerst fundamentele kennis nodig over mogelijke bouwstenen. Met mijn promotie-onderzoek heb ik een klein steentje bijgedragen aan het wetenschappelijke bouwwerk van deze fundamentele kennis.

De titel van mijn thesis **'Assembling Anisotropic Colloidal Building Blocks'** verraadt al een beetje hoe ik mijn steentje heb bijgedragen. Zoals uitgelegd kunnen colloiden bouwstenen zijn voor grotere materialen en structuren, dit zijn dus de **'Colloidal Building Blocks'**. Deze bouwstenen kunnen verschillende vormen hebben en alles wat niet bolvorming, isotroop, is noemen we **'Anisotropic'**. De colloidale bouwstenen kunnen we samenvoegen, assembleren, tot ze gezamenlijk grotere structuren vormen. Daar komt de term **'Assembling'** vandaan.

In **Hoofdstuk 2** heb ik colloidale bouwstenen gemaakt van verschillende vormen en met verschillende type ruwheid op de buitenkant van de deeltjes. Het maken van moleculen of colloiden wordt in de wetenschap *synthese* genoemd. De vorm van de deeltjes kon veranderd worden door het volume in bollen te veranderen tijdens de synthese. Door bollen eerst groter te maken, te zwellen, en vervolgens de inhoud van de bol te verkleinen klapte de schil naar binnen waardoor er 1 of meerdere deuken zichtbaar werden. Dit is te vergelijken met een lekke voetbal. De ruwheid van de deeltjes werd gecontroleerd door een extra chemische stof, hydroquinone, toe te voegen tijdens de synthese. Zonder hydroquinone ontstaan er nanodeeltjes die op de grote bollen gaan zitten en de bollen een ruw uiterlijk geven. Met hydroquinone wordt de vorming van deze kleine deeltjes voorkomen en krijg je dus gladde bollen. Deze ruwheid kunnen we gebruiken om andere eigenschappen te geven aan zachte materialen. Een creme met gladde deeltjes is bijvoorbeeld beter smeerbaar dan een creme met ruwe deeltjes.

In **Hoofdstuk 3** presenteer ik een nieuwe methode, de *Colloidal Recycling method*, om simpele bollen te assembleren tot clusters met complexe vormen. De clusters zijn anisotroop in vorm en de exacte vorm hangt af van de hoeveelheid bollen in het cluster. Deze complexe clusters worden gemaakt in twee stappen. In de eerste stap worden losse bollen attractief, plakkerig, gemaakt waardoor ze aan elkaar plakken als ze tegen elkaar aan botsen. De bollen vormden zo willekeurige clusterstructuren. In een tweede stap wordt een extra vloeistof toegevoegd die als druppeltjes tussen de bollen gaat zitten en als een smeerolie fungeert. De bollen

in een cluster kunnen nu over elkaar heen bewegen en herschikken wat leidde tot compacte clustervormen omdat de kleine druppeltjes samenvoegden tot 1 grote druppel. Een deel van de oorspronkelijke bollen steekt uit deze druppel naar buiten wat patches worden genoemd: Delen van een deeltje die attractief kunnen worden gemaakt. Deze structuren worden daarom *patchy particles* genoemd. De Colloidal Recycling method onderscheidt zich van andere methodes, doordat grote hoeveelheden deeltjes kunnen worden gemaakt en het type colloiden en type druppeltjes sterk varieerbaar is. Hierdoor kan een grote diversiteit aan complexe patchy particles worden gerealiseerd. De patchy particles zijn op hun buurt ook weer interessant als bouwstenen voor nog grotere structuren.

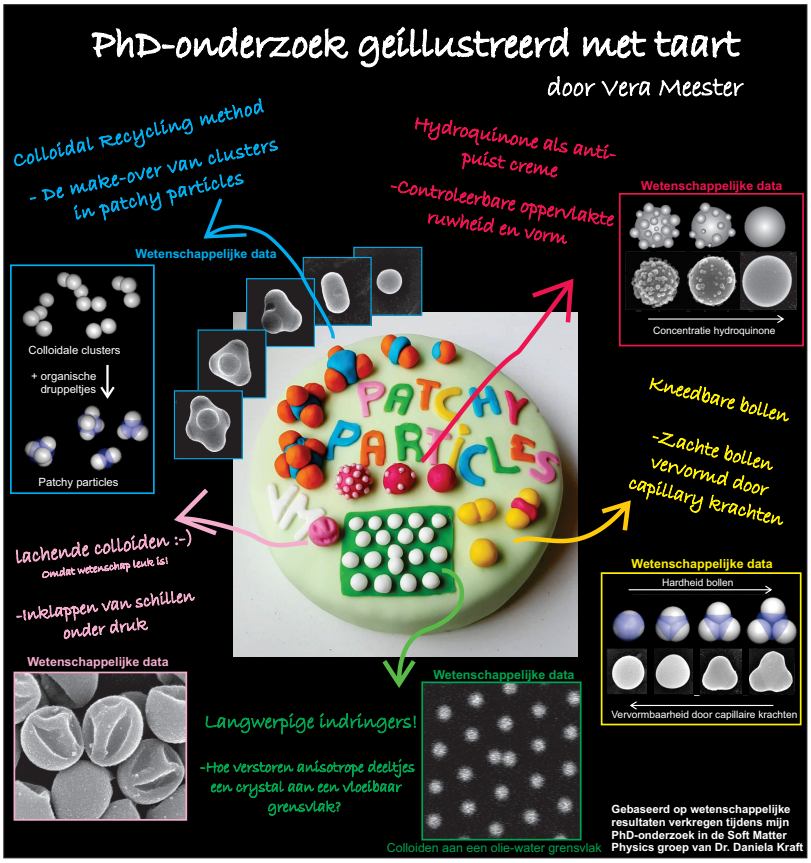
In **Hoofdstuk 4** ga ik dieper in op de *Colloidal Recycling method* en onderzoek ik wat voor effect de kleine druppeltjes tussen de bollen hebben op de vorm van de bollen en hoe de bollen herschikken. Druppels willen het liefste bolvormig zijn, omdat dan het contact-oppervlak van de druppel met de buitenwereld zo klein mogelijk is. Aan de andere kant hebben de bollen een voorkeur voor een andere vorm van het druppeltje omdat de colloiden de druppel willen verspreiden over hun oppervlak. Om een balans te vinden zien we dat de krachten van de druppel, de capillaire krachten, zo sterk zijn dat ze bepaalde bollen kunnen vervormen. Hele zachte bollen worden zo sterk vervormd dat de bollen in de clusters samenvloeien tot 1 grotere bol. Hardere bollen vervormen minder waardoor de originele bollen een cluster blijven vormen. We kunnen dus de zachtheid van de bollen gebruiken om de vorm van het uiteindelijke cluster aan te passen.

In **Hoofdstuk 5** gebruik ik de kennis uit hoofdstuk 3 en 4 om nog complexere patchy particles te vormen. Dit werd bereikt door de Colloidal Recycling method toe te passen op mengsels van bollen met verschillende grootte en zachtheid. Het combineren van zachte en harde bollen leverde unieke clustervormen op. De zachte bollen vervormden door de capillaire krachten die de druppeltjes op de bollen uitoefenden, terwijl de harde bollen niet vervormden. De clustervormen die ontstaan door het combineren van deeltjes van verschillende grootte hangt af van de ratio tussen de bollen. Bollen van 1.06 micrometer en 0.23 micrometer, een grootte ratio van 4.6, vormen structuren waarbij de grote bollen de geometrie bepalen en de kleine bollen gezamenlijk een soort jasje vormen over de grotere bollen. Dit jasje introduceert ruwheid aan het cluster wat extra mogelijkheden biedt voor de assemblage van deze deeltjes.

In **Hoofdstuk 6** heb ik bestudeerd hoe sterk repulsieve colloiden ordenen aan een grensvlak tussen water en olie. Vergelijkbaar met zeepmoleculen binden colloiden aan olie-water grensvlakken. Hier vormen de deeltjes geordende patronen, zogenoemde *colloidale kristallen*. Bollen worden vaak omringd door 6 andere bollen en vormen zo een hexagonaal patroon. Dit hexagonale patroon hebben wij

met opzet verstoord door langwerpige anisotrope deeltjes, dumbbells, toe te voegen aan het kristal. De *kristaldefecten* die ontstonden uit deze verstoring waren afhankelijk van de lengte van de dumbbells. Als de concentratie deeltjes aan het grensvlak hoog was konden de dumbbells niet meer bewegen, de tranlationele en rotationele beweging was beperkt, en dit gaf ons de mogelijkheid om ook de orientatie van de dumbbells te bestuderen welke af bleek te hangen van de lengte van de dumbbell. De dumbbells kunnen gebruikt worden om de eigenschappen van colloidale kristallen, zoals de mechanische sterkte, aan te passen aangezien deze beinvloedt worden door kristal defecten. De resultaten geven ook meer inzicht in defectvorming door anisotrope deeltjes, wat ook voorkomt in biologische systemen zoals virus capsides.

Als laatste, een creatieve eetbare illustratie van mijn promotie onderzoek:



Publication List

Work presented in this thesis

- Vera Meester and Daniela J. Kraft, *Spherical, dimpled and crumpled hybrid colloids with tunable surface morphology*, Langmuir, 32 (41), 10668-10677, **2016**.
(results from Chapter 2)
- Vera Meester, Ruben W. Verweij, Casper M. van der Wel and Daniela J. Kraft, *Colloidal recycling: Reconfiguration of random aggregates into patchy particles*, ACS nano, 10 (4), 4322-4329, **2016**.
(results from Chapter 3)
- Vera Meester and Daniela J. Kraft, *Complex patchy particles shaped from deformable seed particles by capillary interactions*, Soft Matter, 14, 1162-1170, **2018**.
(results from Chapter 4)
- Vera Meester and Daniela J. Kraft, *Patchy particles with two distinct patch types*, in preparation.
(results from Chapter 5)
- Vera Meester, Casper M. van der Wel, Ruben W. Verweij, Giovanni Biondaro and Daniela J. Kraft, *Anisotropic distortions in hexagonal crystals at fluid interfaces*, in preparation.
(results from Chapter 6)

Additional appreciation for work in this thesis

- Vera Meester, LION image award, Leiden University, published in Volkskrant in November **2016**.
(results from Chapter 2)
- Vera Meester, Best presentation award, Casimir Spring School, presentation title: *Colloidal recycling: Reconfiguration of random aggregates into patchy particles*, **2016**.
(results from Chapter 3)

Other publications

- Janne-Mieke Meijer, Vera Meester, Fabian Hagemans, Albert P. Philipse and Andrei Petukhov, *Convectively assembled crystals of colloidal cubes*, in preparation.
- Indrani Chakraborty, Vera Meester, Casper M. van der Wel and Daniela J. Kraft, *Colloidal joints with designed motion range and tunable joint flexibility*, Nanoscale, 9, 7814-7821, **2017**.
- Jan Hilhorst, Vera Meester, Esther Groeneveld, Jan K. G. Dhont and Henk N. W. Lekkerkerker, *Structure and Rheology of Mixed Suspensions of Montmorillonite and Silica Nano-particles*, Journal of Physical Chemistry B, 118 (40), 11816-11825, **2014**.
- Peter Holmqvist, Vera Meester, Fabian Westermeijer and Dzina Kleshchanok, *Rotational diffusion in concentrated platelet systems measured with X-ray photon correlation spectroscopy*, The Journal of Chemical Physics, 139, 084905, **2013**.
- Dzina Kleshchanok, Vera Meester, Cornelia E. Pompe, Jan Hilhorst and Henk N. W. Lekkerkerker, *Effects of added silica nanoparticles on hectorite gels*, Journal of Physical Chemistry B, 116 (31), 9532-9539, **2012**.

Curriculum Vitae

I was born in 1988 in Amersfoort and grew up in a small town nearby, Spakenburg. In 2008 I enrolled in the bachelor *Chemisty* at Utrecht University, where I specialized in physical chemistry with the minor *Nanosciences*. My bachelor graduation project was performed in collaboration with NIZO food research in Ede where we studied the effect of casein molecules on the texture of clay suspensions. During my studies I've also worked as a study coach for teenagers with study and social difficulties.
I graduated in 2011 (GPA 3.72) and subsequently started with the master *Nanomaterials: Chemistry and Physics* at Utrecht University. Two research projects were performed. One study was performed at Utrecht University at the department of Physical and Colloid Chemistry, where I synthesized hollow silica cubes and studied their self-assembly into large compact structures. The second project was performed at Oxford University where I formed networks of alternating strings of dia- and superparamagnetic particles under the influence of an external magnetic field. I finished my masters in 2014 (GPA 4.00). During my master I also worked as a researcher on a separate research project at Utrecht University involving the visco-elastic and dynamic properties of clay suspensions.
In March 2014 I started as a PhD-candidate in the newly established Soft Matter Physics group of Dr. Daniela Kraft at Leiden University. I developed a method to recycle colloidal aggregates by reconfiguration into patchy shapes and formed anisotropic colloids of various shapes. I also studied the effect of anisotropic particles on the hexagonal order of spheres at a fluid interface and the dynamics of these impurities under confinement. During my PhD I've supervised research projects of high school, bachelor, master and MBO students and presented my work at several national and international conferences. Besides research I've been motivated to promote and communicate science to a wider audience via interviews, labtours, competitions and presentations, which led to participation in Famelab and winning the LION Image Award and the Best Presentation Prize at the Casimir Spring School in 2016.
In June 2018 I'll start a new adventure as a Junior Scientist Innovator at the department of Explosions, Ballistics and Protection of TNO in Rijswijk.

Acknowledgements

I gratefully thank my supervisor Dr. Daniela Kraft for her guidance in the past four years. During scientific discussions you always provided me with renewed enthusiasm and options for further research, thanks to your knowledge and passion for science. Additionally, you have been a great mentor for both my scientific and personal development.
Many thanks to Casper, who has been my office buddy for 3.5 years. I appreciated our scientific discussions and your support with Python. We were also a very good team in managing the practicalities in the young Kraft laboratory and I value our friendship. Ruben, when I started my PhD research in Leiden you immediatly performed your bachelor research project with me. I admired your independent working attitude and your results on the colloidal recyling method have contributed to a nice chapter in this thesis. In the last year I thank you as a fellow PhD-colleague for your support. I also thank my colleagues Indrani, Melissa, Stefania and Rachel for their input during group meetings which I highly appreciated. Other students that contributed to my research are Giovanni, Sergio, Jelle, Esmee, Pim and Nuri. I thank you all for your contributions and for allowing me to develop my supervising and teaching skills. I also thank our secretary Danielle Duijn-ter Veer for her support with administration.
Besides members of the Kraftlab, other people contributed as well. I gratefully thank Prof. Martin van Hecke for acting as promotor and his insights in teaching. I also acknowledge my colleagues Merlijn, Luuk, Bastiaan, Peter, Geert, Anne, Scott, Koen, Ireth, Dan and Piermarco for introducing me to a physics perspective on research problems. Dr. Michiel Hermes and Prof. Wilson Poon (University of Edinburgh) are thanked for fruitful discussions on the visco-elastic behavior of colloidal suspensions and for allowing experiments in Edinburgh with their equipment. The input of Prof. Roel Dullens (University of Oxford) involving the anisotropic distortion of the hexagonal order of spheres at fluid interfaces is also highly appreciated.

Ook wil ik een aantal dierbaren bedanken zonder wie dit proefschrift niet tot stand was gekomen. Allereerst mijn liefdevolle ouders, Aart en Tamara, omdat ze altijd in mij geloofd hebben, ervoor gezorgd hebben dat ik kon studeren en mij

vrij hebben gelaten in mijn keuzes. Ook mijn zus en broers; Elise, Roelof, Joram en Martijn hebben mij altijd gesteund en met twee benen op de grond gezet met hun nuchtere kijk op dingen. Als laatste bedank ik mijn liefdevolle partner Alexander voor al zijn liefde, steun en geduld in de afgelopen jaren. Met jouw achtergrond in de gamma-wetenschappen heb je mij soms anders naar problemen laten kijken, waar ik ook inspiratie uit haalde voor mijn wetenschappelijk onderzoek binnen de natuurkunde.

Bibliography

[1] P. C. Hiemenz and R. Rajagopalan, *Principles of Colloid and Surface Chemistry*, Third (Marcel Dekker Inc, New York, 1997).

[2] S. C. Glotzer and M. J. Solomon, "Anisotropy of building blocks and their assembly into complex structures", Nature Materials **6**, 557–562 (2007).

[3] S. Sacanna, M. Korpics, K. Rodriguez, L. Colón-Meléndez, S.-H. Kim, D. J. Pine, and G.-R. Yi, "Shaping colloids for self-assembly.", Nature Communications **4**, 1688 (2013).

[4] H. R. Sheu, M. S. El-Aasser, and J. W. Vanderhoff, "Phase separation in polystyrene latex interpenetrating polymer networks", Journal of Polymer Science, Part A: Polymer Chemistry **28**, 629–651 (1990).

[5] G.-R. Yi, V. N. Manoharan, E. Michel, M. T. Elsesser, S.-M. Yang, and D. J. Pine, "Colloidal Clusters of Silica or Polymer Microspheres", Advanced Materials **16**, 1204–1208 (2004).

[6] S. Sacanna, W. T. M. Irvine, and D. J. Pine, "Lock and key colloids through polymerization-induced buckling of monodisperse silicon oil droplets", Soft Matter **7**, 1631–1634 (2011).

[7] H. R. Sheu, M. S. El-Aasser, and J. W. Vanderhoff, "Uniform nonspherical latex particles as model interpenetrating polymer networks", Journal of Polymer Science Part A: Polymer Chemistry **28**, 653–667 (1990).

[8] R. Arshady, "Suspension, emulsion, and dispersion polymerization: A methodological survey", Colloid and Polymer Science **270**, 717–732 (1992).

[9] J. W. Kim, R. J. Larsen, and D. A. Weitz, "Uniform nonspherical colloidal particles with tunable shapes", Advanced Materials **19**, 2005–2009 (2007).

[10] B. G. P. Van Ravensteijn and W. K. Kegel, "Tuning particle geometry of chemically anisotropic dumbbell-shaped colloids", Journal of Colloid and Interface Science **490**, 462–477 (2017).

[11] S. Sacanna, W. T. M. Irvine, P. M. Chaikin, and D. J. Pine, "Lock and key colloids", Nature **464**, 575–578 (2010).

[12]S. Knoche and J. Kierfeld, "Buckling of spherical capsules", Physical Review E **84**, 046608 (2011).

[13]G. Meng, N. Arkus, M. P. Brenner, and V. N. Manoharan, "The Free-Energy Landscape of Clusters of Attractive Hard Spheres", Science **327**, 560–563 (2010).

[14]V. Manoharan, M. Elsesser, and P. D.J., "Dense packing and symmetry in small clusters of microspheres", Science **301**, 483–487 (2003).

[15]A. B. Pawar and I. Kretzschmar, "Patchy particles by glancing angle deposition", Langmuir **24**, 355–358 (2008).

[16]D. J. Kraft, W. S. Vlug, C. M. Van Kats, A. Van Blaaderen, A. Imhof, and W. K. Kegel, "Self-assembly of colloids with liquid protrusions", Journal of the American Chemical Society **131**, 1182–1186 (2009).

[17]J. Du and R. K. O'Reilly, "Anisotropic particles with patchy, multicompartment and Janus architectures: preparation and application", Chemical Society Reviews **40**, 2402–2416 (2011).

[18]A. B. Pawar and I. Kretzschmar, "Fabrication , Assembly , and Application of Patchy Particles", Macromolecular rapid communications **31**, 150–168 (2010).

[19]Z. Zhang and S. C. Glotzer, "Self-assembly of patchy particles", Nano Letters **4**, 1407–1413 (2004).

[20]Y. Wang, A. D. Hollingsworth, S. K. Yang, S. Patel, D. J. Pine, and M. Weck, "Patchy Particle Self-Assembly via Metal Coordination", Journal of the American Chemical Society **135**, 14064–14067 (2013).

[21]Q. Chen, S. C. Bae, and S. Granick, "Directed self-assembly of a colloidal kagome lattice", Nature **469**, 381–384 (2011).

[22]S. Jiang, Q. Chen, M. Tripathy, E. Luijten, K. S. Schweizer, and S. Granick, "Janus Particle Synthesis and Assembly", Advanced Materials **22**, 1060–1070 (2010).

[23]L. Hong, S. Jiang, and S. Granick, "Simple method to produce janus colloidal particles in large quantity", Langmuir **22**, 9495–9499 (2006).

[24]J. W. Kim, R. J. Larsen, and D. A. Weitz, "Synthesis of nonspherical colloidal particles with anisotropic properties", Journal of the American Chemical Society **128**, 14374–14377 (2006).

[25]Y. Wang, Y. Wang, D. R. Breed, V. N. Manoharan, L. Feng, A. D. Hollingsworth, M. Weck, and D. J. Pine, "Colloids with valence and specific directional bonding", Nature **491**, 51–55 (2012).

[26]J. Israelachvili, *Intramolecular and surface forces*, Third ed. (Academic Press, Santa Barbara, 2011), pp. 253–266.

[27] V. Meester, *Magnetic-field induced structure formation in mixtures of superparamagnetic and diamagnetic colloids in a ferrofluid*, tech. rep. (University of Oxford, Oxford, 2014).

[28] M. E. Leunissen, A. van Blaaderen, A. D. Hollingsworth, M. T. Sullivan, and P. M. Chaikin, "Electrostatics at the oil-water interface, stability, and order in emulsions and colloids.", Proceedings of the National Academy of Sciences **104**, 2585–2590 (2007).

[29] D. J. Kraft, R. Ni, F. Smallenburg, M. Hermes, K. Yoon, D. A. Weitz, and A. V. Blaaderen, "Surface roughness directed self-assembly of patchy particles into colloidal micelles", Proceedings of the National Academy of Sciences **109**, 10787–10792 (2012).

[30] P. Pieranski, "Two-dimensional interfacial colloidal crystals", Physical Review Letters **45**, 569–572 (1980).

[31] Y. Yang, Z. Fang, X. Chen, W. Zhang, Y. Xie, Y. Chen, Z. Liu, and W. Yuan, "An overview of pickering emulsions: Solid-particle materials, classification, morphology, and applications", Frontiers in Pharmacology **8**, 1–20 (2017).

[32] M. Kamp, M. Hermes, C. M. Van Kats, D. J. Kraft, W. K. Kegel, M. Dijkstra, and A. Van Blaaderen, "Selective Depletion Interactions in Mixtures of Rough and Smooth Silica Spheres", Langmuir **32**, 1233–1240 (2016).

[33] W. T. M. Irvine, M. J. Bowick, and P. M. Chaikin, "Fractionalization of interstitials in curved colloidal crystals", Nature Materials **11**, 948–951 (2012).

[34] V. W. A. de Villeneuve, R. Dullens, D. Aarts, E. Groeneveld, H. Scherff, W. Kegel, and H. Lekkerkerker, "Colloidal Hard-Sphere Crystal Growth Frustrated by Large Spherical Impurities", Science **309**, 1231–1233 (2005).

[35] P. Pieranski, "Colloidal crystals", Contemporary Physics **24**, 25–73 (1983).

[36] D. R. Nelson, *Defects and Geometry in Condensed Matter Physics*, First edit (Cambridge University Press, Cambridge, 2002).

[37] W. T. M. Irvine, V. Vitelli, and P. M. Chaikin, "Pleats in crystals on curved surfaces", Nature **468**, 947–951 (2010).

[38] S. J. Gerbode, S. H. Lee, C. M. Liddell, and I. Cohen, "Restricted dislocation motion in crystals of colloidal dimer particles", Physical Review Letters **101**, 1–4 (2008).

[39] S. J. Gerbode, D. C. Ong, C. M. Liddell, and I. Cohen, "Dislocations and vacancies in two-dimensional mixed crystals of spheres and dimers", Physical Review E **82**, 1–7 (2010).

[40] E. Vignati, R. Piazza, and T. P. Lockhart, "Pickering Emulsions : Interfacial Tension , Colloidal Layer Morphology , and Trapped-Particle Motion", Langmuir **19**, 6650–6656 (2003).

[41]Y. C. Jung and B. Bhushan, "Contact angle , adhesion and friction properties of micro- and nanopatterned polymers for superhydrophobicity", Nanotechnology **17**, 4970–4980 (2006).

[42]V. N. Manoharan, "Colloids at interfaces: Pinned down", Nature Materials **14**, 869–870 (2015).

[43]B. M. Guy, M. Hermes, and W. C. K. Poon, "Towards a Unified Description of the Rheology of Hard-Particle Suspensions", Physical Review Letters **115**, 088304 (2015).

[44]J. R. Royer, D. L. Blair, and S. D. Hudson, "Rheological Signature of Frictional Interactions in Shear Thickening Suspensions", Physical Review Letters **116**, 188301 (2016).

[45]N. Y. C. Lin, B. M. Guy, M. Hermes, C. Ness, J. Sun, W. C. K. Poon, and I. Cohen, "Hydrodynamic and Contact Contributions to Continuous Shear Thickening in Colloidal Suspensions", Physical Review Letters **115**, 228304 (2015).

[46]S. Badaire, C. Cottin-Bizonne, and A. D. Stroock, "Experimental investigation of selective colloidal interactions controlled by shape, surface roughness, and steric layers", Langmuir **24**, 11451–11463 (2008).

[47]J. R. Wolters, G. Avvisati, F. Hagemans, T. Vissers, D. J. Kraft, M. Dijkstra, and W. K. Kegel, "Self-assembly of "Mickey Mouse" shaped colloids into tube-like structures: experiments and simulations", Soft Matter **11**, 1067–1077 (2015).

[48]K. Zhao and T. G. Mason, "Directing colloidal self-assembly through roughness-controlled depletion attractions", Physical Review Letters **99**, 268301 (2007).

[49]C. I. Zoldesi and A. Imhof, "Synthesis of monodisperse colloidal spheres, capsules, and microballoons by emulsion templating", Advanced Materials **17**, 924–928 (2005).

[50]M. Okubo, H. Minami, and K. Morikawa, "Influence of shell strength on shape transformation of micron-sized , monodisperse , hollow polymer particles", Colloid and Polymer Science **281**, 214–219 (2003).

[51]G. A. Vliegenthart and G. Gompper, "Compression, crumpling and collapse of spherical shells and capsules", New Journal of Physics **13**, 045020 (2011).

[52]C. Quilliet, C. Zoldesi, C. Riera, A. V. Blaaderen, and A. Imhof, "Anisotropic colloids through non-trivial buckling", The European Physical Journal E **27**, 13–20 (2008).

[53]L. Zhang, J. Wu, Y. Wang, Y. Long, N. Zhao, and J. Xu, "Combination of Bioinspiration: A General Route to Superhydrophobic Particles", Journal of the American Chemical Society **134**, 9879–9881 (2012).

[54] A. Perro, S. Reculusa, E. Bourgeat-Lami, E. Duguet, and S. Ravaine, "Synthesis of hybrid colloidal particles: From snowman-like to raspberry-like morphologies", Colloids and Surfaces A: Physicochemical and Engineering Aspects **284**, 78–83 (2006).

[55] M. D'Acunzi, L. Mammen, M. Singh, X. Deng, M. Roth, G. K. Auernhammer, and H.-j. Butt, "Superhydrophobic surfaces by hybrid raspberry-like particles", Faraday Discussions **146**, 35–48 (2010).

[56] N. Puretskiy and L. Ionov, "Synthesis of Robust Raspberry-like Particles Using Polymer Brushes", Langmuir **27**, 3006–3011 (2011).

[57] T. Song, T. Liu, X. Yang, and F. Bai, "Raspberry-like particles via the heterocoagulated reaction between reactive epoxy and amino groups", Colloids and Surfaces A: Physicochemical and Engineering Aspects **469**, 60–65 (2015).

[58] B. Peng and A. Imhof, "Surface morphology control of cross-linked polymer particles via dispersion polymerization", Soft Matter **11**, 3589–3598 (2015).

[59] M. T. Elsesser, A. D. Hollingsworth, K. V. Edmond, and D. J. Pine, "Large Core - Shell Poly(methyl methacrylate) Colloidal Clusters : Synthesis , Characterization , and Tracking", Langmuir **27**, 917–927 (2011).

[60] B. Thomson, A. Rudin, and G. Lajoie, "Dispersion Copolymerization of Styrene and Divinylbenzene . II . Effect of Crosslinker on Particle Morphology", Journal of Applied Polymer Science **59**, 2009–2028 (1996).

[61] C. Graf, D. L. J. Vossen, A. Imhof, and A. V. Blaaderen, "A General Method To Coat Colloidal Particles with Silica", Langmuir **19**, 6693–6700 (2003).

[62] Y. Lu, J. Mclellan, and Y. Xia, "Synthesis and Crystallization of Hybrid Spherical Colloids Composed of Polystyrene Cores and Silica Shells", Langmuir **20**, 3464–3470 (2004).

[63] A. Perro and V. N. Manoharan, "Bulk Synthesis of Polymer - Inorganic Colloidal Clusters", Langmuir **26**, 18669–18675 (2010).

[64] Y. Lan, Y. Wu, A. Karas, and O. A. Scherman, "Photoresponsive Hybrid Raspberry-Like Colloids Based on Cucurbit[8]uril Host – Guest Interactions", Angewandte Chemie - International Edition **53**, 2166–2169 (2014).

[65] W. Ming, D. Wu, R. V. Benthem, and G. D. With, "Superhydrophobic Films from Raspberry-like Particles", Nano Letters **5**, 2298–2301 (2005).

[66] R.-k. Wang, H.-r. Liu, and F.-w. Wang, "Facile Preparation of Raspberry-Like Superhydrophobic Polystyrene Particles via Seeded Dispersion Polymerization", Langmuir **29**, 11440–11448 (2013).

[67] C. Sun, Z.-z. Gu, and H. Xu, "Packing the Silica Colloidal Crystal Beads: A Facile Route to Superhydrophobic Surfaces", Langmuir **25**, 12439–12443 (2009).

[68]C. M. Tseng, Y. Y. Lu, and J. W. Vanderhoff, "Uniform Polymer Particles by Dispersion Polymerization in Alcohol", Journal of Polymer Science Part A: Polymer Chemistry **24**, 2995–3007 (1986).

[69]L. R. Herndon and E. E. Reid, "the Decomposition of Organic Compounds At High Temperatures and Pressures", J. Am. Chem. Soc. **50**, 3066–3073 (1928).

[70]Y. Wei, G.-W. Jang, C.-C. Chan, K. F. Hsueh, R. Hariharan, S. A. Patel, and C. K. Whitecar, "Polymerization of Aniline and Alkyl ring-Substituted Anilines in the Presence of Aromatic Additives", Journal of Physical Chemistry **94**, 7716–7721 (1990).

[71]C. I. Zoldesi, I. L. Ivanovska, C. Quilliet, G. J. L. Wuite, and A. Imhof, "Elastic properties of hollow colloidal particles", Physical Review E **78**, 051401 (2008).

[72]S. S. Datta, S.-h. Kim, J. Paulose, A. Abbaspourrad, D. R. Nelson, and D. A. Weitz, "Delayed Buckling and Guided Folding of Inhomogeneous Capsules", Physical Review Letters **109**, 134302 (2012).

[73]M. Okubo, R. Takekoh, and A. Suzuki, "Preparation of micron-sized , monodisperse poly (methyl methacrylate)/polystyrene composite particles having a large number of dents on their surfaces by seeded dispersion polymerization in the presence of decalin", Journal of Polymer Science **280**, 1057–1061 (2002).

[74]C. van der Wel, K. B. Rohit, R. W. Verweij, H. C. Frijters, Z. Gong, A. D. Hollingsworth, S. Sacanna, and D. J. Kraft, "Preparation of colloidal organosilica spheres through spontaneous emulsification", Langmuir **33**, 8174–8180 (2017).

[75]W. M. Haynes, D. Lide, and T. Bruno, *Handbook of Chemistry and Physics*, 94 (2013), pp. 15046–15047.

[76]S. I. R. Castillo, S. Ouhajji, S. Fokker, B. H. Erné, C. T. W. M. Schneijdenberg, D. M. E. Thies-Weesie, and A. P. Philipse, "Silica cubes with tunable coating thickness and porosity: From hematite filled silica boxes to hollow silica bubbles", Microporous and Mesoporous Materials **195**, 75–86 (2014).

[77]J. D. Halverson and A. V. Tkachenko, "DNA-programmed mesoscopic architecture", Physical Review E **87**, 062310 (2013).

[78]Z. Zeravcic, V. N. Manoharan, and M. P. Brenner, "Size limits of self-assembled colloidal structures made using specific interactions", Proceedings of the National Academy of Sciences **111**, 15918–15923 (2014).

[79]F. Romano and F. Sciortino, "Colloidal self-assembly: patchy from the bottom up", Nature Materials **10**, 171–173 (2011).

[80]P. F. Damasceno, M. Engel, and S. C. Glotzer, "Predictive Self-Assembly of Polyhedra into Complex Structures", Science **337**, 453–458 (2012).

[81] E. Bianchi, R. Blaak, and C. N. Likos, "Patchy colloids: state of the art and perspectives", Physical Chemistry Chemical Physics **13**, 6397–6410 (2011).

[82] A. Reinhardt and D. Frenkel, "Numerical Evidence for Nucleated Self-Assembly of DNA Brick Structures", Physical Review Letters **112**, 238103 (2014).

[83] A. Murugan, Z. Zeravcic, M. P. Brenner, and S. Leibler, "Multifarious assembly mixtures : Systems allowing retrieval of diverse stored structures", Proceedings of the National Academy of Sciences **112**, 54–59 (2014).

[84] K. L. Young, M. L. Personick, M. Engel, P. F. Damasceno, S. N. Barnaby, R. Bleher, T. Li, S. C. Glotzer, B. Lee, and C. a. Mirkin, "A directional entropic force approach to assemble anisotropic nanoparticles into superlattices", Angewandte Chemie **52**, 13980–13984 (2013).

[85] J. A. Millan, D. Ortiz, G. Van Anders, and S. C. Glotzer, "Self-assembly of archimedean tilings with enthalpically and entropically patchy polygons", ACS Nano **8**, 2918–2928 (2014).

[86] G. Van Anders, D. Klotsa, N. K. Ahmed, M. Engel, and S. C. Glotzer, "Understanding shape entropy through local dense packing", Proceedings of the National Academy of Sciences **111**, E4812–E4821 (2014).

[87] B. Ruzicka, E. Zaccarelli, L. Zulian, R. Angelini, M. Sztucki, A. Moussaïd, T. Narayanan, and F. Sciortino, "Observation of empty liquids and equilibrium gels in a colloidal clay", Nature Materials **10**, 56–60 (2011).

[88] F. Smallenburg and F. Sciortino, "Liquids more stable than crystals in particles with limited valence and flexible bonds", Nature Physics **9**, 554–558 (2013).

[89] L. Hong, A. Cacciuto, E. Luijten, and S. Granick, "Clusters of Charged Janus Spheres", Nano Letters **6**, 2510–2514 (2006).

[90] Q. Chen, E. Diesel, J. K. Whitmer, S. C. Bae, E. Luijten, and S. Granick, "Triblock Colloids for Directed Self-Assembly", Journal of the American Chemical Society **133**, 7725–7727 (2011).

[91] K. Chaudhary, Q. Chen, J. J. Jua, S. Granick, and J. A. Lewis, "Janus Colloidal Matchsticks", Journal of the American Chemical Society **134**, 12901–12903 (2012).

[92] J. Yan, M. Bloom, S. C. Bae, E. Luijten, and S. Granick, "Linking synchronization to self-assembly using magnetic Janus colloids", Nature **491**, 578–581 (2012).

[93] J. Yan, K. Chaudhary, S. C. Bae, J. A. Lewis, and S. Granick, "Colloidal ribbons and rings from Janus magnetic rods", Nature Communications **4**, 1516–1519 (2013).

[94]A. A. Shah, M. Ganesan, J. Jocz, and M. J. Solomon, "Direct Current Electric Field Assembly of Colloidal Crystals Displaying Reversible Structural Color", ACS nano **8**, 8095–8103 (2014).

[95]A. Ruditskiy, B. Ren, and I. Kretzschmar, "Behaviour of iron oxide (Fe3O4) Janus particles in overlapping external AC electric and static magnetic fields", Soft Matter **9**, 9174–9181 (2013).

[96]S. Sacanna, L. Rossi, and D. J. Pine, "Magnetic click colloidal assembly", Journal of the American Chemical Society **134**, 6112–6115 (2012).

[97]A. A. Shah, B. Schultz, W. Zhang, S. C. Glotzer, and M. J. Solomon, "Actuation of shape-memory colloidal fibres of Janus ellipsoids.", Nature Materials **14**, 117–124 (2014).

[98]Q. Chen, S. C. Bae, and S. Granick, "Directed self-assembly of a colloidal kagome lattice", Nature **469**, 381–384 (2011).

[99]Q. Chen, S. C. Bae, and S. Granick, "Staged self-assembly of colloidal metastructures", Journal of the American Chemical Society **134**, 11080–11083 (2012).

[100]S. Sacanna and D. J. Pine, "Shape-anisotropic colloids: Building blocks for complex assemblies", Current Opinion in Colloid and Interface Science **16**, 96–105 (2011).

[101]K. J. Lee, J. Yoon, and J. Lahann, "Recent advances with anisotropic particles", Current Opinion in Colloid and Interface Science **16**, 195–202 (2011).

[102]M. Grzelczak, J. Vermant, E. M. Furst, and L. M. Liz-Marzán, "Directed self-assembly of nanoparticles", ACS Nano **4**, 3591–3605 (2010).

[103]D. D. L. Heras, J. M. Tavares, and M. M. T. Da Gama, "Phase diagrams of binary mixtures of patchy colloids with distinct numbers and types of patches: The empty fluid regime", Journal of Chemical Physics **134**, 5615–5626 (2011).

[104]J. Appel, S. Akerboom, R. G. Fokkink, and J. Sprakel, "Facile one-step synthesis of monodisperse micron-sized latex particles with highly carboxylated surfaces.", Macromolecular rapid communications **34**, 1284–8 (2013).

[105]A. M. Yake, R. A. Panella, C. E. Snyder, and D. Velegol, "Fabrication of colloidal doublets by a salting out-quenching-fusing technique", Langmuir **22**, 9135–9141 (2006).

[106]C. van der Wel, N. Bossert, Q. J. Mank, M. G. T. Winter, D. Heinrich, and D. J. Kraft, "Surfactant-free Colloidal Particles with Specific Binding Affinity", Langmuir **33**, 9803–9810 (2017).

[107]D. A. Weitz, J. S. Huang, and Sung, "Dynamics of Diffusion-Limited Kintetic Aggregation", Physical Review Letters **53**, 1657–1660 (1984).

[108] P. J. Flory and J. Rehner, "Statistical Mechanics of Cross-Linked Polymer Networks", The Journal of Adhesion **11**, 521–526 (1943).

[109] A. B. Pawar, M. Caggioni, R. W. Hartel, and P. T. Spicer, "Arrested coalescence of viscoelastic droplets with internal microstructure", Faraday Discussions **158**, 341–350 (2012).

[110] E. B. Mock, H. De Bruyn, B. S. Hawkett, R. G. Gilbert, and C. F. Zukoski, "Synthesis of anisotropic nanoparticles by seeded emulsion polymerization", Langmuir **22**, 4037–4043 (2006).

[111] J. Russo, J. M. Tavares, P. I. C. Teixeira, M. M. T. Da Gama, and F. Sciortino, "Re-entrant phase behaviour of network fluids: A patchy particle model with temperature-dependent valence", Journal of Chemical Physics **135**, 034501 (2011).

[112] W. K. Kegel, D. Breed, M. Elsesser, and D. J. Pine, "Formation of Anisotropic Polymer Colloids by Disparate Relaxation Times", Langmuir **22**, 7135–7136 (2006).

[113] D. J. Kraft, J. Groenewold, and W. K. Kegel, "Colloidal molecules with well-controlled bond angles", Soft Matter **5**, 3823–3826 (2009).

[114] M. Y. Lin, H. M. Lindsay, D. A. Weitz, R. C. Ball, R. Klein, and P. Meakin, "Universality in colloid aggregation", Nature **339**, 360–362 (1989).

[115] M. Smoluchowski, "Drei vortrage uber diffusion, Brownsche bewegung und koagulation von kolloidteilchen", Zeitschrift fur Physik **17**, 557–585 (1916).

[116] M. Smoluchowski, "Versuch einer mathematischen Theorie der Koagulationskinetic kolloider Losungen", Zeitschrift fur Physik **92**, 129–168 (1917).

[117] E. Koos, "Current Opinion in Colloid & Interface Science Capillary suspensions : Particle networks formed through the capillary force", Current Opinion in Colloid & Interface Science **19**, 575–584 (2014).

[118] B. G. P. Van Ravensteijn, M. Kamp, A. Van Blaaderen, and W. K. Kegel, "General route toward chemically anisotropic colloids", Chemistry of Materials **25**, 4348–4353 (2013).

[119] C. Van Der Wel, A. Vahid, A. Šarić, T. Idema, D. Heinrich, and D. J. Kraft, "Lipid membrane-mediated attraction between curvature inducing objects", Scientific Reports **6**, 1–10 (2016).

[120] S. S. Velankar, "A non-equilibrium state diagram for liquid/fluid/particle mixtures", Soft Matter **11**, 8393–8403 (2015).

[121] G.-R. Yi, D. J. Pine, and S. Sacanna, "Recent progress on patchy colloids and their self-assembly.", Journal of physics. Condensed matter **25**, 193101 (2013).

[122]F. Li, D. P. Josephson, and A. Stein, "Colloidal assembly: The road from particles to colloidal molecules and crystals", Angewandte Chemie **50**, 360–388 (2011).

[123]S. Sacanna, D. J. Pine, and G.-R. Yi, "Engineering shape: the novel geometries of colloidal self-assembly", Soft Matter **9**, 8096–8106 (2013).

[124]Q. Chen, J. K. Whitmer, S. Jiang, S. C. Bae, E. Luijten, and S. Granick, "Supracolloidal reaction kinetics of Janus spheres", Science **331**, 199–202 (2011).

[125]E. Bianchi, C. N. Likos, and G. Kahl, "Self-Assembly of Heterogeneously Charged Particles under Confinement", ACS Nano **7**, 4657–4667 (2013).

[126]Z. Zhang, A. S. Keys, T. Chen, and S. C. Glotzer, "Self-Assembly of Patchy Particles into Diamond Structures through Molecular Mimicry", Langmuir **21**, 11547–11551 (2005).

[127]E. G. Noya, C. Vega, J. P. Doye, and A. A. Louis, "The stability of a crystal with diamond structure for patchy particles with tetrahedral symmetry.", The Journal of Chemical Physics **132**, 234511 (2010).

[128]X. Mao, Q. Chen, and S. Granick, "Entropy favours open colloidal lattices", Nature Materials **12**, 217–222 (2013).

[129]F. Sciortino, E. Bianchi, J. F. Douglas, and P. Tartaglia, "Self-assembly of patchy particles into polymer chains : A parameter-free comparison between Wertheim theory and Monte Carlo simulation", The Journal of Chemical Physics **126**, 194903 (2007).

[130]L. Lu, X. Li, P. G. Vekilov, and G. E. Karniadakis, "Probing the Twisted Structure of Sickle Hemoglobin Fibers via Particle Simulations", Biophysics journal **110**, 2085–2093 (2016).

[131]J. J. McManus, P. Charbonneau, E. Zaccarelli, and N. Asherie, "The physics of protein self-assembly", Current Opinion in Colloid and Interface Science **22**, 73–79 (2016).

[132]F. Romano, E. Sanz, and F. Sciortino, "Role of the Range in the Fluid-Crystal Coexistence for a Patchy Particle Model", The Journal of Physical Chemistry B **113**, 15133–15136 (2009).

[133]S. H. Kim, G. R. Yi, K. H. Kim, and S. M. Yang, "Photocurable pickering emulsion for colloidal particles with structural complexity", Langmuir **24**, 2365–2371 (2008).

[134]Y.-S. Cho, G.-R. Yi, J.-M. Lim, S.-H. Kim, V. N. Manoharan, D. J. Pine, and S.-M. Yang, "Self-Organization of Bidisperse Colloids in Water Droplets", Journal of the American Chemical Society **127**, 15968–15975 (2005).

[135] A. Desert, C. Hubert, Z. Fu, L. Moulet, J. Majimel, P. Barboteau, A. Thill, M. Lansalot, E. Bourgeat-lami, E. Duguet, and S. Ravaine, "Synthesis and Site-Specific Functionalization of Tetravalent , Hexavalent , and Dodecavalent Silica Particles", Angewandte Chemie **52**, 11068–11072 (2013).

[136] X. Zheng, Y. Wang, Y. Wang, D. J. Pine, and M. Weck, "Thermal Regulation of Colloidal Materials Architecture through Orthogonal Functionalizable Patchy Particles", Chemistry of Materials **28**, 3984–3989 (2016).

[137] B. Bharti, D. Rutkowski, K. Han, A. U. Kumar, C. K. Hall, and O. D. Velev, "Capillary Bridging as a Tool for Assembling Discrete Clusters of Patchy Particles", Journal of the American Chemical Society **138**, 14948–14953 (2016).

[138] V. Meester, R. W. Verweij, C. Van Der Wel, and D. J. Kraft, "Colloidal Recycling: Reconfiguration of Random Aggregates into Patchy Particles", ACS Nano **10**, 4322–4329 (2016).

[139] N. Arkus, V. N. Manoharan, and M. P. Brenner, "Minimal energy clusters of hard spheres with short range attractions", Physical Review Letters **103**, 118303 (2009).

[140] M. Hoare and P. Pal, "Physical cluster mechanics: Statics and energy surfaces for monatomic systems", Advances in Physics **20**, 161–196 (1971).

[141] S. Mossa, F. Sciortino, P. Tartaglia, and E. Zaccarelli, "Ground-State Clusters for Short-Range Attractive and Long-Range Repulsive Potentials", Langmuir **20**, 10756–10763 (2004).

[142] E. Koos and N. Willenbacher, "Particle configurations and gelation in capillary suspensions", Soft Matter **8**, 3988–3994 (2012).

[143] E. Lauga and M. P. Brenner, "Evaporation-driven assembly of colloidal particles", Physical Review Letters **93**, 238301 (2004).

[144] Y. Min, M. Akbulut, K. Kristiansen, Y. Golan, and J. Israelachvili, "The role of interparticle and external forces in nanoparticle assembly", Nature Materials **7**, 527–538 (2008).

[145] Y. G. Durant and D. C. Sundberg, "Effects of Cross-Linking on the Morphology of Structured Latex Particles. 1. Theoretical Considerations", Macromolecules **29**, 8466–8472 (1996).

[146] C. S. Wagner, Y. Lu, and A. Wittemann, "Preparation of Submicrometer-Sized Clusters from Polymer Spheres Using Ultrasonication", Langmuir **24**, 12126–12128 (2008).

[147] D. J. Kraft, W. S. Vlug, C. M. Van Kats, A. Van Blaaderen, A. Imhof, and W. K. Kegel, "Self-Assembly of Colloids with Liquid Protrusions", Journal of the American Chemical Society **131**, 1182–1186 (2008).

[148]D. J. Kraft, J. Hilhorst, M. A. P. Heinen, M. J. Hoogenraad, B. Luigjes, and W. K. Kegel, "Patchy Polymer Colloids with Tunable Anisotropy Dimensions", The Journal of Physical Chemistry B **115**, 7175–7181 (2011).

[149]H. Mehrabian, J. Harting, and J. H. Snoeijer, "Soft particles at a fluid interface", Soft Matter **12**, 1062–1073 (2016).

[150]C. S. Wagner, B. Fischer, M. May, and A. Wittemann, "Templated assembly of polymer particles into mesoscopic clusters with well-defined configurations", Colloid and Polymer Science **288**, 487–498 (2010).

[151]P. A. Kralchevskyt and K. Nagayama, "Capillary Forces between Colloidal Particles", Langmuir **10**, 23–36 (1994).

[152]D. Stamou, C. Duschl, and D. Johannsmann, "Long-range attraction between colloidal spheres at the air-water interface: The consequence of an irregular meniscus", Physical Review E **62**, 5263 (2000).

[153]Z. Gong, T. Hueckel, G. R. Yi, and S. Sacanna, "Patchy particles made by colloidal fusion", Nature **550**, 234–238 (2017).

[154]V. Meester and D. J. Kraft, "Complex Patchy Colloids shaped from Deformable Seed Particles through Capillary Interactions", Soft Matter **14**, 1162–1170 (2018).

[155]S. Ni, J. Leemann, I. Buttinoni, L. Isa, and H. Wolf, "Programmable colloidal molecules from sequential capillarity-assisted particle assembly", Science advances **2**, 1–7 (2016).

[156]Y. S. Cho, G. R. Yi, S. H. Kim, M. T. Elsesser, D. R. Breed, and S. M. Yang, "Homogeneous and heterogeneous binary colloidal clusters formed by evaporation-induced self-assembly inside droplets", Journal of Colloid and Interface Science **318**, 124–133 (2008).

[157]E. Bianchi, G. Doppelbauer, L. Filion, M. Dijkstra, and G. Kahl, "Predicting patchy particle crystals: Variable box shape simulations and evolutionary algorithms", Journal of Chemical Physics **136** (2012) 10.1063/1.4722477.

[158]W. Bollman, *Crystal Defects and Crystalline Interfaces*, first (Springer-Verlag, Berlin, 1970).

[159]T. Wood, J. Lintuviori, A. Schofield, B. Marenduzzo, and W. Poon, "A Self-Quenched Defect Glass in a Colloid-Nematic Liquid Crystal Composite", Science **334**, 79–83 (2011).

[160]U. Gasser, "Crystallization in three- and two-dimensional colloidal suspensions", Journal of Physics: Condensed Matter **21**, 203101 (2009).

[161]P. V. Braun, S. A. Rinne, and F. García-Santamaría, "Introducing defects in 3D photonic crystals: State of the art", Advanced Materials **18**, 2665–2678 (2006).

[162]C. López, "Materials Aspects of Photonic Crystals", Advanced Materials **15**, 1679–1704 (2003).

[163] A. M. Alsayed, M. F. Islam, J. Zhang, P. J. Collings, and A. G. Yodh, "Premelting at Defects Within Bulk Colloidal Crystals", Science **309**, 1207–1210 (2005).

[164] W. Lechner, E. Scholl-Paschinger, and C. Dellago, "Displacement fields of point defects in two- dimensional colloidal crystals", Journal of Physics: Condensed Matter **20**, 1–7 (2008).

[165] G. Meng, J. Paulose, D. R. Nelson, and V. N. Manoharan, "Elastic Instability of a Crystal Growing on a Curved Surface", Science **343**, 634–637 (2014).

[166] D. J. Wales, "Chemistry, geometry, and defects in two dimensions", ACS Nano **8**, 1081–1085 (2014).

[167] D. Ershov, J. Sprakel, J. Appel, M. A. Cohen Stuart, and J. van der Gucht, "Capillarity-induced ordering of spherical colloids on an interface with anisotropic curvature", Proceedings of the National Academy of Sciences **110**, 9220–9224 (2013).

[168] H. Kusumaatmaja and D. J. Wales, "Defect motifs for constant mean curvature surfaces", Physical Review Letters **110**, 1–5 (2013).

[169] F. A. Lavergne, S. Diana, D. G. A. L. Aarts, and R. P. A. Dullens, "Equilibrium Grain Boundary Segregation and Clustering of Impurities in Colloidal Polycrystalline Monolayers", Langmuir **32**, 12716–12724 (2016).

[170] J. A. G. Briggs, J. D. Riches, B. Glass, V. Bartonova, G. Zanetti, and H.-G. Krausslich, "Structure and assembly of immature HIV", Proceedings of the National Academy of Sciences **106**, 11090–11095 (2009).

[171] R. P. Dullens, M. Claesson, D. Derks, A. Van Blaaderen, and W. K. Kegel, "Monodisperse core-shell poly (methyl methacrylate) latex colloids", Langmuir **19**, 5963–5966 (2003).

[172] M. T. Elsesser and A. D. Hollingsworth, "Revisiting the Synthesis of a Well-Known Comb-Graft Copolymer Stabilizer and Its Application to the Dispersion Polymerization of Poly(methyl methacrylate) in Organic Media", Langmuir **26**, 17989–17996 (2010).

[173] M. T. Elsesser, A. D. Hollingsworth, K. V. Edmond, and D. J. Pine, "Large Core-Shell Poly(methyl methacrylate) Colloidal Clusters: Synthesis, Characterization, and Tracking", Langmuir **27**, 917–927 (2011).

[174] R. Aveyard, B. P. Binks, J. H. Clint, P. D. Fletcher, T. S. Horozov, B. Neumann, V. N. Paunov, J. Annesley, S. W. Botchway, D. Nees, A. W. Parker, A. D. Ward, and A. N. Burgess, "Measurement of long-range repulsive forces between charged particles at an oil-water interface", Physical Review Letters **88**, 2461021 (2002).

[175]D. N. ten Napel, P. Liu, and A. P. Philipse, "Synthesis, Characterization and Interfacial Self-Assembly of Spherical Magnetic Colloids", Master (Utrecht University, 2016).

[176]J. Crocker and D. Grier, "Methods of Digital Video Microscopy for Colloidal Studies", Journal of Colloid and Interface Science **179**, 298–310 (1996).

[177]D. Allan, T. Caswell, N. Keim, and C. van der Wel, *Trackpy*, 2017.

[178]C. van der Wel and D. J. Kraft, "Automated tracking of colloidal clusters with sub-pixel accuracy and precision", Journal of Physics: Condensed Matter **29**, 044001 (2016).

[179]C. P. Kelleher, A. Wang, G. I. Guerrero-García, A. D. Hollingsworth, R. E. Guerra, B. J. Krishnatreya, D. G. Grier, V. N. Manoharan, and P. M. Chaikin, "Charged hydrophobic colloids at an oil-aqueous phase interface", Physical Review E - Statistical, Nonlinear, and Soft Matter Physics **92**, 062306 (2015).

[180]M. Oettel and S. Dietrich, "Colloidal Interactions at Fluid Interfaces", Langmuir **24**, 1425–1441 (2008).

[181]C. P. Kelleher, R. E. Guerra, A. D. Hollingsworth, and P. M. Chaikin, "Phase behavior of charged colloids at a fluid interface", Physical Review E **95**, 022602 (2017).

[182]F. Ghezzi and J. C. Earnshaw, "Formation of meso-structures in colloidal monolayers", Journal of Physics: Condensed Matter **9**, L517–L523 (1997).

[183]J. C. Fernández-Toledano, A. Moncho-Jordá, F. Martínez-López, and R. Hidalgo-Álvarez, "Spontaneous formation of mesostructures in colloidal monolayers trapped at the air-water interface: A simple explanation", Langmuir **20**, 6977–6980 (2004).

[184]M. N. van der Linden, D. El Masri, M. Dijkstra, and A. van Blaaderen, "Expansion of charged colloids after centrifugation: formation and crystallisation of long-range repulsive glasses", Soft Matter **9**, 11618 (2013).

[185]J. C. Everts, M. N. van der Linden, A. van Blaaderen, and R. van Roij, "Alternating strings and clusters in suspensions of charged colloids", Soft Matter **12**, 6610–6620 (2016).

[186]K. D. Danov, P. A. Kralchevsky, B. N. Naydenov, and G. Brenn, "Interactions between particles with an undulated contact line at a fluid interface: Capillary multipoles of arbitrary order", Journal of Colloid and Interface Science **287**, 121–134 (2005).

[187]V. S. J. Craig, "Very small bubbles at surfaces—the nanobubble puzzle", Soft Matter **7**, 40–48 (2011).

[188]H. Peng, G. R. Birkett, and A. V. Nguyen, "Progress on the Surface Nanobubble Story: What is in the bubble? Why does it exist?", Advances in Colloid and Interface Science **222**, 573–580 (2015).

[189]H. An, G. Liu, and V. S. J. Craig, "Wetting of nanophases: Nanobubbles, nanodroplets and micropancakes on hydrophobic surfaces", Advances in Colloid and Interface Science **222**, 9–17 (2015).

[190]F. A. Lavergne, "Dynamics of grain boundaries in two-dimensional colloidal crystals", PhD (University of Oxford, 2016).